การหาสภาพเหมาะที่สุดของเครื่องพลาสมาโฟกัสที่ถูกดัดแปรเพื่อการกำเนิดลำไอออน

นายดุสิต งามรุ่งโรจน์

วิทยานิพนธ์นี้เป็นส่วนหนึ่งของการศึกษาตามหลักสูตรปริญญาวิทยาศาสตรดุษฎีบัณฑิต
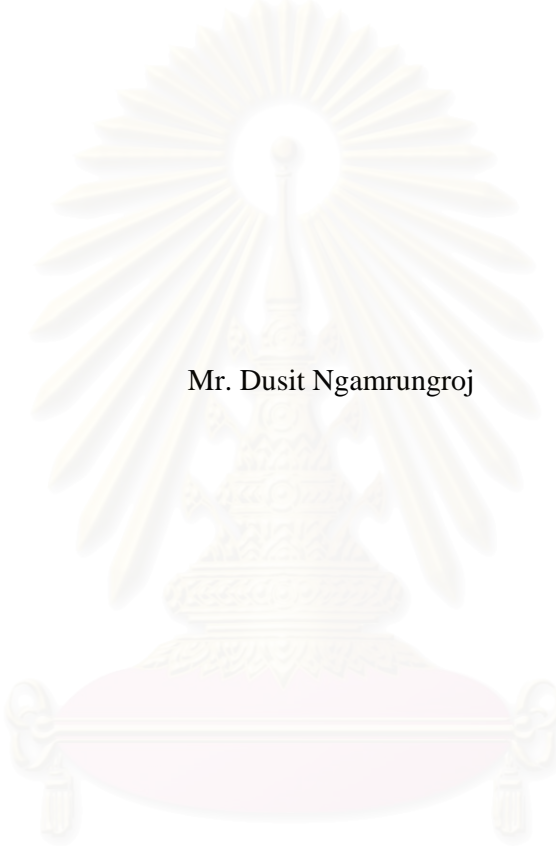สาขาวิชาฟิสิกส์   ภาควิชาฟิสิกส์
คณะวิทยาศาสตร์ จุฬาลงกรณ์มหาวิทยาลัย
ปีการศึกษา 2550

OPTIMIZATION OF A MODIFIED PLASMA FOCUS

FOR ION BEAM GENERATION

Mr. Dusit Ngamrungroj

A Dissertation Submitted in Partial Fulfillment of the Requirements
for the Degree of Doctor of Philosophy Program in Physics
Department of Physics
Faculty of Science Chulalongkorn University
Academic year 2007

Thesis Title   OPTIMIZATION OF A MODIFIED PLASMA FOCUS FOR ION BEAM GENERATION

By   Mr. Dusit Ngamrungroj

Field of Study   Physics

Thesis Advisor   Assistant Professor Rattachat Mongkolnavin, Ph.D.

Thesis Co-advisor   Professor Chiow San Wong, Ph.D.

Accepted by the Science, Chulalongkorn University in Partial Fulfillment of the Requirements for the Doctoral Degree

.... Dean of the Faculty of Science

(Professor Supot Hannongbua, Ph.D.)

THESIS COMMITTEE

.... Chairman

(Assistant Professor Kajornyod Yoodee, Ph.D.)

.... Thesis Advisor

(Assistant Professor Rattachat Mongkolnavin, Ph.D.)

.... Thesis Co-advisor

(Professor Chiow San Wong, Ph.D)

.... External Member

(Emeritus Professor Thiraphat Vilaithong, Ph.D.)

.... Member

(Associate Professor Wichit Sritrakool, Ph.D.)

.... Member

(Assistant Professor Tonphong Kaewkongka, Ph.D.)

นายดุสิต งามรุ่งโรจน์ : การหาสภาพเหมาะที่สุดของเครื่องพลาสมาโฟกัสที่ถูกดัดแปรเพื่อการ กำเนิดลำไอออน. (OPTIMIZATION OF A MODIFIED PLASMA FOCUS FOR ION BEAM GENERATION) อ. ที่ปรึกษา : ผศ. ดร. รัฐชาติ มงคลนาวิน, อ.ที่ปรึกษาร่วม : PROF. CHIOW SAN WONG, Ph.D. จำนวนหน้า 98 หน้า.

ในงานวิจัยนี้ได้ทำการศึกษากระบวนการเกิดของไอออนของเครื่อง UNU/ICTP พลาสมาโฟกัส พลังงานต่ำ 3.3 กิโลจูล และได้อธิบายการหาสภาพที่ดีสุดของเครื่องเพื่อการกำเนิดลำไอออน ใน การศึกษานี้ได้ใช้การทดลองและทฤษฎีมาช่วยในการวิเคราะห์ เทคนิคที่ใช้ในการวิเคราะห์เป็นเทคนิค ได้มีการพัฒนาให้เหมาะสมกับเครื่องพลาสมาโฟกัสในการวิเคราะห์ลำไอออน แบบจำลองที่ใช้มี พื้นฐานทางกลศาสตร์ และอิเล็กทรอนิกส์ ได้นำมาใช้ในการอธิบายการเกิดพลาสมาในเครื่องพลาสมา โฟกัส นอกจากนี้ได้ศึกษาผลกระทบของการเคลื่อนที่และพลังงานของชั้นกระแสของพลาสมาต่อการ กำเนิดลำไอออน หัววัดไอออนแบบสะสม หัววัดพินไดโอด (PIN-diode) และหัววัดโลโกวีสกี้ (Rogowski coil) ได้นำมาใช้เพื่อวัดอัตราเร็ว พลังงานจลน์และความหนาแน่นของลำไอออน ที่เกิดจาก เครื่องพลาสมาโฟกัส ภายใต้การเปลี่ยนแปลงความดันและความต่างศักย์ตกคร่อมตัวเก็บประจุความต่าง ศักย์สูงของแต่ละความยาวและรูปร่างของขั้วแอโนด

ในการศึกษานี้ได้แสดงให้เห็นว่าความหนาแน่นของไอออน ได้เพิ่มขึ้นมากกว่า 300% และ 80% ของพลังงานไอออน เมื่อเทียบกับเครื่อง UNU/ICTP พลาสมาโฟกัสแบบเดิม พลังงานของไอออน มีความสัมพันธ์กับพลังงานที่เข้าสู่พลาสมา ซึ่งความหนาแน่นสัมพันธ์กับพลังงานเริ่มต้นที่ประจุในตัว เก็บประจุ เครื่องพลาสมาโฟกัสที่ปรับปรุงมีขั้วแอโนดยาว 19 เซนติเมตร โดยมีลักษณะปลายแอโนด เรียว (taper anode) ภายใต้เงื่อนไขของก๊าซอาร์กอนที่ความดัน 0.8 mbar กับพลังงานเก็บสะสม 2.53 kJ จะทำให้ได้พลังงานเฉลี่ยและความหนาแน่นของอาร์กอนไอออน ประมาณ 1.47 MeV และ 4.49×10^{-19} ion/m^2 ตามลำดับ

ภาควิชาฟิสิกส์   ลายมือชื่อนิสิต..

สาขาวิชาฟิสิกส์   ลายมือชื่ออาจารย์ที่ปรึกษา.................................

ปีการศึกษา 2550   ลายมือชื่ออาจารย์ที่ปรึกษาร่วม...........................

This thesis presents a study of ion production process of a UNU/ICTP Plasma Focus which is a low energy device of 3 kJ. The optimization of the device for better ion beam production is also discussed. The study is based on both experimental and theoretical aspects, where suitable diagnostic techniques for the device characterization and ion beam characterization have been developed and employed, as well as, the simulation model based on both the kinematics and electronic aspects of the plasma generated by the device. Furthermore, the effects of the dynamics and the energy of the plasma current sheath on the ion beam generation are also investigated. The measurements of ion beam such as speed, kinetic energy and density are carried out using ion collector, PIN diode and Rogowski coil, when the device is operated at various pressures and charging voltages, as well as, various physical configurations such as length and shape of the anode.

It has been demonstrated that more than 300 % increase in ion density and 80% of the ion energy from the original UNU/ICTP Plasma Focus configuration can be obtained. The ion beam energy is found to be related to the energy transferred into the plasma where the ion density is found to be related to the initially stored energy to the capacitor bank. Average Ar ion energy and Ar ion density of 1.47 MeV and approximately 4.49×10^{19} ions/m^2, respectively, have been obtained from the plasma focus that is modified with a 19 cm taper anode and operating with 0.8 mbar Ar gas with the stored energy of 2.53 kJ.

Department Physics   Student's signature........ _____

Field of study Physics   Advisor's signature....... _____

Academic year 2550   Co-advisor's signature.. _____

ACKNOWLEDGEMENTS

CONTENTS

List of Tables

List of Figures

CHAPTER I

INTRODUCTION

1.1 Background

For many decades, plasma focus device has been an interesting device because of its special characteristics as a powerful source of neutron [1,2] as well as ion [3,4] for material processing, EUV [5,6] and X-ray source for lithography[7,8,9,10] and other applications[11].

The plasma focus device, shown in Figure 1.1 is a cylindrical coaxial tube, which has six outer electrodes surrounding an inner electrode pointing in Z-axis direction. A glass insulator is used to insulate between the inner and the outer electrode.

Centre electrode
or anode

Cathode

Pyrex Glass
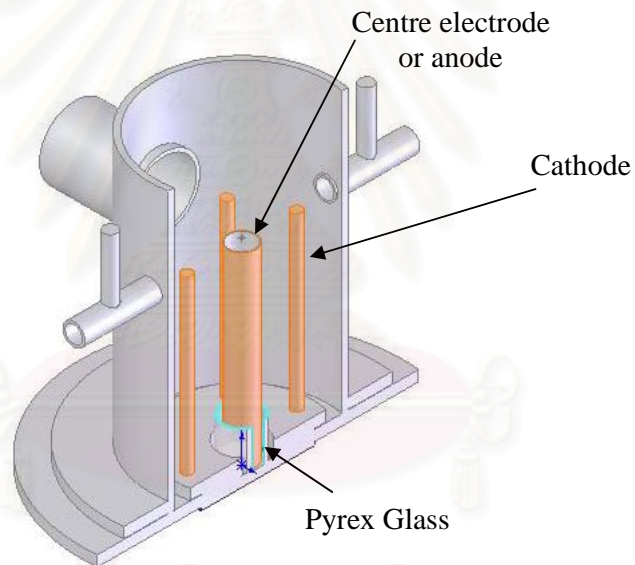
Figure 1.1: Diagram showing typical plasma focus tube configuration.

The main aim of this research is to modify a Mather-type 3 kJ Plasma Focus (PF) [12] to have an enhanced ion beam generation capability. The investigation will be concentrated specifically on the ion beam generation aspect of UNU/ICTP PF configuration. Both experimental and numerical studies have been carried out to explain the ion beams production mechanism as well as to explore their characteristics.

There are reports of plasma focus that has been applied as ion source in many applications. For example Rico et al.[13] used argon and oxygen plasma generated

from a plasma focus device to promote crystallization on amorphous ZrO_2–2.5 mol% Y_2O_3 film deposited by chemical solution deposition onto silica glass substrate. Boonlear et al.[14] used plasma focus to clean oxides on Fe surface. Kelly et al.[15] and Hassan et al.[16] also worked on room temperature surface treatment of metallic samples irradiated by a nitrogen ion beam generated by a co-axial plasma gun and 2.3 kJ plasma focus device, respectively. This was done by using a titanium insert at the end of the inner electrode to produce TiN coating on the surface of samples. Kant et al.[17] have also deposited carbon film on glass, silicon and quartz substrate by using argon plasma. The plasma etched a graphite target to produce carbon ion that is deposited onto a substrate. Similarly, Nayak et al.[18] used nitrogen ion from nitrogen plasma produced by Mather type plasma focus device to bombard graphite surface for 20 and 30 times (shots) to produce carbon nitride. Rattachat et al.[19] has demonstrated the use of ion beam from plasma focus device to modified surface of textile (Polypropylene/Polyester/Cotton Composites).

As well as many applications of ions produced by plasma focus mentioned, measurement methods and characteristics of the ions produces are also interesting. Bhuyan et al.[20] have measured energy flux of methane ion beam generated from small plasma by time of fight technique (TOF). The energy of C^{+4} and C^{+5} ions were found to be about 200-400 keV and 400-600 keV respectively. Kelly et al. [21] also studied nitrogen ion spectrum generated from a low energy Mather-type plasma focus device. They used Thomson parabolas spectrometer to measure the type of species of nitrogen ions such as N^{+1}, N^{+2}, and N^{+3}. The densities of the nitrogen ions are also found to be more than 10^{16} cm^{-2} by observing tracks on CR-39 plate. The use of CR-39 plate will be described in Chapter 3. The energy of these ions was reported to be more than 170 keV. Similarly, Takao et al.[22], used Mather type plasma focus device filled with H_2 at 2.3 torr to produce proton with distributed energy between 0.15 MeV to 2 MeV measured by Thomson parabola spectrometer. The ion current density is reported to be 2,400 A/cm^2. Wong et al.[23] have modified a small plasma focus device to operate at low pressure (in the range of 0.01 mbar to 0.03 mbar) for enhancing nitrogen ion beam production. They used ion collectors and time of fight technique to measure ion beam energy. It was found to have energy about 225 ± 66 keV and ion density about 2.7×10^9 cm^{-2}. Another type of ion diagnostics was demonstrated by Gerdin et al.[24]. They used a Faraday cup as well as the time of fight technique to measure

energy of ion beam. The faraday cup was located in differentially pumped ($<20\mu Pa$) chamber which is separated from the main plasma focus chamber by a pin hole with 0.0457 cm in diameter at 16 cm above the anode. This arrangement used the bias voltage of –400 V for stop moving electrons and allowed the observation of deuteron energy down to ~25 keV.

Jakubowski et al.[25] have also studied the energetic ion beams and their correlation with pulsed relativistic electron beams. Time integrated and time resolved measurements were performed with an ion pinhole camera equipped with solid state nuclear track and scintillation detector. These allow a determination of ion energy spectrum on the basis of the time of flight technique. Further more, Hoon Heo and Park [26] investigated the characteristics of X-rays and ions generated in argon plasma focus discharge, and analyzed correlation between X-ray and ion emissions, again, using the time of flight method with a Faraday cup, a capacitive current monitor, and PIN diodes covered with Ross filters. These measurement techniques will be discussed in Chapter 3. He obtained energy spectra of argon ion beams, and observed X-rays of Ar Kα line and Cu Kα line. It was found that the optimum pressure range for ion emissions agreed with that for X-ray emissions, and ion energy distributions were shifted toward higher energies when X-ray emissions were good. He went on to suggest that the enhancement of the ion acceleration is due to some mechanism of X-ray emission. Although the observed time correlation cannot be explained by conventional ion acceleration models, but it can be explained by a hybrid model describing the electric field induced by the moving current distribution, an anomalous resistivity, and the Hall effect.

Other interesting works that have been done and reported are from Zakaullah et al. [27] where they carried out an experiment to measure X-ray and ion beam from a 2.3 kJ Mather type plasma focus that was operated with argon gas and three different shapes of anode. It was found that the radiation yield strongly depends on the anode shape. An appropriate tapering of the anode end can enhance the emission by threefold for both X-rays and ions. The intensities of the signal were also found to be in correlation with the high-voltage probe signal intensity. Furthermore, time-integrated pinhole images revealed that the X-rays originate predominantly from the anode end surface. In other words, an appropriate shaping of the anode end switches the device to a high-emission mode for both X-rays and a charged particle beam.

Another factor that may influence the energy of the ion beam is the speed of the plasma sheath during the axial acceleration. Al-Hawat [28] used a magnetic probe to study the current sheath in 2.8 kJ plasma focus device. He measured the speed of argon plasma under an operating pressure of about 1 mbar and obtained, both experimentally and theoretically, the axial distribution of trajectory, average axial velocity, and magnetic field of the current sheath at a certain radial distance along the axis of the plasma focus tube.

Example of application that uses ion generated by a plasma focus was first presented by Zeb [29], where they deposited amorphous diamond-like carbon (DLC) films on Si (1 0 0), using a low energy (1.45 kJ) dense plasma focus. They inserted a high purity graphite at the tip of the tapered anode, which serves as a carbon source, then a silicon substrate was placed in front of the anode at different axial and angular positions. The films were deposited using multiple focus shots. The results from Raman spectroscopy show formation of good quality amorphous carbon (DLC) films with higher sp^3 content as compared to sp^2 content. Table 1 summarizes research works done with different types of plasma focus for producing ion beam and ion beam application.

.

Table 1.1: Summary of research works done on different types of plasma focus for producing ion beam and ion beam application.

	Plasma Focus Type	Operating Gas	Operating Pressure	Ion energy	Ion density	Measurement Method
G. Gerdin et al.[24]	17 kJ	^2_1H	0.667-13.33 mbar	~200 keV	10^{12} cm^{-3}	FC, TOF
Heo and Park et al.[26]	1.2-2.7 kJ	Ar	0.133-0.933 mbar	200 keV – 1 Mev	-	TPA,CCM and FC, TOF
C.S. Wong et al. [23]	UNU/ICTP,3.3 kJ	N_2	0.01 -0.03 mbar	225 ± 66 keV	2.7 x 10^9 cm^{-2}	IC ,TOF
		Ar	0.01 -0.03 mbar	285 ± 23 keV	0.34 x 10^9 cm^{-2}	
		H_2	0.01 -0.03 mbar	296 ± 12 keV	3.7 x 10^9 cm^{-2}	
Takao et al.[22]	Mather-type,19.44 kJ	H_2	3.06 mbar	0.15 -2 MeV	2400 A/cm^2	IC CR39, TOF
Bhuyan et al.[20]	Mather-type, 1.8 kJ	CH_4	0.413 -0.533 mbar	H^+ 200-400 keV C^{+4} 400-600 keV C^{+5} 900-1100 keV	-	TPA and IC,TOF
Nayak et al.[18]	Mather-type, 2.2 kJ	N_2	0.4 mbar	1-2 MeV	-	Ref
Kant et al.[17]	Mather-type, 3.3 kJ	Ar and Carbon target	0.8 mbar	25 keV – 8 MeV	-	Ref
Kelly[21,30]	Mather-type,4.75 kJ	N_2	0.4 mbar	N^+, N^{+2}, N^{+3} 0.17-4.0 MeV	8x10^{12} ion/stereorad	TPA CR39

TPA = Thomson parabola analyzer   TOF = Time of fight   FC = Faraday cup   CCM = Capacitive current monitor   IC = Ion collector

1.2 Objective

The objective for this research is to study further the aspect of ion production process of a UNU/ICTP Plasma Focus and to optimize the plasma focus device for better ion beam production. This includes the measurement of the ion beams characteristics by various diagnostic techniques Furthermore, it is also important to investigate experimentally and numerically the effect of the dynamics and the energy of the characteristic plasma current sheath on the ion beam generation. The measurements of ion beam such as speed, kinetic energy and density are carried out by using ion collector, PIN diode, Rogowski coil and magnetic probe operating at various pressures and charging voltages, as well as variable physical configuration such as length and shape of the anode.

We are expecting to obtain more than 10 % increase in ion density and energy from the original UNU/ICTP Plasma Focus configuration.

1.3 Thesis Structure

In this chapter, a survey of works related to plasma focus ion beam generation is presented as well as the objective of the research. In Chapter 2, a detailed theory of plasma focus and the operational aspect are described, including the device component, the dynamics of plasma and the numerical simulation based on shock theory. Chapter 3 presents different diagnostics used to measure the ion density, ion energy and X-ray radiation for the plasma focus. Chapter 4 is divided into subsections which describe different experiments carried out in this research and report on the results found for each experiment. In Chapter 5, the discussion of the results is presented as well as an attempt is made to explain the phenomena with support from the result obtained by the simulation model. Chapter 6 presents the conclusion of the research as well as a recommendation for further work.

CHAPTER II

PLASMA FOCUS DYNAMICS
AND SIMULATION MODEL

In this chapter, the process for generating plasma and ion beam is described by closely looking at the movement of the plasma sheath or the plasma dynamics. The dynamics can also be simplified and described by an equation of motion [31]. Using numerical methods, a simulation of the plasma dynamics is carried out giving results that correspond to experimental data obtained. A details set up of the plasma focus device will be presented first in this section, to ensure a general understanding of the operation of the device.

2.1 Plasma Focus System
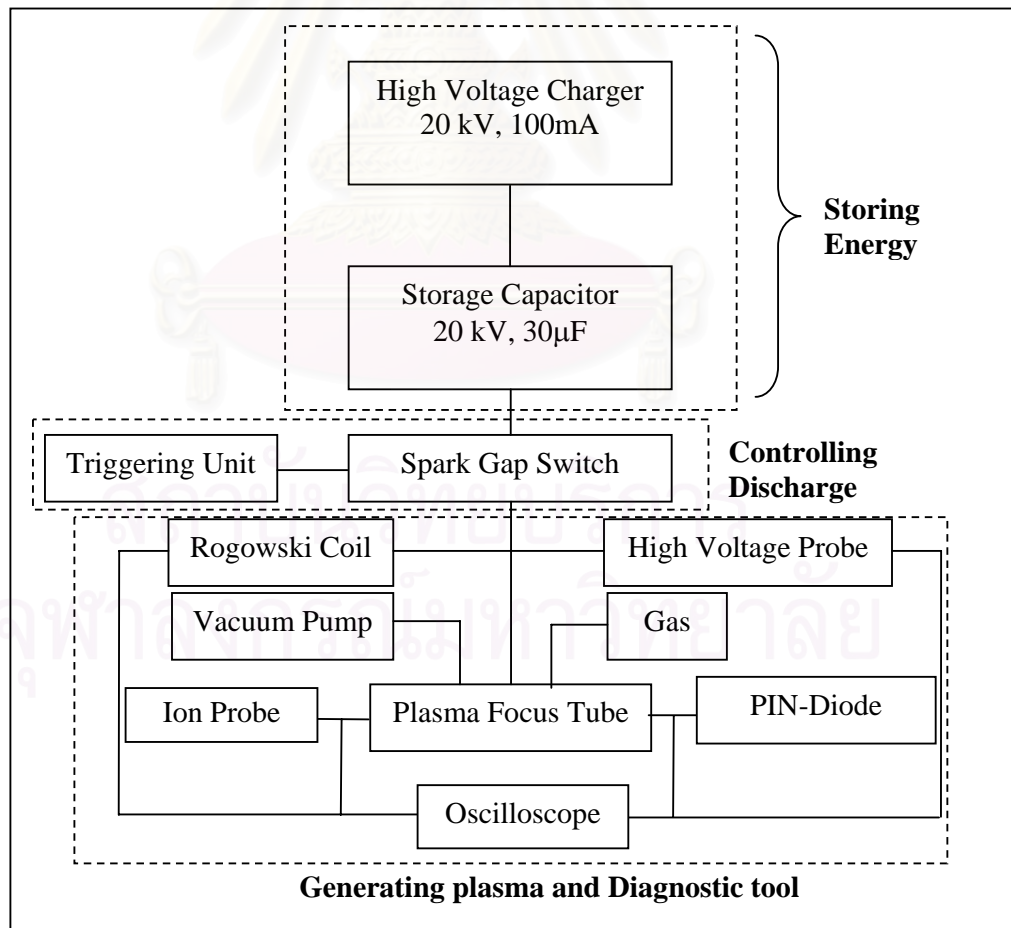
Figure 2.1: Schematic showing overall components of a plasma focus device.

Plasma focus device works on a principle of releasing stored electrical energy within a short period of time to produce a fast moving plasma sheath as described previously by its dynamics. The system is made up of three main functional parts which are; the electrical energy storage, the discharge control circuit and the plasma chamber, where plasma and radiation are generated, as well as essential diagnostics tools. A schematic of overall components of a plasma focus is shown in Figure 2.1.

2.1.1 Electrical Energy Storage

The electrical energy storage part comprises of a high voltage charger and storage capacitor or commonly known as a capacitor bank. The high voltage charger shown in Figure 2.2(a) was built in the laboratory. It converts 220 V AC from the main to a maximum of 20 kV DC with full-wave rectification. The operating current is about 100 mA. The circuit diagram is shown in Figure 2.2(b). The charger unit was connected to a Maxwell Inc. capacitor bank. The capacitor bank has a capacitance of 30 μF and a full charging voltage of 20 kV. With this combination, electrical energy of 3.3 kJ can be stored when the capacitor bank is charged to 15 kV. The range of operation in this research is based on energies between 2 kJ and 3.3 kJ and charging voltages of 12 kV and 15 kV respectively.

(a)   (b)
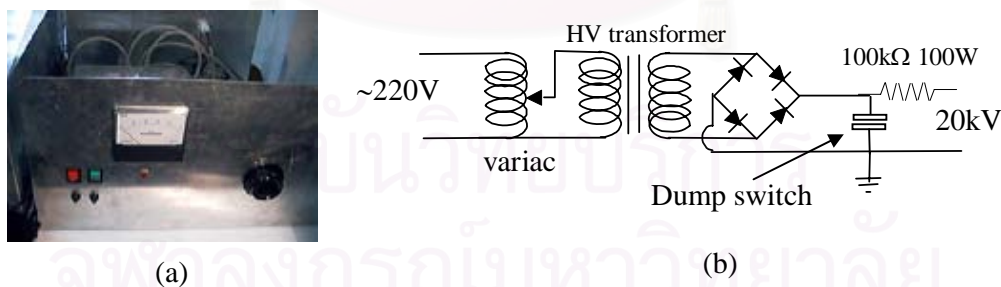
Figure 2.2: (a) Picture of a high voltage charger and (b) circuit diagram of the high voltage charger**.**

2.1.2 Discharge Control Circuit

The discharge control circuit is separated into two parts which are a triggering unit and a spark gap switch. The spark gap switch used in the experiments is a cascade type made up of three conducting plates. The first plate is connected to the capacitor bank. The center plate is connected to a trigger unit and the other plate is connected to the anode located at the center of the plasma focus tube. Diagram of triggering unit and spark gap switch is shown in Figure 2.3 below.
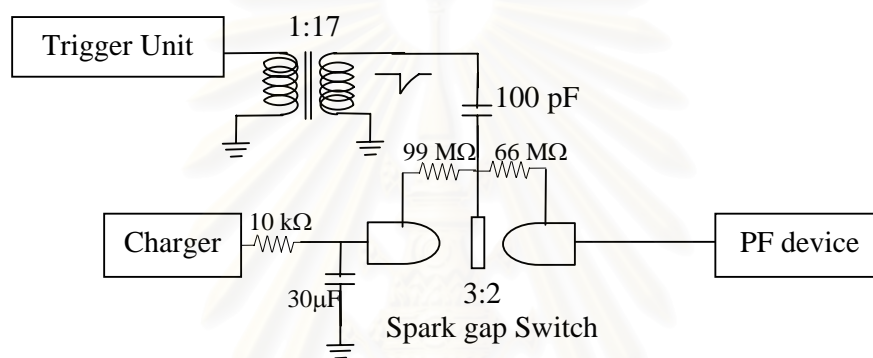
Figure 2.3: Diagram showing components of the electrical discharge control system.

The triggering unit consists of a low voltage pulse circuit for generating a low negative voltage pulse through a transformer. The transformer steps up the low negative voltage pulse to a higher voltage of -40 kV. The distance of the conducting plates is set so that this voltage is sufficient to allow the breakdown between the conducting plates which it then allows the charge in the capacitor bank to transfer to the anode resulting in a large current flow.

2.1.3 Plasma Chamber

In this part, a cylindrical stainless steel is constructed in such a way that high vacuum can be maintained as well as accommodating for various diagnostics through different port outlets. This is generally known as a plasma focus tube. Coaxial electrodes made up of six cathodes surrounding a central anode sit inside the tube. A diagram of the plasma focus tube is shown in Figure 1.1. Between the anode and

cathodes, a cylindrical Pyrex glass is placed for insulating and separating both electrodes. Pyrex glass has a diameter of 2.5 cm and 5 cm in length. The centre electrode or anode has a diameter of 1.95 cm and the length varies according to the various experiments carried out in this research. The diagnostic tools will be presented in Chapter 3.

2.2 Plasma Focus Dynamics

In order to simplify the explanation, the dynamics process of the plasma focus can be separated into 4 phases [25], namely, breakdown phase, axial phase, radial phase and focusing phase. Figure 2.4 shows diagrams of all four phases of a plasma focus.
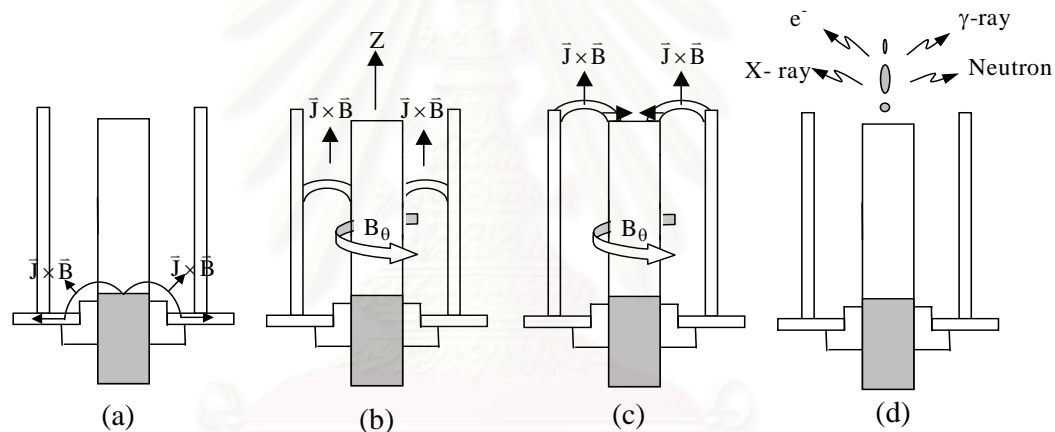
Figure 2.4: Phases of plasma formation: (a) Break down Phase ,(b) Axial phase, (c) Radial Phase and (d) Focusing Phase.

2.2.1 Breakdown Phase

Plasma focus process begins when a charged capacitor bank at a voltage V_o discharges to the plasma focus tube. The high voltage causes a gas to breakdown initially on the surface of the glass insulator at the base of the anode. The gas between electrodes are broken down into electrons and ions [32,33]. At a low pressure between 0.1 mbar to1 mbar shown in Figure 2.5, a diffuse volume discharge fills space between the electrodes above the insulator, and extending along the electrode when the filling pressure is reduced. Conversely, when the pressure is high (about 5 mbar < pressure <20 mbar), a current sheath or a plasma sheath is formed symmetrically

along the electrode axis as shown in Figure 2.6. At operating pressures between 1 mbar to 3 mbar where the atomic density is 5.4×10^{16} cm^{-3} [32], the current sheath is believed to lift off from the glass insulator and then propelled by the Lorentz force ($\vec{J} \times \vec{B}$). Here, $\vec{J}$ is the current density and $\vec{B}$ is the self-induced magnetic field.

In this phase, the speed of the current sheath in radial direction is about 200 cm/μs [32,33] for operating pressure of 1 mbar. The duration is shown in Figure 2.7 to be around 20 ns to 300 ns. According to Bruzzone et al.[32], the electron temperature during this phase is deduced to be about 2 eV to 3 eV. Generally, this phase is defined as "breakdown phase" or "surface discharge phase"[31].
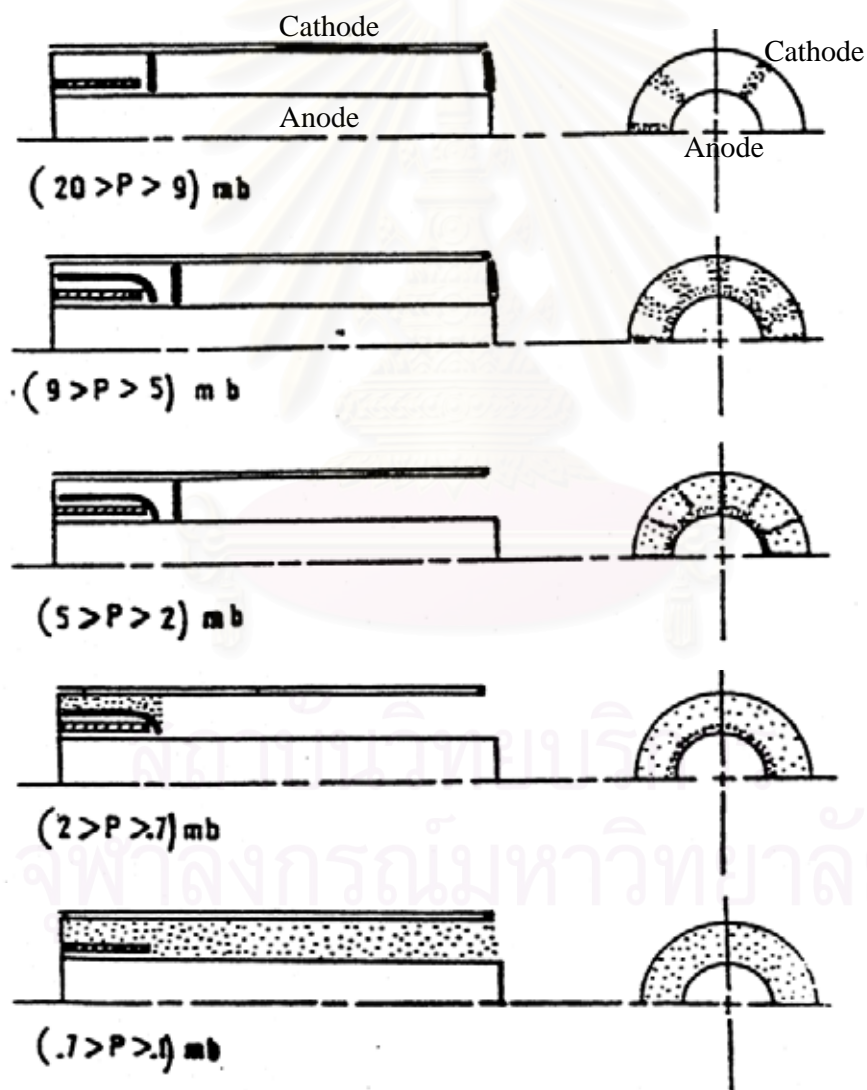
Figure 2.5: Diagrams showing modes of breakdown that depend on operating gas pressure [33].
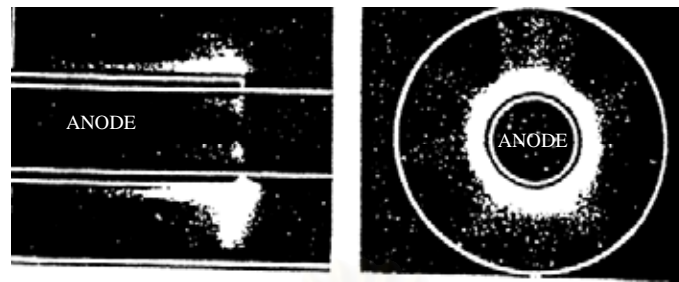
Figure 2.6: Pictures showing (a) plasma sheath discharge sliding along insulator surface and (b) current sheet lift-off from the insulator surface by the $\vec{J} \times \vec{B}$ force [33].
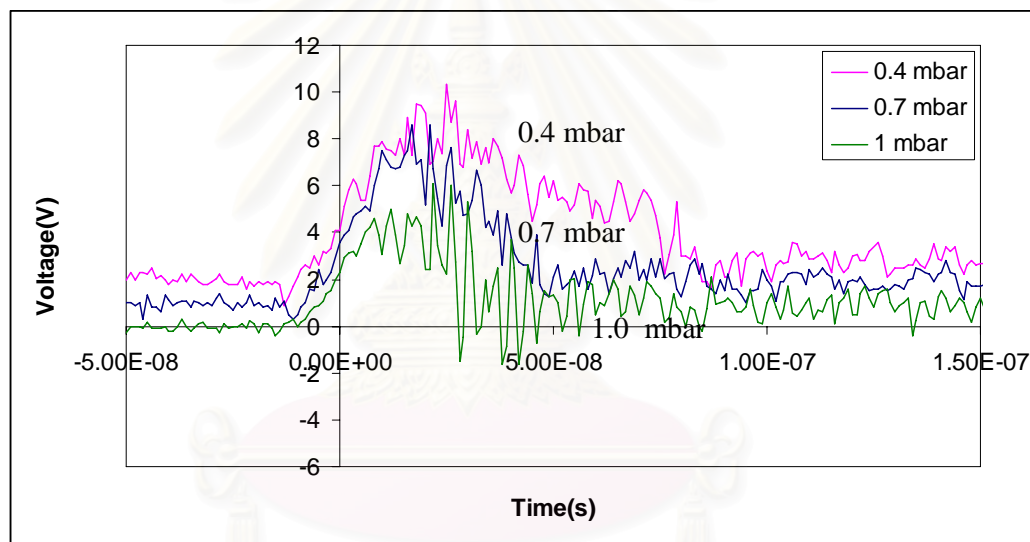
Figure 2.7: A plot showing voltage signal, $V(t)$, in breakdown phase for argon gas for operating pressure of 0.4 ,0.7 and 1 mbar. Voltage scale is in kV.

2.2.2 Axial Phase

The axial phase starts when current sheath lift off is completed and the current is flowing radially outward from the inner anode to the outer cathode. The $\vec{J} \times \vec{B}$ force then continually pushes the current sheath along the Z-direction towards the end of the electrodes. The current sheath sweeps up all the charged particles it encountered

leaving behind a vacuum immersed in the magnetic field of the current sheath. As this happens, a thicker current sheath is being built up. A shock front is formed in front of the current sheath when it is moving out with supersonic speed [31,33,34]. During this movement the gas is shock heated to a highly ionized state and a plasma slug is formed between the shock front and the current sheath while the ambient gas is assumed to be undisturbed ahead of the shock front. This second phase is called the axial acceleration phase[35]. Figure 2.8 shows a diagram representing the movement in the axial acceleration phase, where ρ_1 is the density of ambient gas, ρ_2 is the density of plasma slug, a is the radius of anode, b is the distance between anode and cathode, z is shock front position, B is the induced magnetic field and μ_o is the permeability of free space.

The duration of this phase increases with pressure as shown in Figure 2.9. The axial velocity measured by a magnetic probe is found to be between 3 to 8 cm/μs according to my previous work [34]. From the figure, the peak magnetic fields can be estimated to be about 8 to 28 kGauss when the plasma focus is operating with charging voltage between 10 to 22 kV for a plasma focus with UNU/ICTP specification. The detail of the components of the plasma focus will be presented later in this chapter [34].
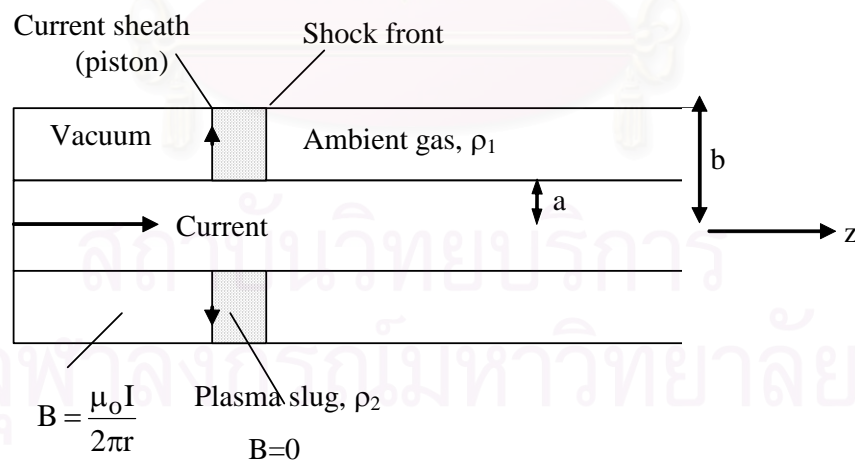
Figure 2.8: A diagram showing "slug model" representing the piston action of a current sheath during the axial phase [31].
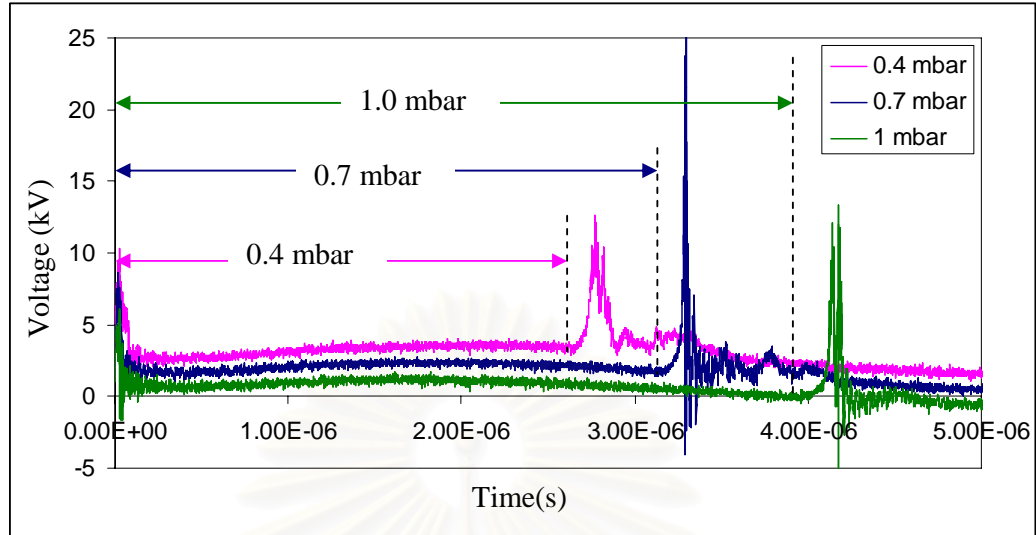
Figure 2.9: Graph showing voltage signal measured from a UNU/ICTP plasma focus operating with argon gas at pressure of 0.4, 0.7 and 1 mbar highlighting the axial acceleration phase in each case. Voltage scale is in kV.

For a theoretical calculation purpose, the plasma movement during the axial acceleration phase can be represented by "1-dimensional slug model" [31]. The model assumes that wall friction can be neglected and the net force that accelerates the total mass of gas swept up by the current sheath is equal to the electromagnetic driving force of the current sheath. The configuration of the plasma tube and plasma "slug" can be simplified and shows in Figure 2.8 [31,33,34]. The equation of motion for the model can be written in term of the rates of change of momentum of the plasma slug as follow;

$$\frac{d}{dt}[\rho_1\pi(b^2 - a^2)z(\frac{\Gamma - 1}{\Gamma}\frac{dz}{dt})] = \int_a^b \frac{B^2}{2\mu_0}2\pi r dr. \tag{2.1}$$

Where

$\Gamma = \dfrac{\rho_2}{\rho_1} = \dfrac{\gamma + 1}{\gamma - 1}$: mass ratio (γ is specific heat),

$\rho_1\pi(b^2 - a^2)$: mass in the slug,

$(\dfrac{\Gamma - 1}{\Gamma}\dfrac{dz}{dt})$: speed of the piston,

$$\frac{dz}{dt}$$: shock speed,

$$\frac{B^2}{2\mu_o}$$: magnetic pressure,

$$\int_a^b \frac{B^2}{2\mu_0} 2\pi r dr$$: $\vec{J} \times \vec{B}$ Lorentz's Force.

From equation 2.1, the acceleration of the current sheath which represents by a piston is,

$$\frac{d^2z}{dt^2} = \frac{\frac{\mu_o}{4\pi^2\rho_1}[\frac{ln(b/a)}{b^2-a^2}](\frac{\Gamma}{\Gamma-1})I^2 - (\frac{dz}{dt})^2}{z}. \tag{2.2}$$

2.2.3 Radial Phase

The radial phase starts when the current sheath reaches the end of the anode. During this phase, the current sheath slides along the surface of the anode in the radial direction due to the $\vec{J} \times \vec{B}$ force. This causes the current sheath to collapse radially as shown in Figure 2.10.
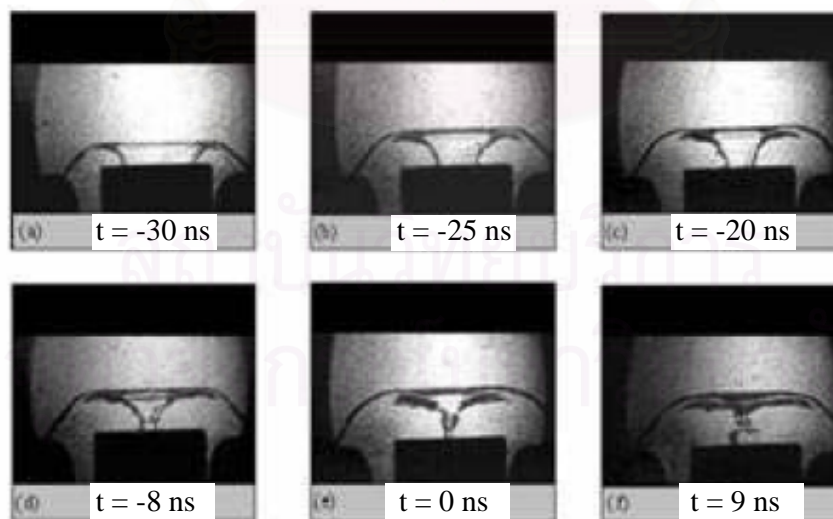
Figure 2.10: Series of picture showing a compression of a plasma sheath in during the radial phase from a UNU/ICTP plasma focus operating with 4.0 mbar deuterium gas [36].

The radial compression can be based on a finite-thickness slug model, shown in Figure 2.11, which may be used to describe the dynamics of this phase. The front position of the slug which is a shock front is designated as r_s and the position of the rear of slug which is the current sheath (or magnetic piston) is designated r_p. The position r_s is obtained through shock-jump equations and by linking the shock pressure to the magnetic pressure[31]. Therefore the radial shock motion is given by;

$$\frac{dr_s}{dt} = -\left\{\frac{\mu_0}{\rho_0}(\gamma+1)\right\}^{\frac{1}{2}} \frac{I}{4\pi r_P}, \tag{2.3}$$

where γ is the specific heat ratio.
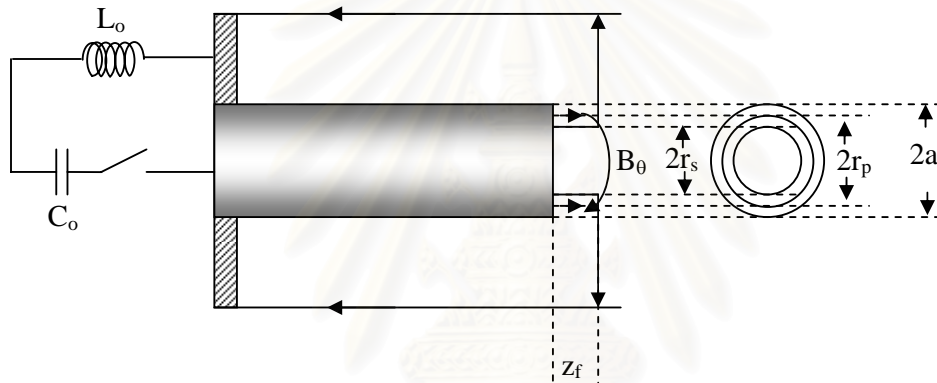
Figure 2.11: Diagram showing parameters in the finite-thickness slug model.

2.2.4 Focusing Phase

At the end of the radial phase, a dense plasma column is formed on the axis of the focus tube just off the face of the anode. During this dense plasma phase, soft X-ray and other types of radiation can be emitted from the plasma. This final phase is called the focusing phase which the photograph can be seen in Figure 3.20.

2.3 Ion Beam and Plasma Jet

Many researches in the past have presented results from experiments which are related to the ion beam and the plasma jet produced from the plasma focus after the final focusing phase. For example, the images shown in Figure 2.12, obtained by Krauz V.I. et al.[37] are rapid framing images showing sequence of event after the focusing phase. One can see that a plasma cloud is present after focusing has occurred

which is immediately after the breaking up of the focus column by its instabilities as shown in Figure 2.12(c).

|←10 cm →|

- 100 ns   220 ns   700 ns   1020 ns

(a)   (b)   (c)   (d)
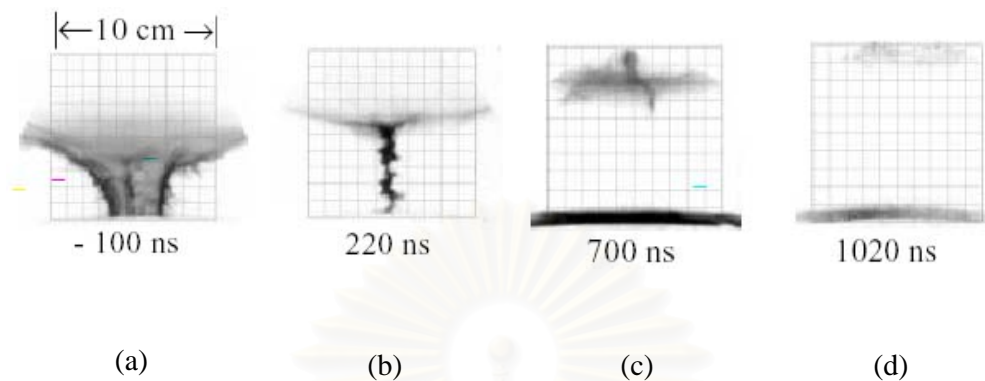
Figure 2.12: Picture taken by a repid framing camera of pure neon plasma during the radial phase (a, b) and after the pinch destruction (c, d) [37].

It is believed that the ion beam produced by the focusing mechanism has higher energy than the moving plasma jet. There are two possible explanations for the process. One is a simple explanation which is based on the shock model where the ion beam is produced during the focusing phase where the plasma sheath undergoes radial compression causing increase in ion density. Later, the sudden change of the electric field due to the instability causes the ions to propel along axial direction at a high speed. Another explanation is introduced by Learner [38]. He described the mechanism from the beginning where the plasma sheath carrying the current moving down the anode due to the interaction of the current and its magnetic field, as shown in Figure 2.13(a-c), then the plasma sheath bends inwards to the center of the anode.

Figure 2.13(d) shows plasma filaments that are formed in counter rotating pairs. At the beginning of the radial phase, the plasma sheath and the filaments contract towards the center forming a focus column. The filaments merge in pairs like a zipper and the energy is transferred from the outside to the central region. During this radial

phase, the plasma sheath and the filaments continue contracting into the center to form a rotating plasma vortex which carries all the current as shown in Figure 2.13(e).
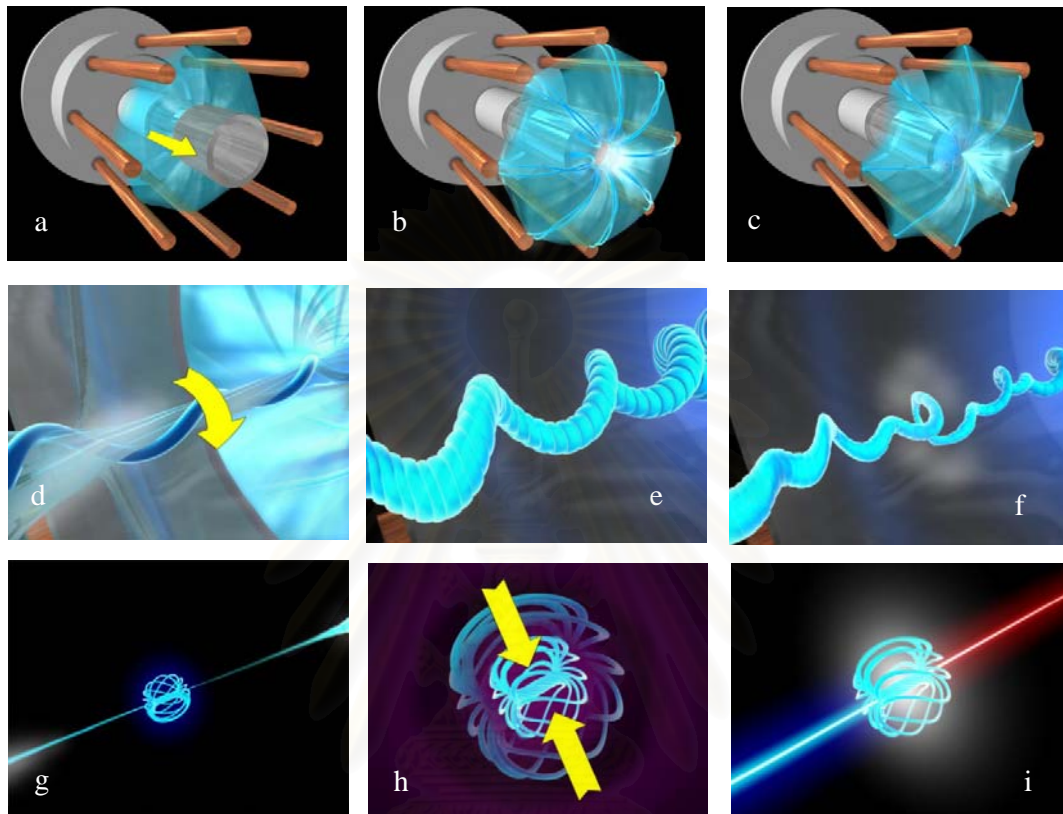
Figure 2.13:Animation pictures showing possible process of ion beam production[38].

At the center of the anode the filaments form one single rotating filament which rapidly tightens forming a plasma helix. This helix in Figure 2.13(f) starts to kink and becomes unstable. These filaments further knot themselves in to a rotating plasmoid, as shown in Figure 2.13(g), whose diameter is only in order of microns. For an ideal case, the plasmoid is assumed to contain the full energy that was fed into the device. Immediately the plasmoid is formed, the magnetic field of the plasmoid causes it to shrink and rotate releasing an electron beam while an electric field creates a beam of fast ions (nuclei) in opposite direction that carry most of the energy (shown in blue), as shown in Figure 2.13(h and i).

At a later time after the ion beam is produced many literatures have shown evidence that there are clouds of charge particles or plasma traveling at a lower speed in the same direction as the ion beam [23,34] as shown in Figure 2.14. This charge particles cloud is normally being called a "plasma jet". Fast framing image in Figure 2.12(c) shows beginning of separation between the ion beam and the plasma jet.
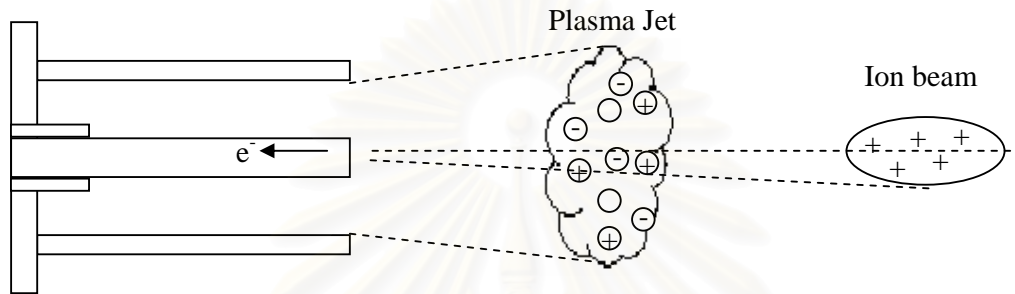
Figure 2.14: Diagram showing ion beam and plasma jet propelled in an axial direction from a plasma focus device.
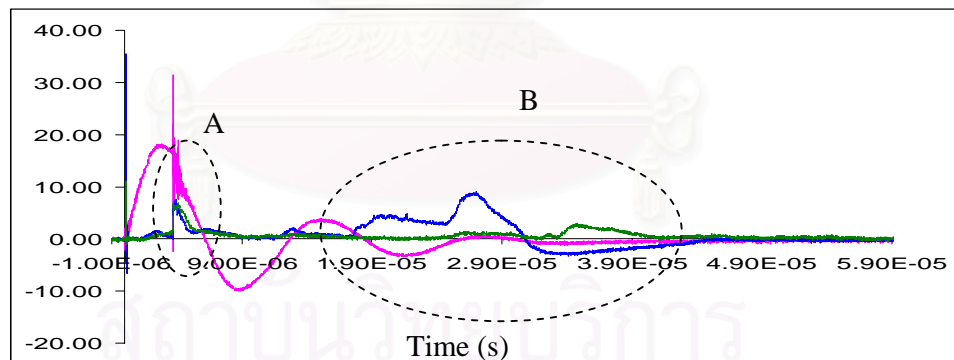
Figure 2.15: Graph showing a current signal (pink) and electric probe signals (blue and green) where area A is the ion beam and B is the plasma jet.

Signals shown in Figure 2.15 are taken from a standard UNU/ICTP plasma focus operating with argon gas using an electric probe (described in Chaprter 3). It can be clearly seen there are two groups of charged particles; group A and B, where signal in

group A happens immediately after the focus and group B occurs around 10 µs later. These results demonstrate the existence of both ion beam and the plasma jet in a single discharge event from a plasma focus device. Although signal of group A can be a combination of the ion beam and the electromagnetic wave produced during the focusing process.
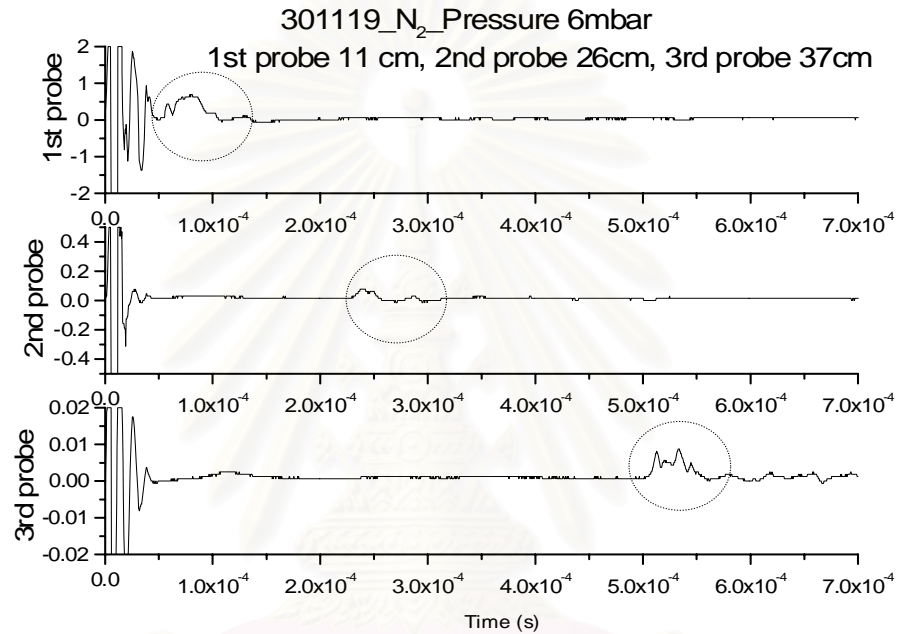
Figure 2.16: Graph showing electric probe signals of a plasma jet produced by a plasma focus device operating at high pressure (6 mbar) [34].

For the ion beam, it is believed that the electrons in the plasma sheath during the radial phase are attracted to the anode and the ions are gaining the energy from the voltage different as $q\Delta V$ during the focusing phase. On the other hand, the plasma jet in group B does not pinch so it moves relatively slower than the ion beam. Further evidence is shown in previous M.Sc work [34] where the plasma jet was recorded during a long period of time after focusing phase of a nitrogen gas which is shown in

Figure 2.16. The movement of a plasma jet passing through three electric probes at different positions can be observed.

2.4 Simulation Model

Simple plasma focus simulation models have been investigated by many people [31,34,39,40] in order to calculate the plasma dynamics for various operating conditions. The more popular models are described by S. Lee [31] and C.S. Wong [31,33]. As described earlier, the dynamics of a plasma focus device generally can be divided into four phases, breakdown phase, axial phase, radial phase and focusing phase or dense plasma focusing phase. Similarly for the simulation, the calculation is separated into four phases. Other people have extensively studied the breakdown phase [41] and the radiation process during the final focusing phase but the emphasis for this research will be on the axial phase and the radial phase. It is believed that these two phases are the most important phases for the ion beam production.

2.4.1 Equivalent Circuit

In the axial phase, snowplow model or slug model is assumed. The equation of motion for this phase is described in Section 2.2.2. An equivalent electronic circuit that represents the flow of current within the plasma focus device is shown in Figure 2.17.
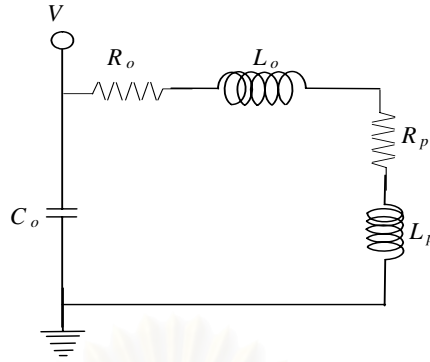
Figure 2.17: Diagram showing an equivalent circuit of a small plasma focus.

From this equivalent circuit, the circuit equation of the axial phase can be written by using Kirchoff's Law. This is the sum of voltages around a close loop circuit;

$$\frac{d}{dt}[(L_o + L_p)I] + I(r_o + r_p) = V_o - \frac{\int_0^t Idt}{C_o}. \tag{2.4}$$

Where L_P is plasma inductance which can be express as:

$$L_P = \frac{\mu_o}{2\pi}\frac{\Gamma - 1}{\Gamma}\ln(\frac{b}{a})z. \tag{2.5}$$

The variables shown in equation 2.4 and 2.5 are;

I : plasma current,

$\Gamma = \dfrac{\rho_2}{\rho_1} = \dfrac{\gamma + 1}{\gamma - 1}$: mass ratio (γ is specific heat),

L_o : circuit inductance,

L_p : plasma inductance,

V_o : changing voltage (voltage across capacitor),

r_o, r_p : circuit resistance and plasma resistance,

a : anode radius,

b : distance from centre of anode to cathode,

Assuming $\dfrac{d}{dt}[(L_o + L_P)I] \gg I(r_o + r_P)$. By re-arranging the equation 2.4, we get:

$$\frac{dI}{dt} = \frac{V_o - \dfrac{\int Idt}{C_o} - \dfrac{\mu_o}{2\pi}\left(\dfrac{\Gamma - 1}{\Gamma}\right)\ln\left(\dfrac{b}{a}\right)I\dfrac{dz}{dt}}{L_o + \dfrac{\mu_o}{2\pi}\left(\dfrac{\Gamma - 1}{\Gamma}\right)\ln\left(\dfrac{b}{a}\right)z} \quad . \tag{2.6}$$

By coupling the circuit equation (Equation 2.2) and the equation of motion (Equation 2.6) together and normalized the variables, the normalized equations can be written as,

$$\frac{d^2\zeta}{d\tau^2} = \frac{\alpha^2 \iota^2 - \left(\dfrac{d\zeta}{d\tau}\right)^2}{\zeta}, \tag{2.7}$$

where the normalizing factors are; $\zeta = \dfrac{z}{z_0}, \tau = \dfrac{t}{t_0}$ and $\iota = \dfrac{I}{I_0}$. The normalizing factors are used as follow;

Z_0 : length of the anode,

$t_0 = \sqrt{(L_0 C_0)}$: discharge characteristic time,

$I_0 = V_0 \sqrt{\dfrac{C_0}{L_0}}$: "short circuit" current.

The scaling parameter for time is represented by α where $\alpha = \dfrac{t_0}{t_a}$ and

$$t_a = \sqrt{\frac{4\pi^2(b^2 - a^2)}{\mu_0 \ln(\frac{b}{a})}(\frac{\Gamma - 1}{\Gamma})\frac{\rho_1 z_0^2}{I_0^2}} \,, \tag{2.8}$$

which is the dynamic characteristic time and $\frac{z_0}{t_a}$ is the characteristic speed, where ρ_l

is the density of ambient gas. ρ_l can be calculated from the operating gas pressure

using an ideal gas equation.

The inductance ratio can be represented by β where $\beta = \frac{L_a}{L_0}$ and

$$L_a = \frac{\mu_0}{2\pi}\frac{\Gamma - 1}{\Gamma}\ln(\frac{b}{a})z_0 \,. \tag{2.9}$$

For a simulation model, value of β and α are set to suitable values. The time

interval dt must also be set to a suitable time in order to resolve the change in the

plasma dynamics. From experiment, a current measurement of the plasma focus gives

the time period of oscillation. For a typical 3.3 kJ UNU/ICTP plasma focus device,

the time period of the current signal is about 12.28 µs.

By knowing the time period from experiment one can calculate other parameters

for the simulation. Initially from $t_o = \frac{T}{2\pi}$ and $t_o = \sqrt{(L_o C_o)}$, we can calculate the

inductance of the device to be 127.33 nH. Also by assuming $\frac{\Gamma - 1}{\Gamma} \approx 1$ and $a = 0.95$

cm, $b=3.2$ cm and $Z_o=16$ cm, the equation 2.9 gives $L_a = 38.72$ nH. Therefore initial

value of the inductance ratio β for the simulation of this device is 0.30409. The

scaling parameter for time α can also be determined based on the assumption that the

current goes to zero when the plasma reaches the ends of the anode, which is estimated to be equal to 0.45. Figure 2.18 shows results from the initial simulation.
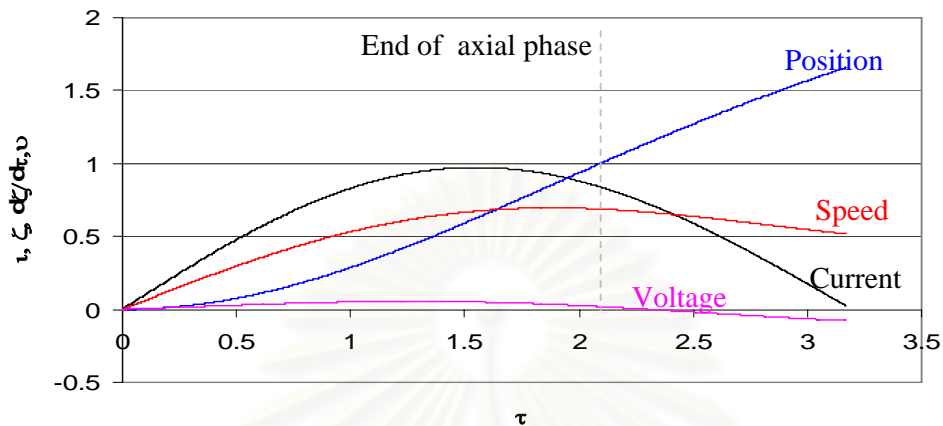
Figure 2.18: Graphs showing initial result of the plasma focus simulation having $\beta = 0.30409$ and $\alpha = 0.45$.

In order to obtain realistic simulation results, an experimental current measurement is made (described in Chapter 3). The current calculation from the simulation is then fitted graphically to the experimental result by varying α, β and Γ. Once suitable values are found, the simulation is then re-executed to give possible values of the plasma sheath speed, current, position and the voltage change, as well as the focusing peak which happens when the condition is suitable. The results obtained from the calculation can be used to further investigate the energy transfer process which is believed to affect the characteristic of the ion beam or the plasma jet. Figure 2.19 shows the fitting of the current obtained by the simulation and the actual experimental result.
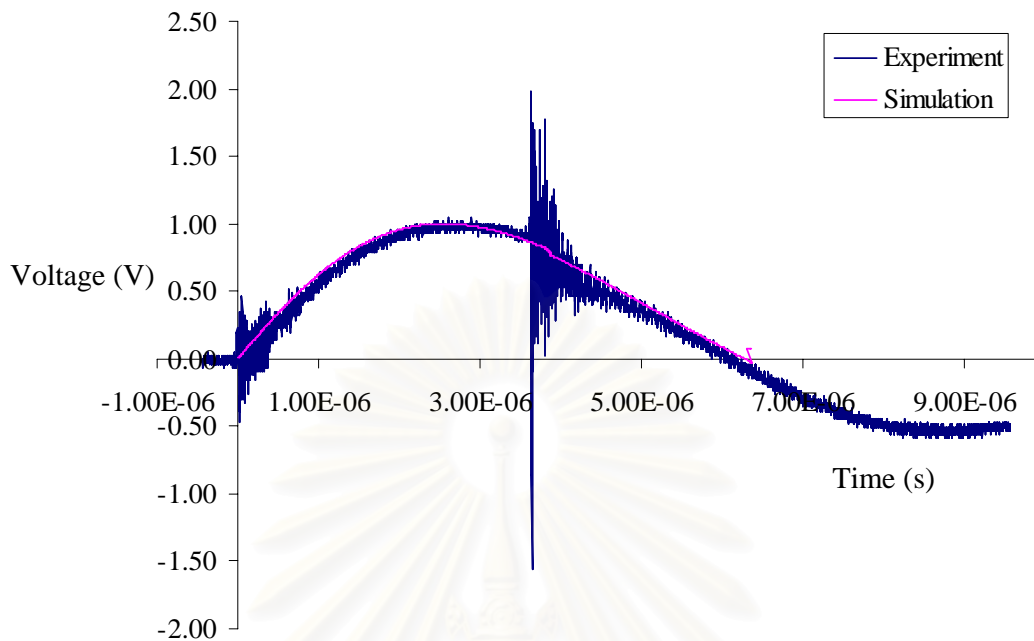
Figure 2.19: Graphs shows the fitting of simulated current signal to an experimental current signal.

2.4.2 Energy Transfer Process

This section describes an investigation on the efficiency of the energy transfer process in a UNU/ICTP plasma focus device. The initial electrical energy of the plasma focus can be calculated from the capacitance and the charging voltage. During the plasma focus discharge, the energy is converted into various forms of energy including the internal energy of the plasma, the kinetic energy of the plasma slug and radiation. In order to have plasma focus device operating efficiently, it is important to optimize the efficiency of energy transfer into the plasma. The energy input to the plasma is calculated based on the plasma current and plasma inductance obtained from the model.
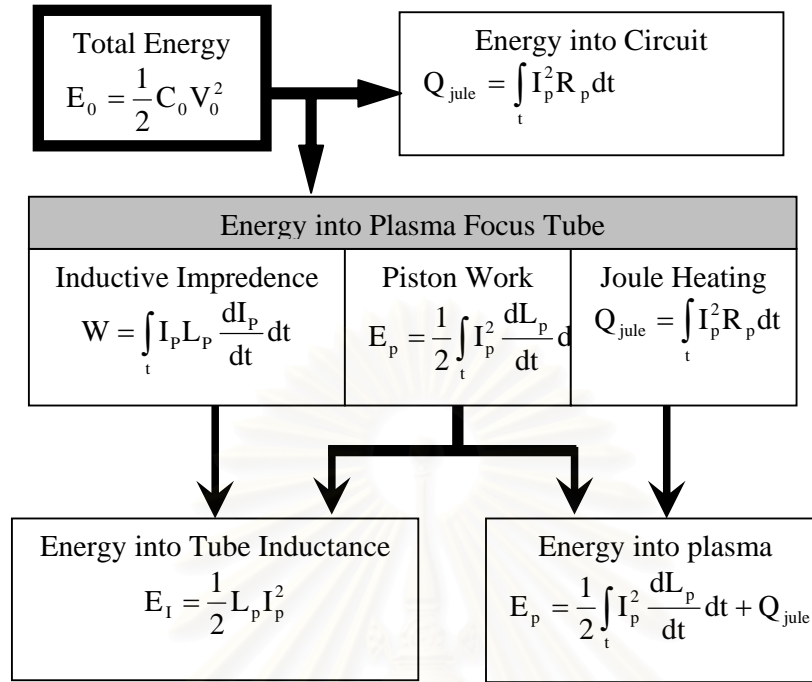
Figure 2.20: Schematic showing energy transfer process of a plasma focus device [42].

According to B. Shan et al [42], the input electrical energy will be divided between energy into the circuit, that is external to the plasma focus tube, and the energy input to the plasma focus tube itself which in turn divides into energy stored inductively, piston work and joule heating as shown in Figure 2.20.

Since the model used in this work assumes an inductive plasma load, the energy input into the plasma focus tube (W_{model})[43] is written as

$$W_{model} = \int I_p^2 \frac{dL_p}{dt} dt + \int I_p L_p \frac{dI_p}{dt} dt = W_m + W_p.$$ (2.10)

Part of this energy is stored as magnetic energy of the system which is given by

$$W_m = \frac{1}{2} L_p I_p^2 = \frac{1}{2} \int I_p^2 \frac{dL_p}{dt} dt + \int I_p L_p \frac{dI_p}{dt} dt , \tag{2.11}$$

and the part of the energy actually goes into the plasma as internal and kinetic energies (neglecting radiation loss) is

$$W_p = \frac{1}{2} \int I_p^2 \frac{dL_p}{dt} dt . \tag{2.12}$$

The experimental results of the energy input to the plasma system can be calculated from

$$W_{experiment} = \int I_p V_p dt . \tag{2.11}$$

The values of $W_{experiment}$ are compared with the energies obtained from the simulation W_{model} given by Equation 2.10. A simple experiment has been set up to investigate the efficiency of the energy transfer in the plasma focus device, where gas operating pressures are varied from 1 to 4 mbar. From the simulation, the mass shedding factor or the mass ratio Γ, is adjusted such that the simulated energy fits to the experimentally measured energy in the axial phase. The efficiency of the energy transferred to the plasma motion is the ratio of the simulated energy input to the plasma (W_p), when the plasma reaches the end of the center electrode ($z = z_o$), and the input energy.
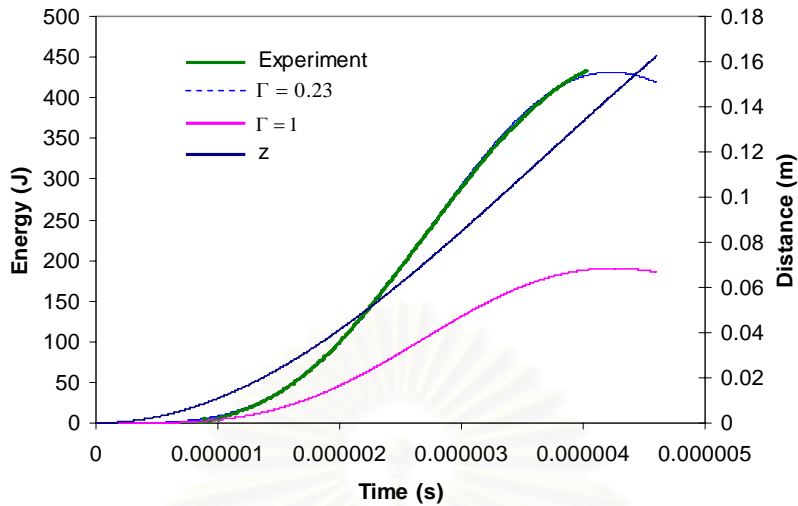
Figure 2.21: Graphs showing calculated energies $W_{experiment}$ and W_{model} as function of

time [43].

Figure 2.21 shows plots of the energies calculated by the model W_{model} and that

obtained from experiment $W_{experiment}$ for the case of mass shedding factor $\Gamma = 1$ and Γ

$= 0.23$. The position of the current sheath as a function of time is also shown in the

same graph. It was found that the fraction of the energy transferred at the end of the

axial phase in the plasma focus varies with pressure. The efficiency decreases as the

pressure is increased. This corresponds to the decrease in the mass shedding factor as

shown in Figure 2.22.

It was found from the calculation based on the results obtained from the modeling

of the plasma focus dynamics that the actual energy input into the plasma is between

224 J to 250 J in the case of a 2.3 kJ plasma focus. The efficiency of energy

transferred calculated was found to have values between 9.6% to 10.7% where the

simulated speed of the plasma sheath is between 3 to 8 cm/μs. It is interesting to note

that, the speed of the plasma slug can be measured for the same condition to have a

value between 3 to 7 cm/μs [2]. This good agreement between the experiment and simulation, together with the good agreement between $W_{experiment}$ and W_{model} as shown in present study show that the plasma focus during its axial acceleration phase is purely inductive and that the joule heating effect may be insignificant.
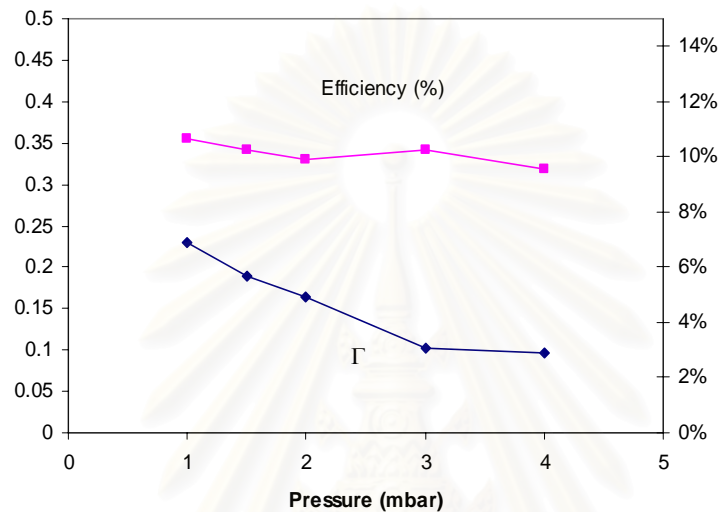
Figure 2.22: Plots showing energy transfer efficiency into plasma (W_p), and the mass ratio Γ as a function of pressure [43].

CHAPTER III

PLASMA DIAGNOSTICS

In this chapter, diagnostic tools required and used in this work are described in detail. The fundamental diagnostics for a plasma focus system are high voltage probe and current probe which is a potential divider and a Rogowski coil respectively. They are commonly used to observe the plasma focus dynamics in term of changing of voltage and current. In this work, another important diagnostic that is used to measure and characterized the ion beam is an electric probe. A photodiode (PIN diode) is also used in conjunction with the electric probe to detect the electromagnetic radiation during the focusing phase. CR39 film is also used to show the ion beam profile.

3.1 High Voltage Probe

A high voltage probe is used to measure voltage across the plasma between a high voltage collector plate (anode plate) and the ground (cathode plate). It is made up of a series (x10) of 500 Ω resistor and one 50 Ω resistor as shown in Figure 3.1. The probe is connected to the plasma focus device as shown in Figure 3.2
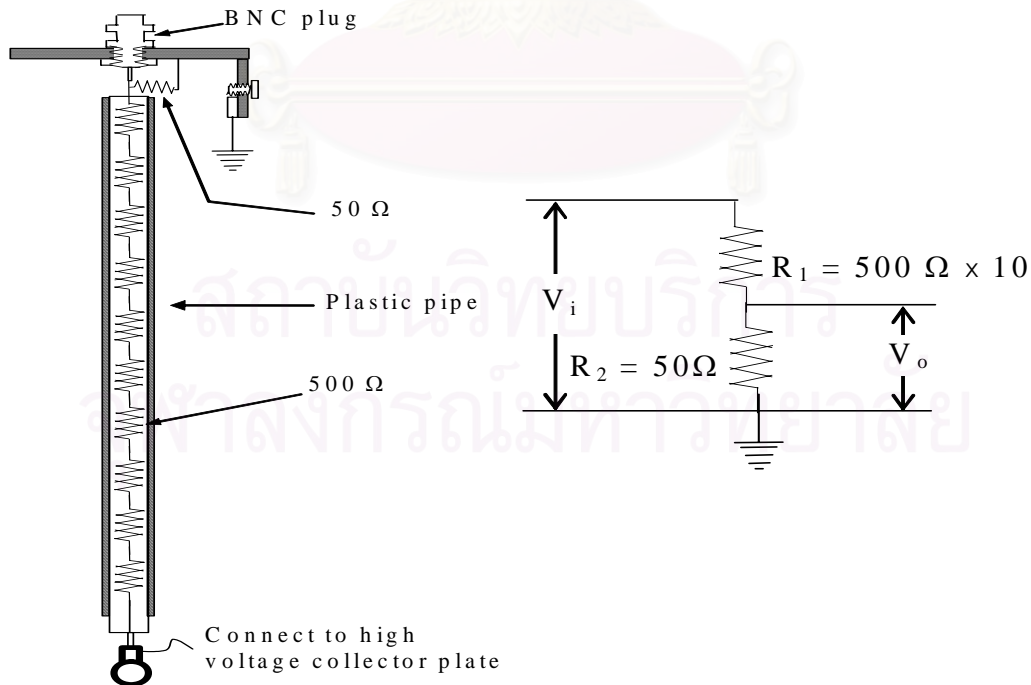
Figure 3.1: Diagram showing a high voltage probe and its circuit.
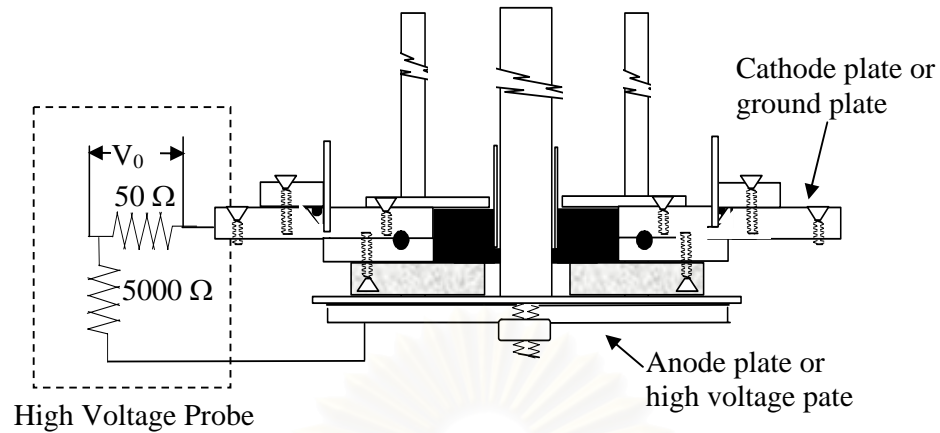
Figure 3.2: Diagram showing how the high voltage probe is coupled to a plasma focus device.

The actual voltage measured by the high voltage probe is reduced by 100 times. From Figure 3.1, the actual voltage output can be calculated from the measured voltage signal using $\frac{V_o}{V_i} = \frac{R_2}{R_1 + R_2}$ where V_o is voltage output, V_i is voltage input, R_1 and R_2 are resistor in series. Figure 3.3 shows a typical voltage signal of a plasma focus operting with argon gas at 1 mbar. LRC oscillation signal is obtained as a baseline which represent the movment of a plasma sheath. The voltage spike at 3.5 μs idicates that there is a focusing phase in this discharge. The spike is a result of an abruply increasing impedance due to the focusing action of the plasma. The current signal also abruply decreases as a result. This will be shown in the next section.
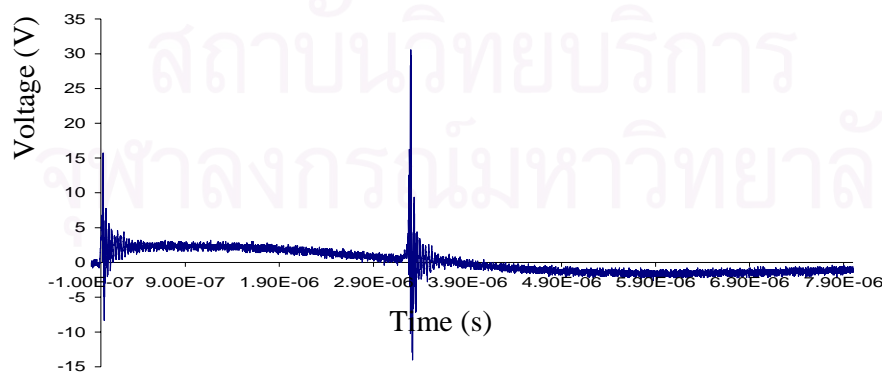
Figure 3.3: Voltage signal of argon at 1 mbar charging voltage 12.5 kV.

3.2 Rogowski Coil

A Rogowski coil is used to measure peak main current of a plasma focus device where the value of the discharge current is very high and in order of 100 kA. A Rogowski coil is a toroidal coil of wire (like a solenoid bent to form a donut). It is used to measure currents as shown in Figure 3.4. In general, a Rogowski coil is a continuous wire turn around a conductor. It does not use a magnetically permeable core, giving it a low inductance [44]. Since it has no permeable core to saturate it can respond linearly to extremely large currents, which is the case of the plasma focus. Being of low inductance it can also respond to very fast frequency pulses. The closer it is to a perfectly symmetric toroidal coil, then the less susceptible for it to external electromagnetic interference; although it can deviate significantly without much loss in performance.
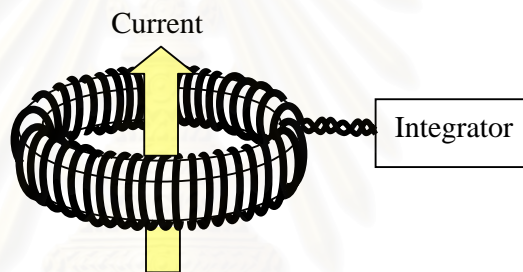
Figure 3.4: Picture showing a Rogowski coil.

Each turn of the Rogowski coil produces voltage proportional to the rate of change of magnetic flux through the turn. Assuming uniform magnetic field density throughout the turn, the rate of change of the magnetic flux is equal to the rate of change of magnetic field density multiply by the cross-sectional area of the turn,

$$V_{turn} = \frac{d\phi}{dt} = A \frac{dB}{dt},$$
(3.1)

where V_{turn} = Voltage output one turn of a Rogowski coil,

ϕ = Magnetic flux passes through a Rogowski coil,

A = Minor cross-sectional area,

B = Magnetic field.

For a coil with n turn, $V_{coil} = nA\dfrac{dB}{dt}$, and the magnetic field B produced by $I(t)$ at the position r is $B = \dfrac{\mu_o I}{2\pi r}$. The voltage of the whole coil is then $V(t) = \dfrac{\mu_0 nA}{2\pi r}\dfrac{dI}{dt}$.

In order to get a voltage proportional to the current, an integrator is used. The total output voltage after integrating is: $V(t) = \dfrac{1}{RC}\dfrac{nA\mu_o}{2\pi r}$.

The coil is mounted around the anode as shown in Figure 3.5. At the end of the conducting wire and the coaxial cable, there is a wire connecting between them as shown in Figure 3.6. The wire is a small resistor or wire resistor used as a self integrator for integrating signal from rate of change of current to current. A typical signal of a current discharge of a plasma focus device is shown in Figure 3.7. Calibration factor of the Rogowski coil can be calculated according to Ngamrungroj [34].
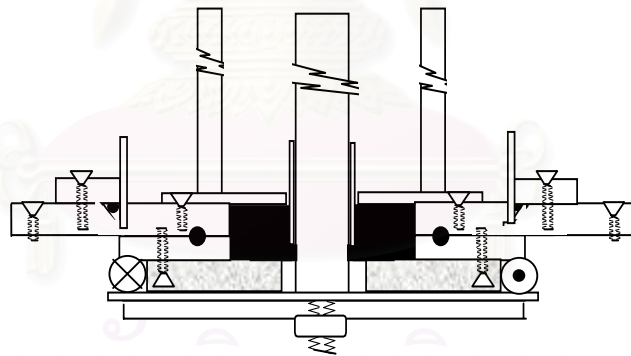
Figure 3.5: Diagram showing the position of a Rogowski that is mounted around anode.
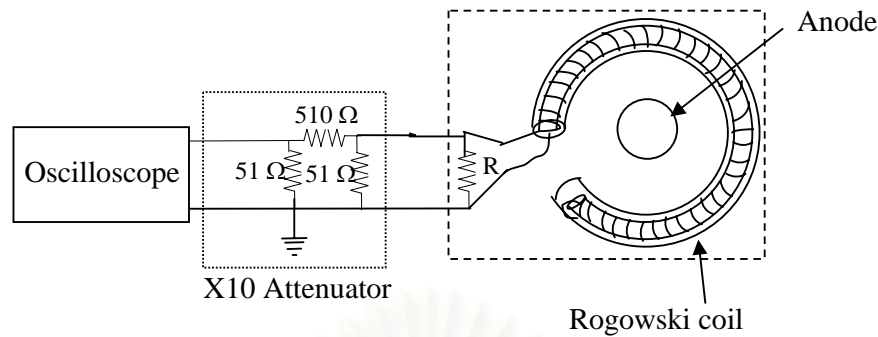
Figure 3.6: Schematic of Rogowski coil circuit connection.
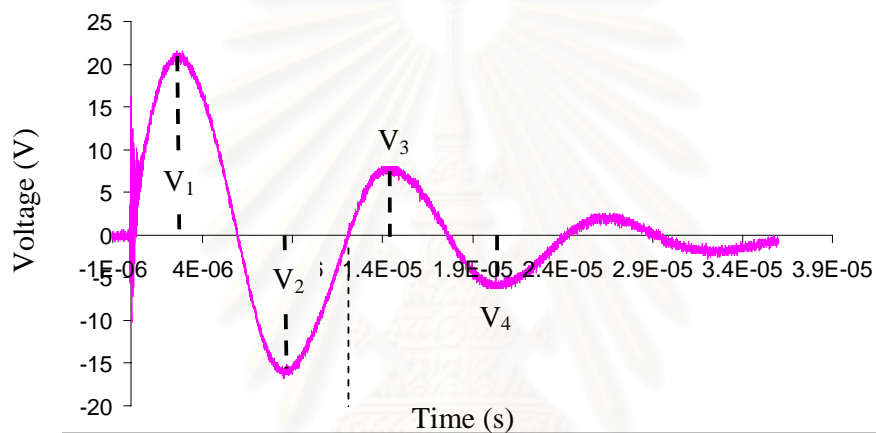
Figure 3.7: Graph showing a current signal of a plasma focus device.

3.3 Bias Ion Collector Probe

In general, Langmuir probe is used to measure ionized particles emitted from continuous plasma but this technique is not suitable for measuring ion densities above 1.3 mbar [45] because the probe dimensions approach those of the ionic and electronic mean free paths. In addition to the invalidity of the Langmuir theory for this case, such a probe can also cause great disturbance to the discharge. However an attempt has been made to use the Langmuir probe type to measure pulse plasma in form of a "Biased ion collector".

In this work, bias ion collector is used for the measurement of ionized particles emitted from the plasma focus. This detector is made essentially of a piece of copper collector connected to a coaxial cable attached to a biasing circuit that provides the bias voltage for the collector. Figure 3.8 shows the diagram of the circuit. Such

detector will have a fast respond and can be easily constructed for the ion beam measurement.
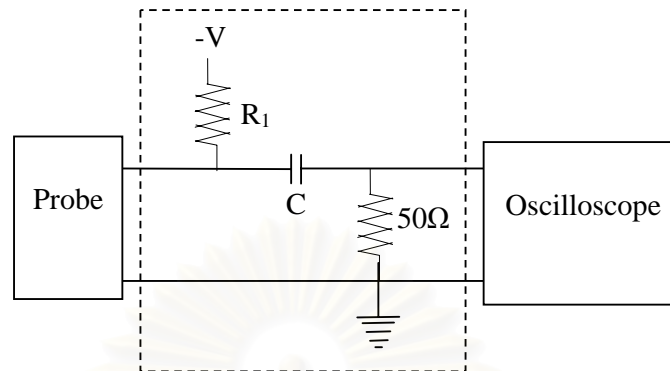
Figure 3.8: Diagram showing a bias circuit used with the electric probe.

The ion collection method is based on the intercept and pickup of ions via the passing ion beam. This method has an advantage that the perturbation has only a minor effect on the ion beam. The energy distribution of the beam, power balance, ion velocity and other parameters remained basically unchanged. The applied biased voltage is used to screen out electrons, either from the beam or photoelectric emission.

Upon pickup of ions, the biased ion collector registers signal as a spike or a sequence of spikes on the digital oscilloscope. A modulation of the current pickup allows us to determine the time of arrival of the ion beam from a known distance. A combination of several biased ion collectors in one direction enables time-of-flight analysis of the ion beam.

There are many types and shapes of bias ion collector probe which are shown in Figure 3.9. Each type of the probe has different detection response to ion because of its shape and the detection area. The probe used in this work is chosen based on fitting criteria to the plasma focus device as well as producing reasonable signal and low noise. The popular type of the probe is one that is adapted from Faraday cup as shown in Figure 3.9 (a) and (e). A large signal can be obtained in comparison to the noise it produces because of its larger detection area. Figure 3.9 (b) shows a probe that is made from a solid coaxial wire. A solid coaxial wire is a copper wire which is covered by insulator with outer copper enclosing. Other types are shown in Figure 3.9 (c) and (d). They are copper wires which fairly easy to make but the detection areas are smaller than the type shown in figure 3.9 (a) and (e). The signal is small for these

types in comparison to the noise pick up. These types of probe are suitable for detecting large number of ions and are practical for the time of flight (TOF) measurement.
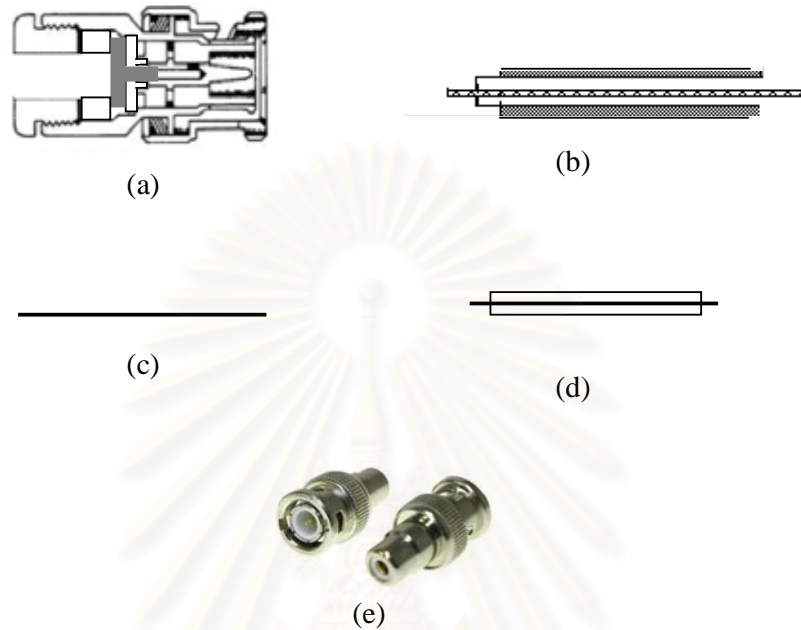
Figure 3.9: Types of bias ion collector probe. (a) and (e) is BNC , (b) solid coaxial ,

(c) and (d) copper wire.

In this work, different types of bias ion collector probe have been experimented in order to find one which is suitable of measuring the ion beam from the plasma focus. It was found that the probe shown in Figure 3.9 (a) and (b) are suitable for experiments that are carried out in this work.

For each type of the probe, the electrical signal produced by the probe will be proportional to the area of the probe. A larger signal will be obtained with the probe that has higher surface area. However the signal obtained from this bias ion collector can be additionally affected by photoelectrons from photoelectric effect, bias voltage, diameter of pin hole, position and distance of the probe.

First effect is the photoelectric effect. It is where a highly energetic electromagnetic wave produces a signal when the wave hits the metal surface of the probe and knocking out electron. The electrons are then conducted to the ground through the wall of the chamber and ground enclosing of the probe as shown in Figure 3.10. If the energy of the electromagnetic wave hf_o, where h is the Planck constant and

f_o is the frequency of the electromagnetic wave, is more than the work function (W) then the photoelectron is released. The kinetic energy of the photoelectron (E_k) is given by,

$$E_k = hf_0 - W .$$ (3.2)

In this work, a bias ion collector probe is made of a piece of copper wire. The work function of copper is 4.70 eV [46]. It is expected that the plasma focus device will generate EM wave ranging from UV to soft X-ray or hard X-ray. From Table 3.1, it shows that the energies from UV and X-ray are sufficient to cause the photoelectric effect on copper.

Table 3.1: Wavelength, frequency and energy of X-ray, UV and visible light [46].

EM wave	Wavelength (m)	Frequency (Hz)	Energy (eV)
X-rays	1×10^{-11} - 2×10^{-8}	1.5×10^{16} - 3×10^{19}	$62.18 - 1.24 \times 10^4$
UV light	2×10^{-8} - 4×10^{-7}	7.5×10^{14} - 1.5×10^{16}	$3.11 - 62.18$
Visible light	4×10^{-7} - 8×10^{-7}	3.7×10^{14} - 7.5×10^{14}	$1.53 - 3.11$
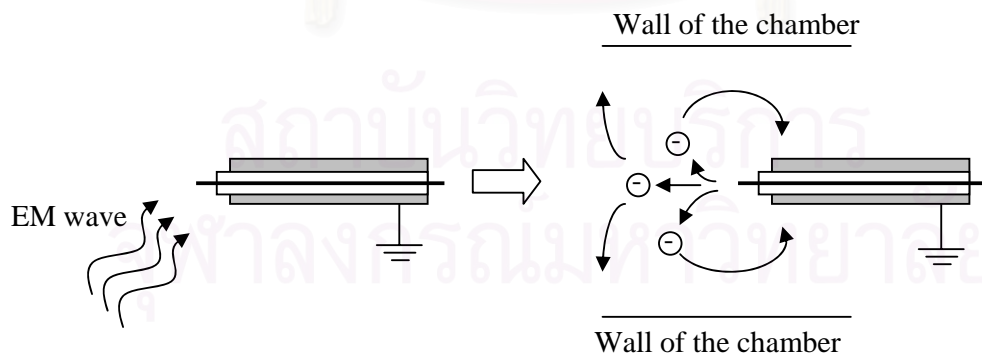
Figure 3.10: Diagram showing the photoelectric effect on a bias ion collector probe.

The ion collector probe used in this work is connected to a bias circuit shown in Figure 3.8. The probe is connected in series with a capacitor and 50 Ω resistor. Tektronix TDS3054 oscilloscope is used to measure voltage across the 50 Ω resistor. A set of 9 V batteries is used to supply the negative bias voltage. Negative voltage is used for selectively detecting ion. However, a large bias voltage can affect the signal as electric field between the probe and the ground can accelerate the ion which can distort the ion velocities. A precaution has been taken to find the lowest negative bias that can still give good signal. The experimental setup is shown in Figure 3.11. Two vacuum chambers are used and the compartments are separated by a hole. The hole is 6.5 cm in diameter. Two ion collector probes that are made by a single copper wire are placed at 20.06 cm. and 28.63 cm from the end of the anode. In this experiment Argon gas is used and the charging voltage is set at 12.5 kV. The anode used is a standard 16 cm length. Biasing voltage of the probes is varied from -9 V to -81 V. Example of signals obtained from the probes with different biasing voltages are shown in Figure 3.12.
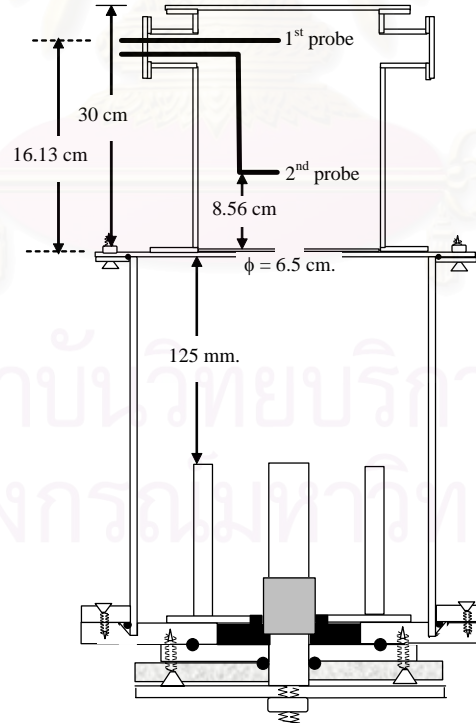
Figure 3.11: Schematic diagram showing the set up of the plasma focus vacuum chamber and the position of two ion collector probes.
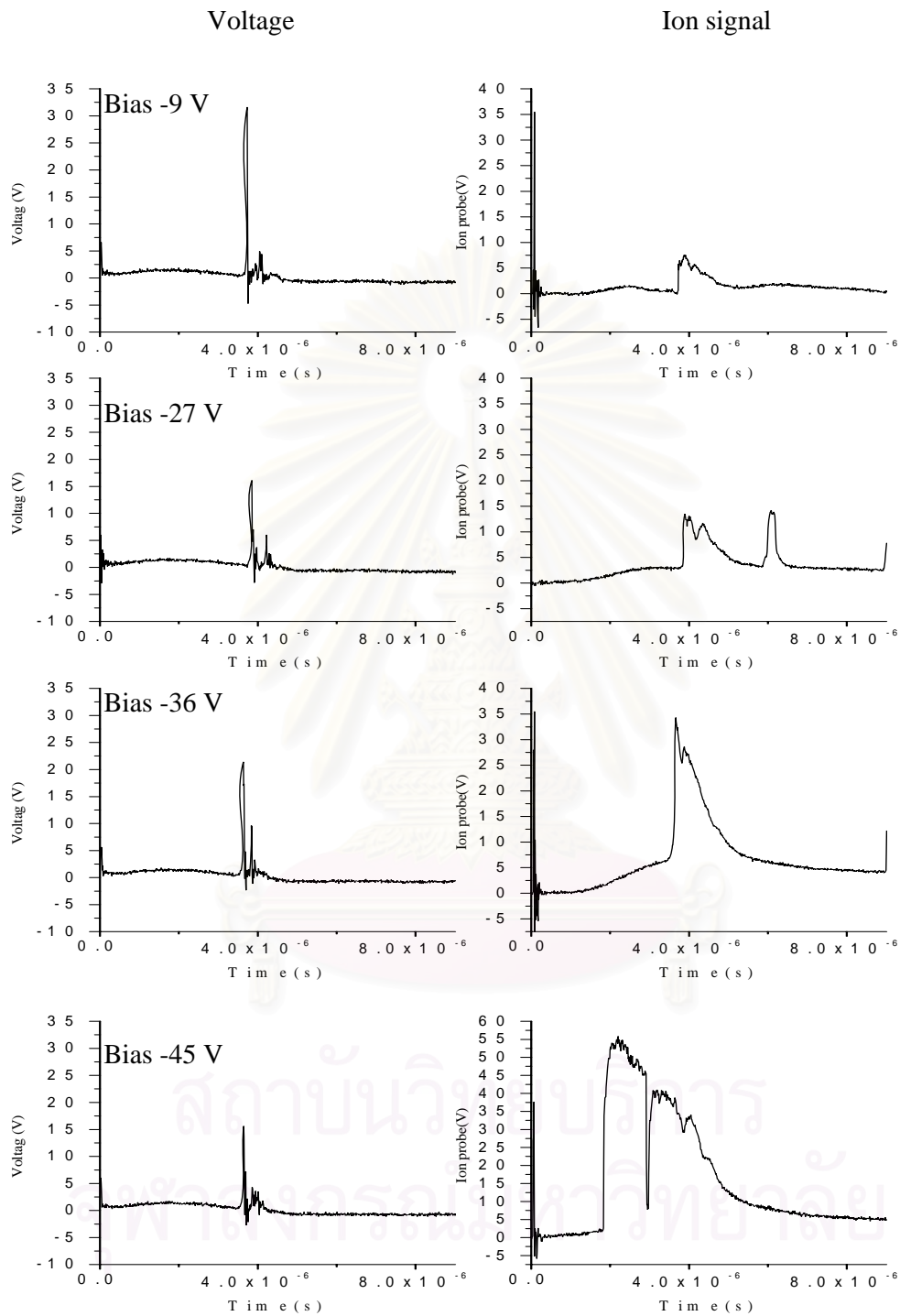
Figure 3.12: Graphs showing voltage and ion signal for various bias voltages applied
            to the ion collector probe.

Another possible way to limit the detected signal is to reduce the size of the hole or the aperture in the setup. This will have effect on the directionality of the ion detected which will be improved. On contrary there will be less number of ions going through. The small size hole will also reduce the number of ion from the plasma jet that will reach the probe.

An experiment has been carried out to obtained optimal aperture where holes of various diameters are experimented. The sizes of the hole are 6 mm, 1.5 cm and 6.5 cm. Various voltage signals from the ion collector probe are shown in Figure 3.13, 3.14 and 3.15 respectively.

Bias -18 V Ar pin hole 6 mm
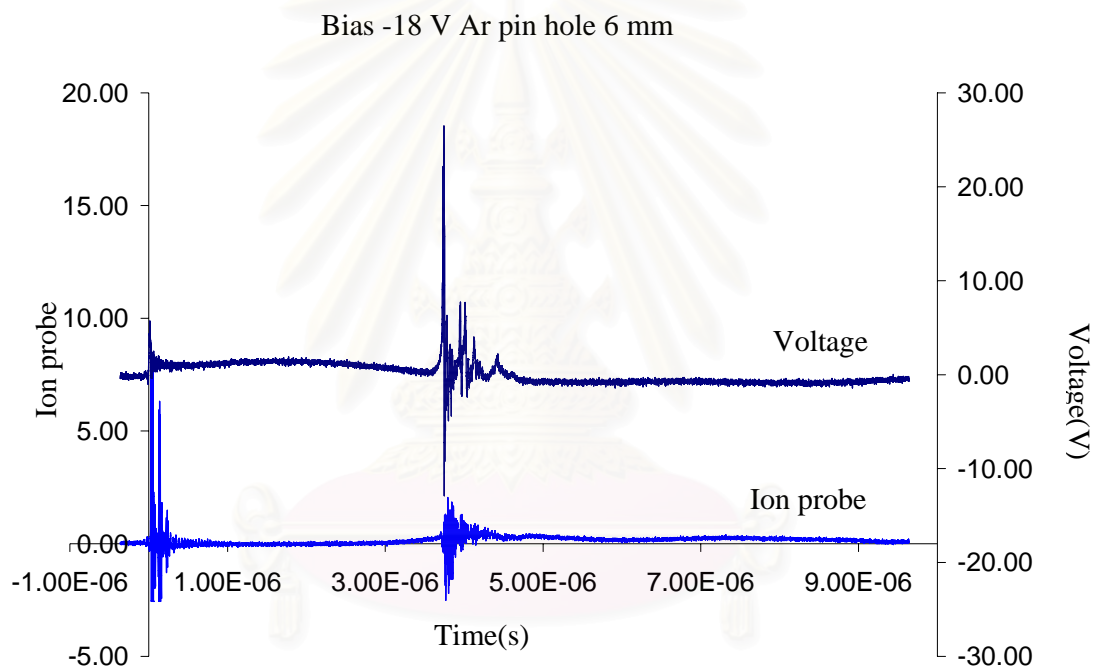
Figure 3.13: Graph showing voltage signal from ion collector probe using -18 V bias and an aperture diameter of 6 mm.
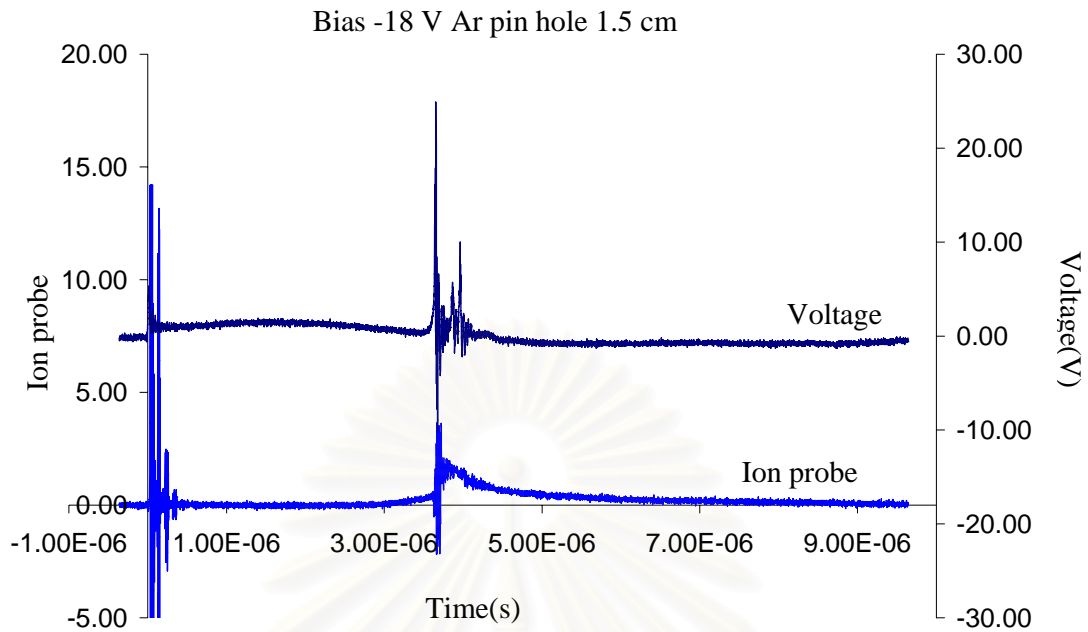
Figure 3.14: Graph showing voltage signal from ion collector probe using -18 V bias and an aperture diameter of 1.5 cm.
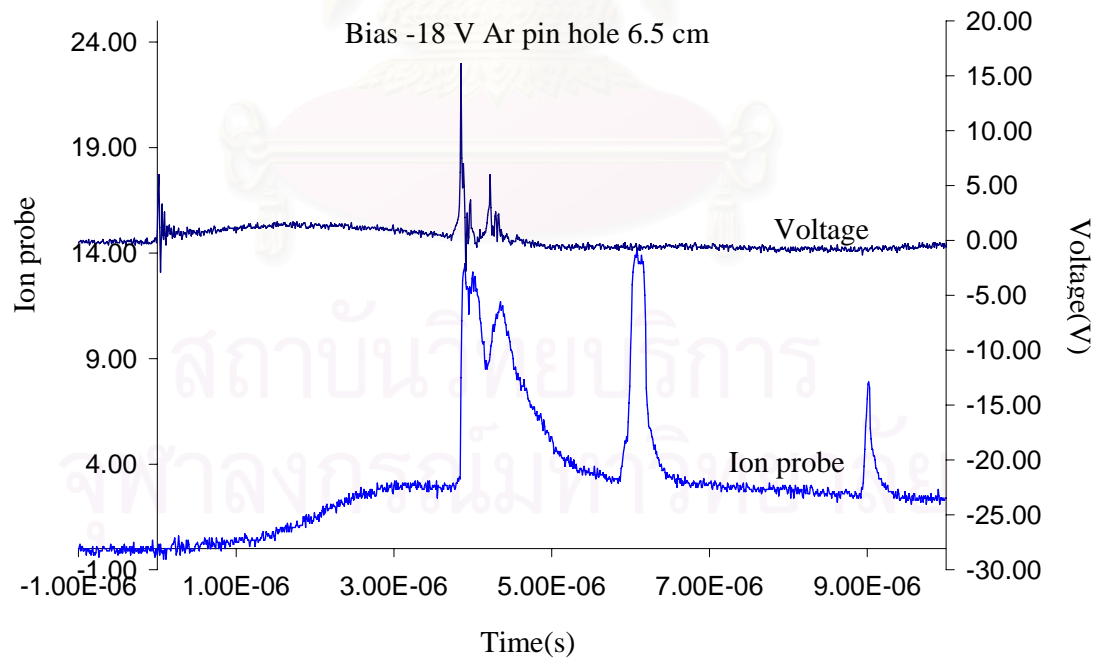
Figure 3.15: Graph showing voltage signal from ion collector probe using -18 V bias and an aperture diameter of 6.5 cm.

From the figures, one can see that the signal is remarkably reduced when the aperture is small. A suitable diameter for the ion beam characterization experiment is 1.5 cm. A reasonable directionality can be achieved as well.

To determine the number of charge detected from the ion beam, we assume that the distribution of the ion beam signal is a combination of Gaussian curves. The peaks that are not directly coinciding with the focusing voltage signal are fitted with the Gaussian curves. The photoelectric effect from any EM waves which gives rise to signal immediately after the focus or during the focus is eliminated. It is assumed that the velocity of the ion beam is much less than the speed of light. Figure 3.16 shows plots of voltage signal from a voltage probe and a signal from a PIN diode (discuss in Section 3.5). One can see that a short EM wave pulse is emitted during the focusing phase and can be immediately detected. The pulse width is less than 17 ns.
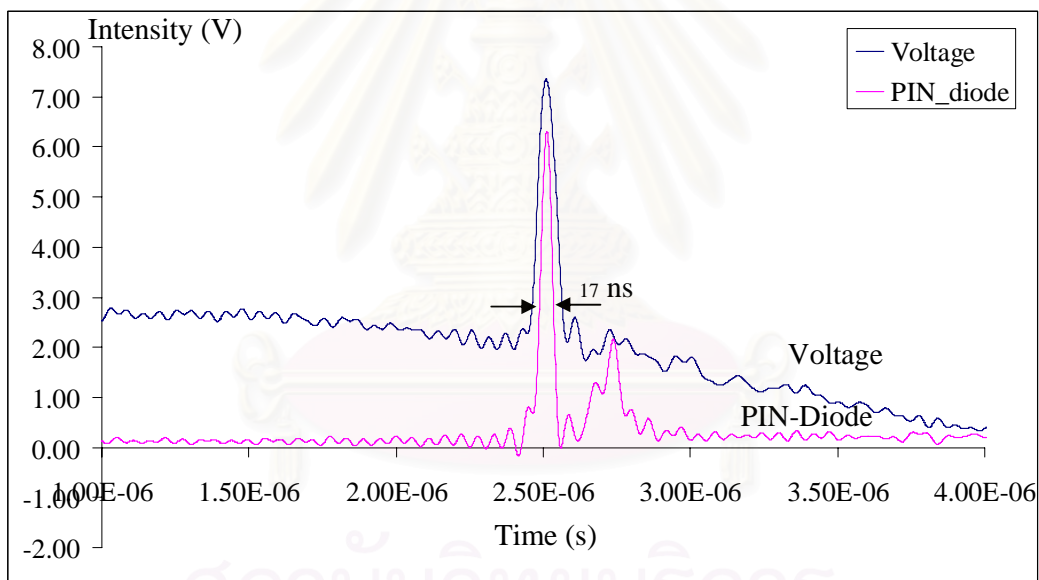
Figure 3.16: Plots showing a voltage and PIN diode signal where the peak of the PIN diode signal occurs at the same time as the focus peak.

Figure 3.17 shows and example of Gaussian curve fitting for determination of charge detected by the ion collector probe. For the first peak a similar pulse width, as in Figure 3.16, is used to simulate the photoelectric effect signal produced during the focusing phase. Other Gaussian peaks are combined to fit the detected signal. The area under this fitted curve that is already subtracted by the first peak (photoelectric

effect) can be used to determined the number of charge collected over the surface area of the probe.

In this case the number of charge detected can be calculated by according to the electronics circuit in Figure 3.8. The current produced, I, that is passing through the resistor R is;

$$I = \frac{V}{R} = \frac{Q}{t},$$
(3.3)

where V is the voltage across the resistor, Q is the charge, t is the time interval. Therefore the charge detected is $Q = \frac{Vt}{R}$. Vt is the area under the curve. In Figure 3.18 the area under the curve after removing the EM-wave signal is 3.15×10^{-6} Vs, therefore the number of charge that reaches the ion collector probe surface is $\frac{3.15 \times 10^{-6}}{50} = 6.30 \times 10^{-8}$ C. The area of the bias ion collector probe is measured and calculated to be 3.14159×10^{-9} m^2. Therefore the charge per unit area is 20.1 C/m^2.
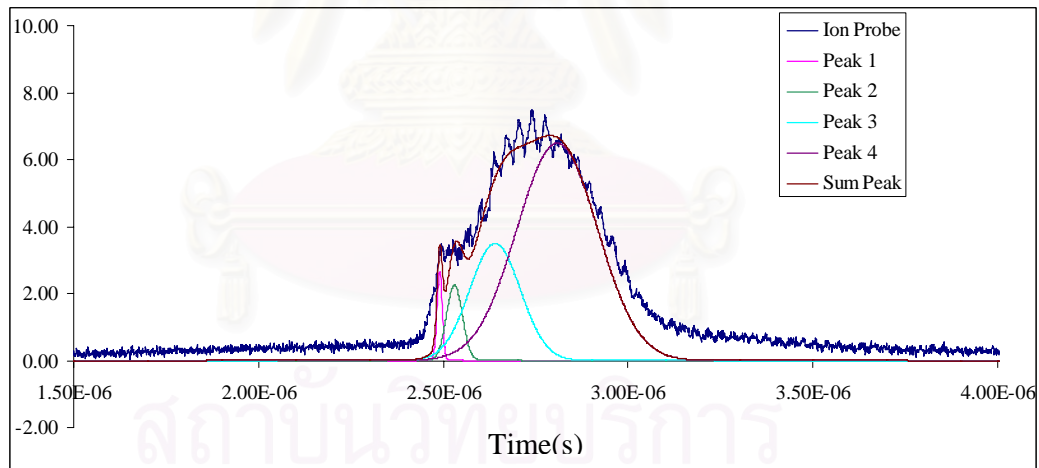
Figure 3.17: Graphs showing an ion beam signal from an ion collector probe fitted with Gaussian curves where peak 1 is assume to be from the EM radiation, Peak 2, 3 and 4 are ions.

A velocity of the ion beam can also be calculated since the position of the probe is known to be at 28 cm from the end of the anode. The peak of the signal after the focusing voltage peak identify the time when the majority of the ions that leave the anode arrive at the probe. In this case, the velocity of 7×10^6 m/s is the result. From the

velocity value, a general kinetic energy of the ion can be obtained by using $E_k = \frac{1}{2}mv^2$ where a mass of natural argon gas of 40 g/mol is assumed therefore one argon atom has a mass of 6.64×10^{-26} kg. The kinetic energy of the ion can be calculated to be 10.2 MeV.

3.4 CR-39 Film [47]

Allyl diglycol carbonate commonly known as **CR-39** film is a plastic polymer used in the manufacture of eyeglass lenses. It has high abrasion resistance, in fact the highest abrasion/scratch resistance of any uncoated optical plastic. CR-39 is a trade marked product of PPG Industries, originally developed by Columbia Chemical Co Inc which evolved through acquisition into the Chemical Division of PPG Industries. A purified CR-39 can be used to measure neutron radiation, a type of ionizing radiation, in neutron dosimetry. CR-39 is transparent in visible spectrum and almost is completely opaque in the ultraviolet range. CR-39 is made by polymerization of diethyleneglycol bis allylcarbonate (ADC) in presence of diisopropyl peroxydicarbonate (IPP) catalyst. The presence of the allyl groups allows the polymer to form cross-links; thus, it is a thermoset resin. The monomer structure is

$CH_2=CH-CH_2-O-CO-O-CH_2CH_2-O-CH_2CH_2-O-CO-O-CH_2-CH=CH_2$.
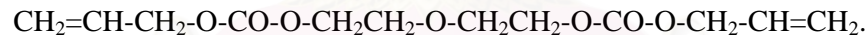
In the radiation detection application, raw CR-39 material is exposed to proton recoils caused by incident neutrons. The proton recoils cause tracks, which are enlarged by an etching process in a caustic solution of sodium hydroxide. The enlarged tracks are normally counted under a microscope (commonly x200), and the number of tracks is proportional to the amount of incident neutron radiation. In this work, CR-39 film is used with a particle pinhole camera to detect ions. The particle pinhole camera is used to create the radial distribution of ions, so that the ion from the pinched plasma column is only allowed to creat a finite area on the CR-39 film.

Figure 3.18 shows set up of CR-39 film to detect the ion beam that is produced from a plasma focus device. The distribution of ion appears on CR39 can be calculated to determined the initial spot size of the plasma column.

Here, the diameter of the image on CR-39 is represented by z, where $z = \dfrac{x' - P}{2}$

and $\tan\theta = \dfrac{h}{z}$. By taking a similar triangle $y' = \dfrac{x'h}{2z}$ and $y = L - y' = L - \dfrac{x'h}{2z}$,

therefore the plasma column spot size is $x = \dfrac{yx'}{y'} = \dfrac{L(x' - P)}{h} - x'$.
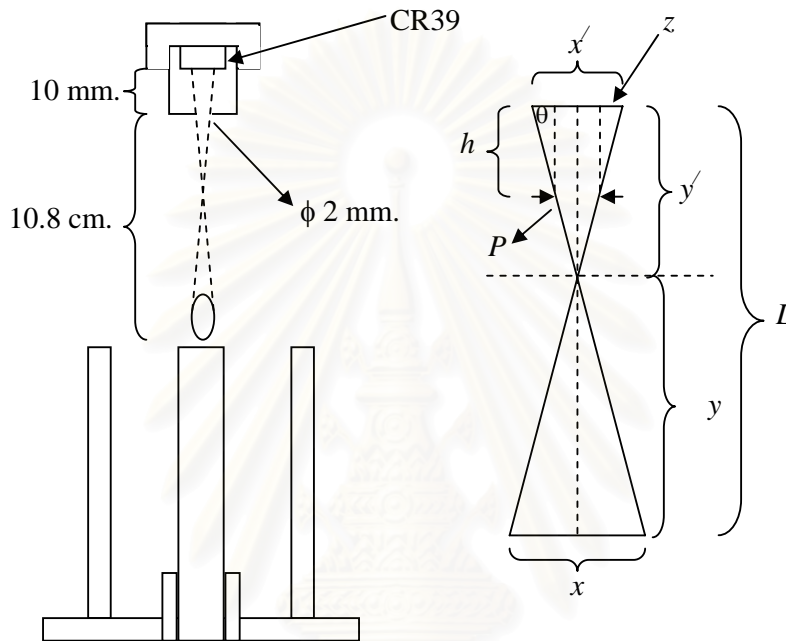
Figure 3.18: Diagram showing CR-39 setup and a geometric diagram for calculating the spot size.

An example of CR-39 application is an experiment done by H.R. Yousefi et al.[4]. A Mather-type plasma focus is energized by a capacitor bank of 44.8 μF 30 kV to generate ion beam. CR39 film was used to measure the distribution of ion from the pinch column. Figure 3.19(a) shows a picture of a pinch column and (b) the ion track distribution from his work.

(a)   (b)
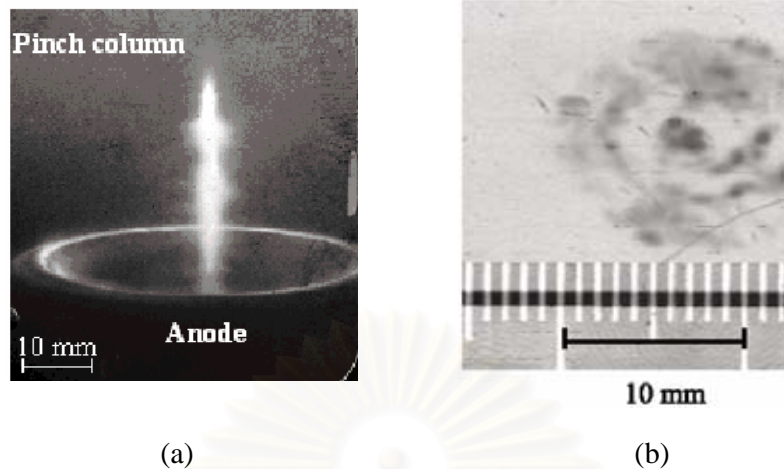
Figure 3.19: Pictures showing (a) a pinch column taken by X-ray pinhole camera and
(b) ion track distribution on CR-39 film [4].

3.5 PIN-diode

In this research, BPX-65 PIN diodes, shown in Figure 3.20, is used to detect EM
radiation especially in our case is X-rays. The front of the PIN diode is covered by
aluminum mylar filter. The diode is biased at – 45 V DC from five 9 V batteries with
the circuit shown in Figure 3.21. The circuit has a blocking 0.047 µF capacitor and
51Ω resistor which are contained in a metal casing.

Figure 3.20: Picture showing the BPX-65 PIN diode[48].
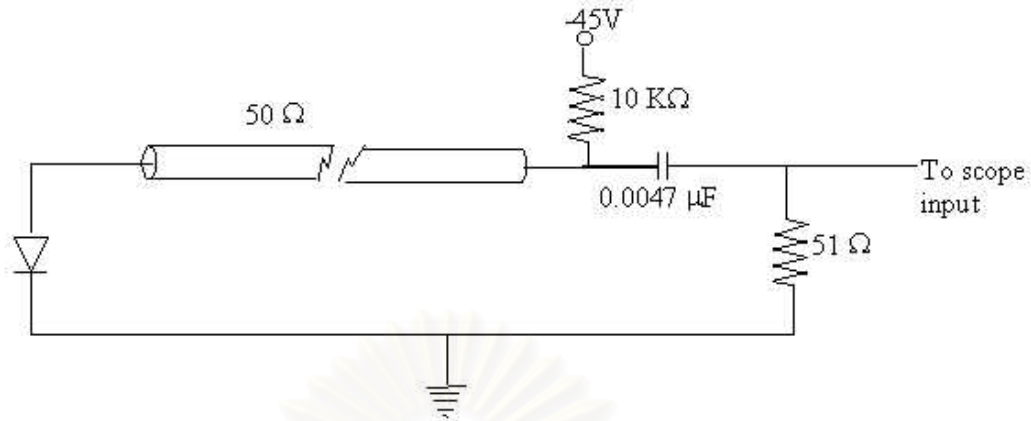
Figure 3.21: Circuit diagram of a PIN diode setup.

A typical PIN diode signal from a plasma focus is shown in Figure 3.17. X-ray is normally produced when there is a strong focus, therefore the signal detected is a burst of X-ray during the focusing phase. This is likely when free electrons collide with other particles yielding the Bremsstrahlung X-ray. The spectrum is a continuum. Electron-electron collisions do not produce radiation except at relativistic velocities. In the plasma focus, important collisions are those between electrons and ions, but in a slightly ionize gas, the more numerous collisions between electrons and neutral atoms, though less effective, are more important.

Recombination process can also happens when a free electron is captured by an ionized atom and makes a transition to a bound state of the ionized atom, the surplus energy may be emitted as X-ray. Recombination may also occur without the emission of radiation if two free electrons collide with the ion simultaneously. One electron is captured while the other carries away the surplus energy. This 'three body' recombination is in competition with the radiative recombination and becomes more probable as the density rises.

Figure 3.22 shows the sensitivity of the BPX-65 PIN diode for various wavelength. In fact multiple PIN diodes can be used to measure X-rays through different absorption fiters allowing for the determination of the peak elecron temperature during the focusing phase. The method is demonstrated in [49]. For the record, the sensitivity of BPX 65 PIN-diode in C/J is given by Equation 3.4 [31];

$$S(\lambda) = 0.28\exp(-\mu_s x_1)\left[1 - \exp(-\mu_s x_2)\right], \tag{3.4}$$

where x_1 : thickness of n-type Si (as window)

                x_2 : thickness of intrinsic layer (detection region)

                μ_s : mass absorption coefficient of Si.

The factor of 0.28 is obtained from the fact that the electron-hole pair production energy of Si is 3.55eV. So, the intensity of X-ray can be detected from the detector is,

$$I_0 \frac{A}{4\pi d^2} S(\lambda) . \tag{3.4}$$

By assuming X-ray radiated from the plasma focus is isotropic. If the detector has an area A and the detector is at a distance D from the x-ray source. The fraction of the X-ray detected at the detector window is, $I_o \dfrac{A}{4\pi d^2}$.
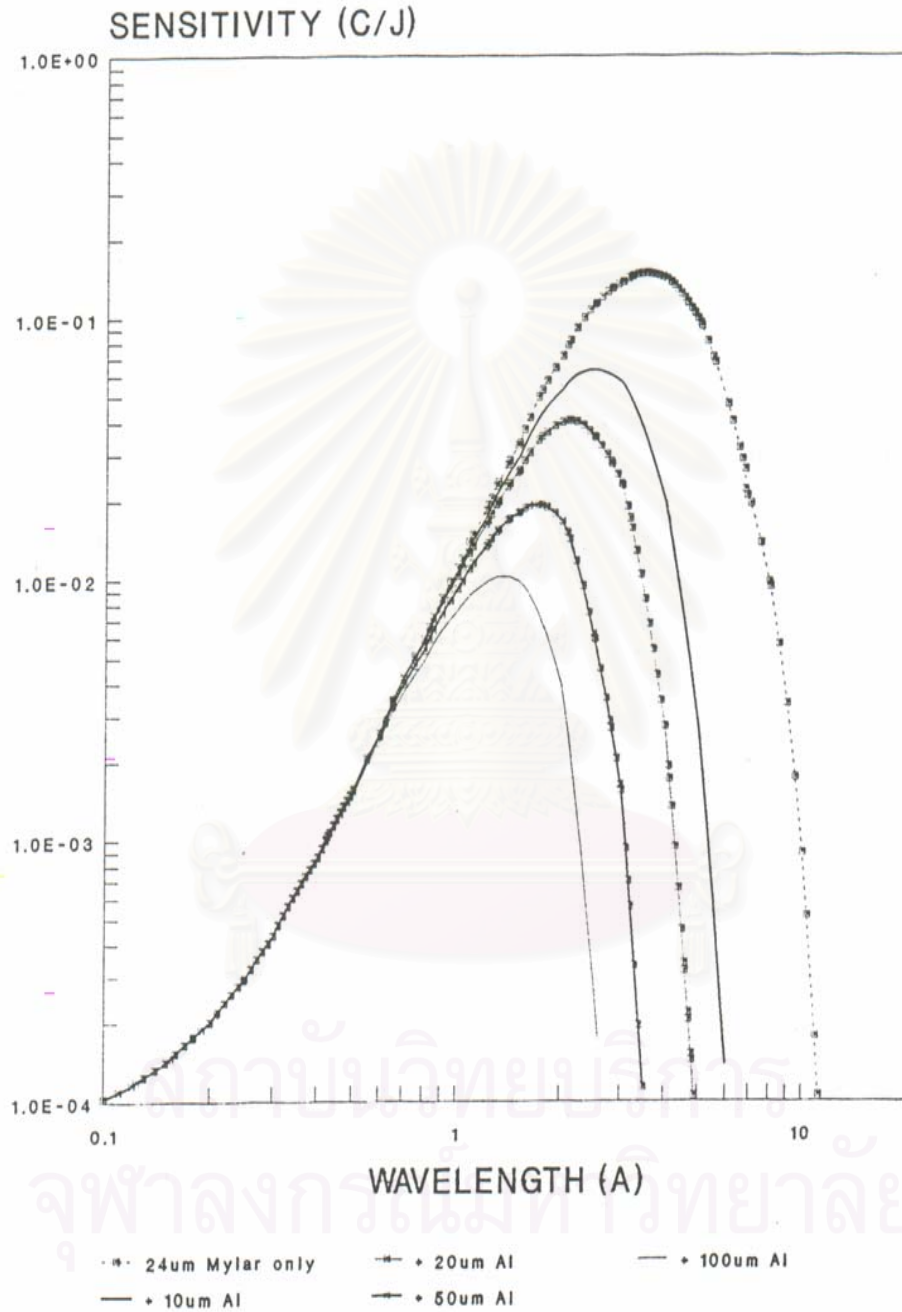
Figure 3.22: Plots showing the sensitivity curve of BPX65 PIN-diode for various

absorption filters [31].

Chapter IV

EXPERIMENT AND RESULT

In this chapter, our experiments on a UNU/ICTP plasma focus to generate ion beams under various operating conditions are explained. The results from each set of experiments are also presented. In the experiment, several diagnostic techniques described in Chapter 3 have been used. An attempt has been made to find a correlation between various operating parameters; such as the shape of the anode, the pressure of the operating gas and the initial charging voltage; with the plasma and the ion beam characteristics that include the voltage peak, the speed of the plasma sheath, the speed and energy of ions produced and the charge density detected. The voltage peak represents the quality of the focus as well as the electric field that accelerates the ions. The discussion of the results is presented in Chapter 5.
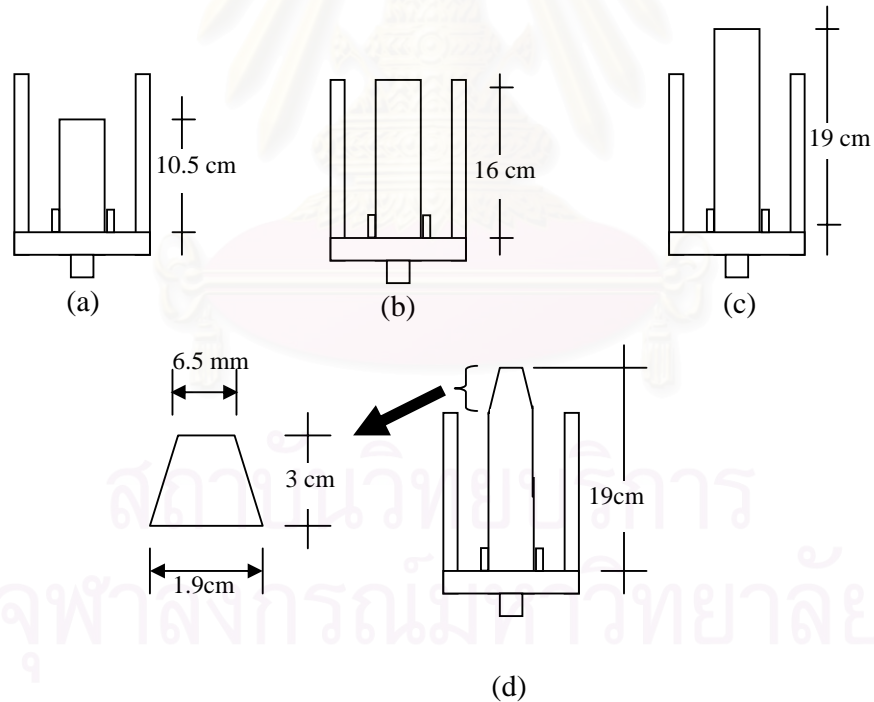
Figure 4.1: Diagrams showing different shapes of cylindrical copper anode, where (a), (b) and (c) are cylindrical with different lengths of 10.5 cm, 16 cm and 19 cm, respectively and (d) is a taper anode.

In general, four types of anode have been used for each experiment. The lengths of three different cooper anode used are 10.5 cm, 16 cm and 19 cm. These anodes are paired up with six 16 cm long copper cathodes with the set up shown in Figure 1.1. Another anode shape that has been experimented is a taper anode as shown in Figure 4.1. The diameter of each cylindrical anode is 1.9 cm. The taper anode has a diameter at the top of 0.65 cm with slanting ratio 1:4.8. It is suspected that each type of anode will produce different quality of focusing column which will affect the characteristics of ion beam produced. Figure 4.1 shows different types of anode used in experiments.

4.1 Experiment I: Variation of Plasma Sheath Velocity with Pressure and Anode Shape

In this experiment, argon gas is used as an operating gas since the halogen gas is inert. The operating voltage for the plasma focus is set at 12.5 kV. This will allow the focus device to have a stored energy of 2.34 kJ. The experimental set up is shown in Figure 4.2.
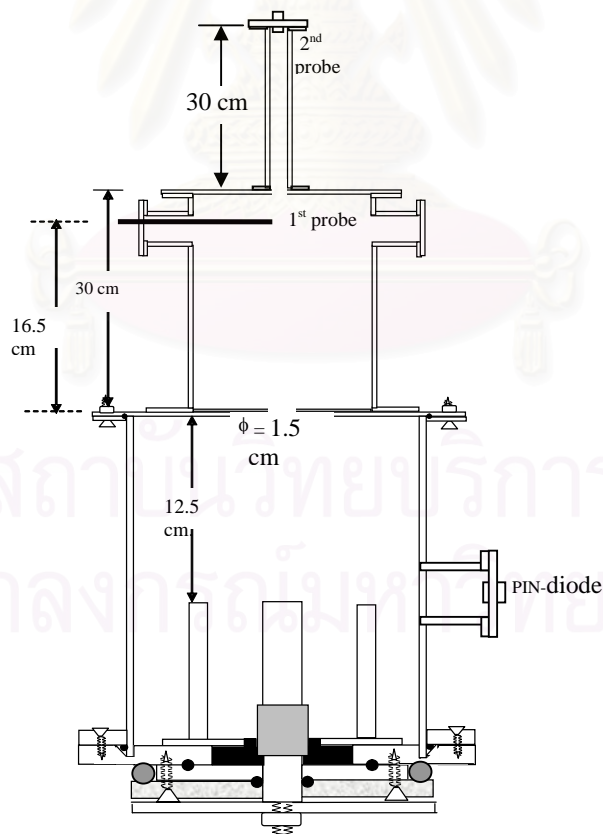
Figure 4.2: Diagram showing the set up of the vacuum chamber and the position of different plasma and ion beam diagnostics.

A small aperture of 1.5 cm diameter is used to collimate and limit the flux of ions as discussed in Chapter 3. It is placed at 12.5 cm from the top of the cathode. Two bias ion collector probes, where the first ion collector probe is made from a solid coaxial is placed at 16.5 cm away from the aperture and the second ion collector probe is placed at 56.5 cm from the aperture. The operating pressure range is selected based on the pressure that the plasma focus can still produce focusing peaks. Figure 4.3 shows example of the result of voltage signal when there is a focusing (a) and non focusing (b).

(a)   (b)
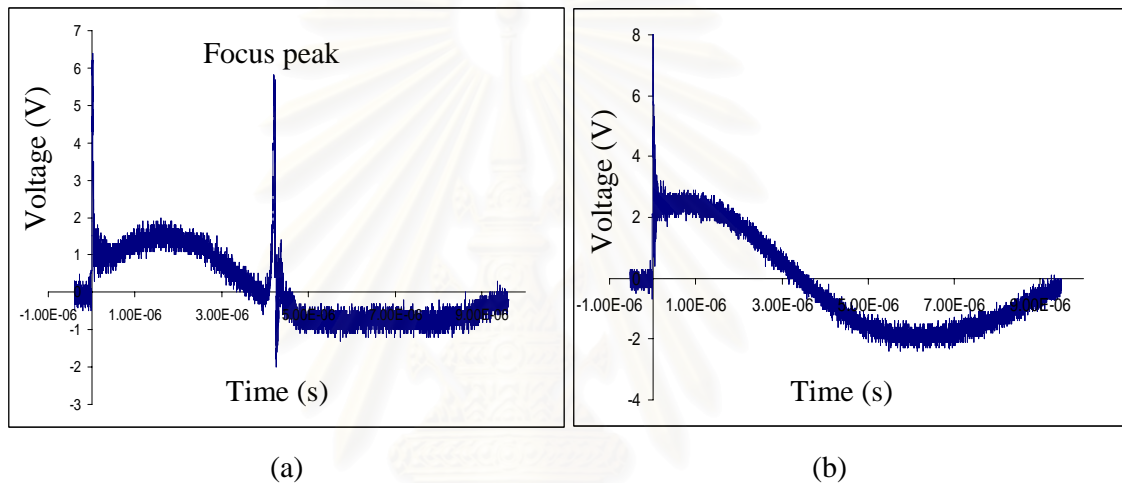
Figure 4.3: Graphs show voltage signal which there is a focus (a) and non focus (b).

The suitable operating pressures found are 0.5 mbar to 1.5 mbar for 16 cm anode long, 1 mbar to 3 mbar for 10.5 cm anode long, 0.5 mbar to 1.2 mbar for 19 cm anode long and 0.5 mbar to 0.9 mbar for taper anode. The results of the voltage signal for each type of anode and various operating pressures are shown in Figure 4.4, 4.5, 4.6 and 4.7.
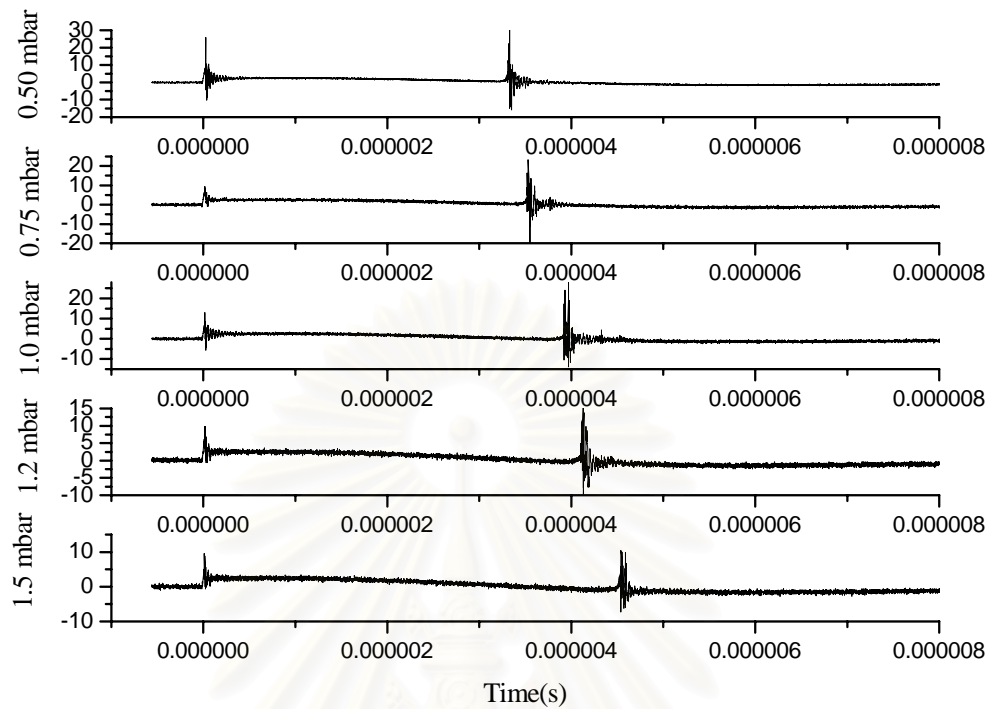
Figure 4.4: Plots showing voltage signal for various operable pressure of a plasma focus device using 16 cm long anode.
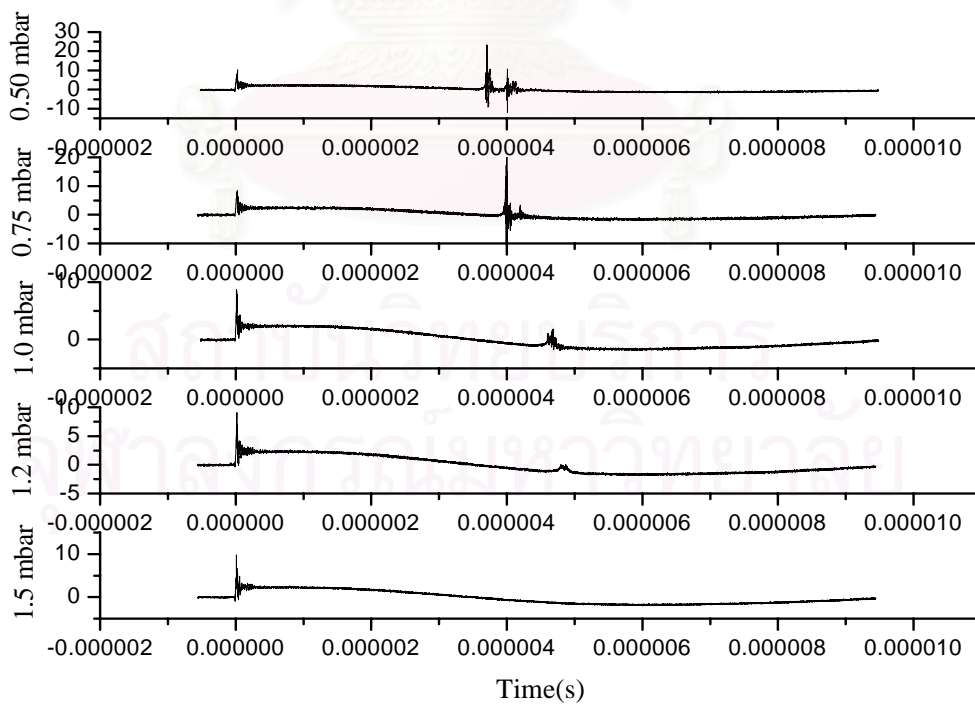
Figure 4.5: Plots showing voltage signal for various operable pressure of a plasma focus device using 19 cm long anode.
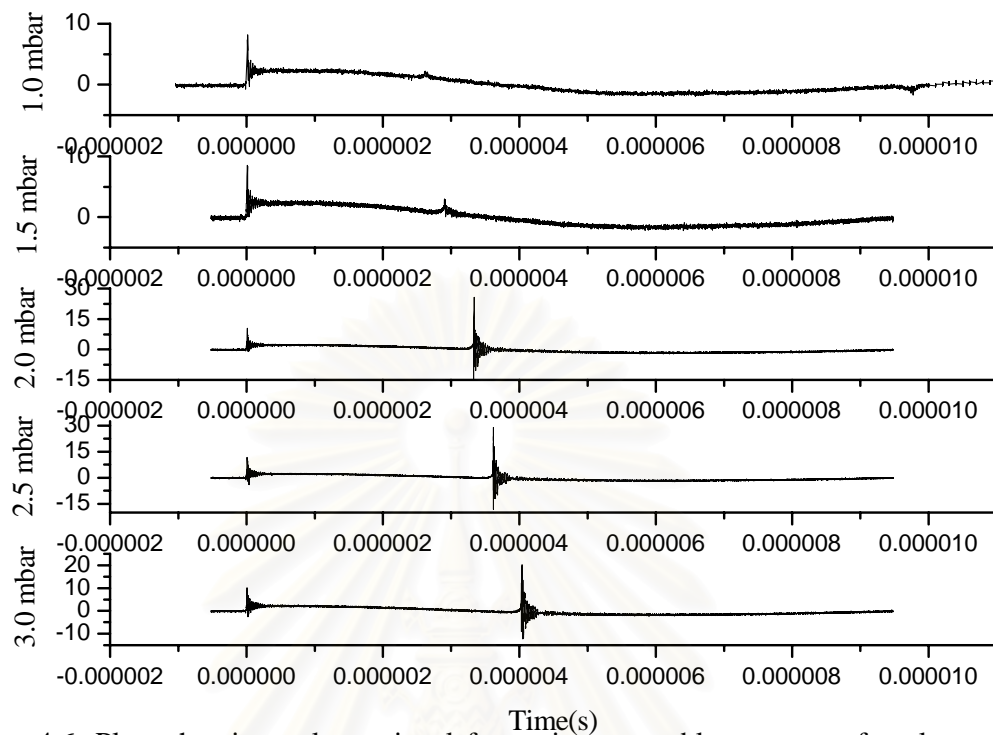
Figure 4.6: Plots showing voltage signal for various operable pressure of a plasma focus device using 10.5 cm long anode.
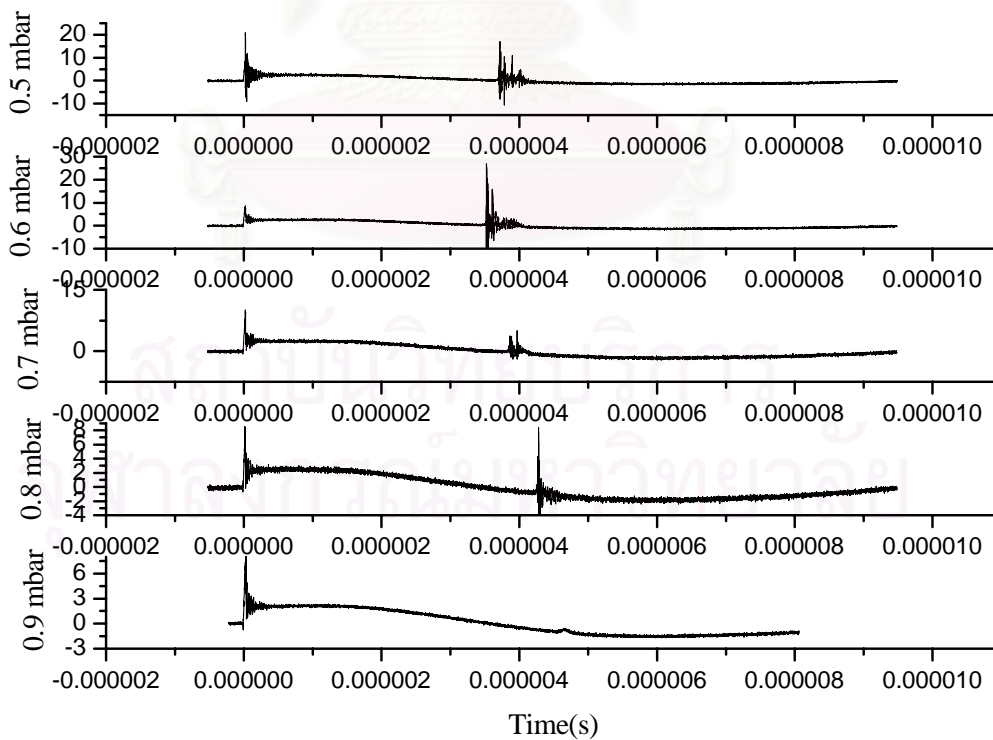
Figure 4.7: Plots showing voltage signal for various operable pressure of a plasma focus device using 19 cm long taper anode.

In each case, voltage signals can be used to estimate the average speed of the plasma sheath during the axial phase for each operating conditions. The first peak marks the start of the axial rundown and the beginning of the focusing peak marks the end of the axial phase which correspond to the distance that plasma sheath has traveled which is the length of the anode. Using this information, one can calculate the average speed of plasma current sheath in the axial phase. The results of the average speed are presented in Table 4.1. Figure 4.8 shows graphical presentation of the results.

Table 4.1: Average speed of plasma sheath in axial phase with various operating pressure

Pressure (mbar)	Average speed (cm/µs)			
	10.5 cm	16 cm	19 cm	taper
0.5	-	4.81	6.04	4.94
0.6	-	-	-	5.37
0.7	-	-	-	4.82
0.75	-	4.52	4.42	-
0.8	-	-	-	4.44
0.9	-	-	-	4.05
1	3.97	4.00	3.99	-
1.2	-	3.87	3.96	-
1.5	3.62	3.53	-	-
2	3.18	-	-	-
2.5	2.88	-	-	-
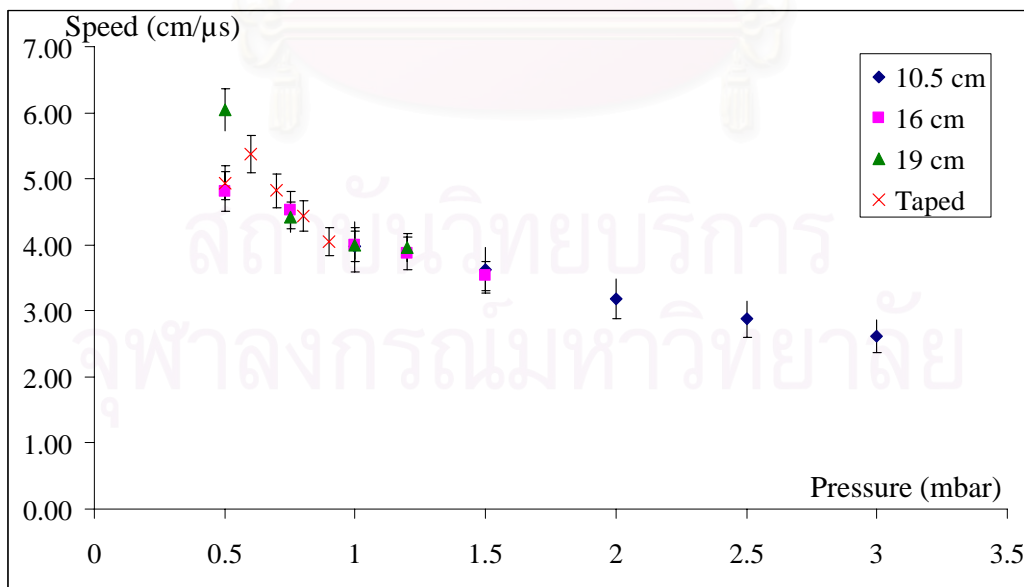
Figure 4.8: Plots showing the variation of average plasma sheath speed with operating argon gas pressure.

It is interesting to see that there is a decrease in the average speed with pressure which is expected as there are more collisions between particles. But the general trend remains even with different anode length. It may be concluded that as the initial stored energy is the same for all operation then the axial speed of the plasma sheath is not affected by the variation of the length. But it has been observed that the different anode length produces focusing peak at different operating pressures. Note that the error bars on the data point is calculated based on the maximum error method.

4.2 Experiment II: Variation of Peak Focusing Voltage with Pressure and Anode Shape

Similar experiments as described for Experiment I are carried out but the emphasis is on the quality and the measurement of the focusing voltage peak. Table 4.2 shows the measured voltage of the voltage peak by a voltage probe and fast oscilloscope (Tektronix TDS5054). Figure 4.9 and Figure 4.10 show graphical plots of the variation of the focusing peak voltage with various operating pressure. It can be seen that the signal is some what fluctuating as this may due to the variation of each operational shot, but a trend can be seen where the peak voltage reduces when the pressure increases. The voltage peak is strongest when the anode length is 16 cm and weaker with 19 cm and taper configuration. For the anode length of 10.5 cm the voltage peak is better when the operating pressure is higher.

Table 4.2: Measured voltage peak from various operating pressure.

Pressure (mbar)	Voltage focus peak (kV)			
	10.5 cm	16cm	19 cm	taper
0.5	-	34.99	18.84	3.62
0.6	-	-	-	26.91
0.7	-	-	-	5.04
0.75	-	23.27	14.58	-
0.8	-	-	-	14.11
0.9	-	-	-	8.39
1.0	2.16	29.32	1.16	-
1.2	-	19.95	0.04	-
1.5	3.02	10.54	-	-
2.0	25.73	-	-	-
2.5	29.03	-	-	-
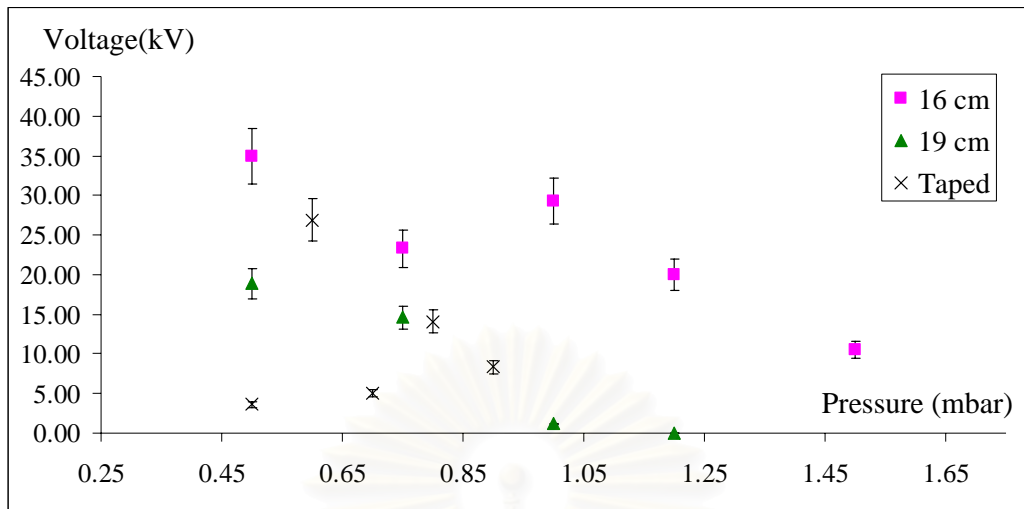
Figure 4.9: Plots showing the variation of focusing voltage peak with operating argon gas pressure.
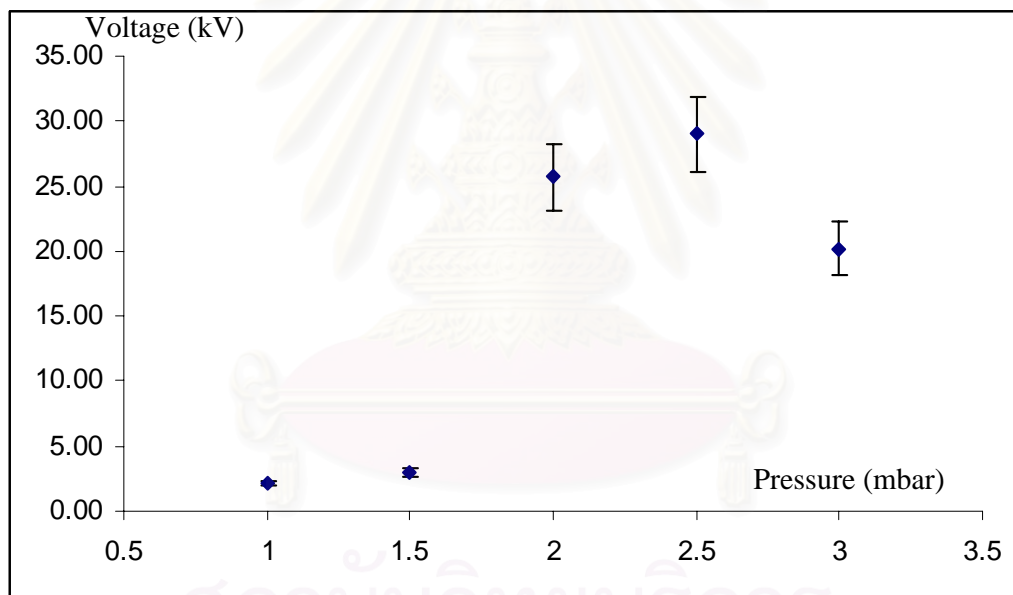
Figure 4.10: Plots showing the variation of focusing voltage peak with operating argon gas pressure for the 10.5 cm anode length.

4.3 Experiment III: Variation of Ions Velocity and Energy with Pressure and Anode Shape

In this experiment, different types of ion collector probe are used to detect the ion produced by a plasma focus. The emphasis is on the ions that are produced immediately after the collapsing of the plasma column. These ions are expelled as a pulse of fast ions or ion beam. The experimental set up resembles that in Figure 4.2. Again, the same energy input is applied where the charging voltage is 12.5kV. Argon gas at various pressures is used. Different anode shapes are similarly applied. The velocity of the ion beam and the energy is determined by the method described in Chapter 3. The operating conditions are chosen only that which produces a focusing plasma column. The focusing column is identified by the voltage peak signals.

The results are shown in Table 4.3. It can be seen, as previously shown, that only some operating conditions produce focusing column. Figure 4.11, 4.12, 4.13 and 4.14 show the variation of the ion velocity and its energy with different operating pressure for anode with 16 cm length, 19 cm length, 10.5 cm length and taper, respectively.

Table 4.3: Ions velocity and energy from various operating pressure and anode shapes.

Pressure (mbar)	Velocity (m/s) and energy (eV) of ion beam							
	10.5 cm		16cm		19 cm		tapered	
	Velocity	Energy	Velocity	Energy	Velocity	Energy	Velocity	Energy
0.50	-	-	1.54E+06	4.93E+05	2.17E+06	9.81E+05	6.97E+05	1.01E+05
0.60	-	-	-	-	-	-	2.33E+06	1.12E+06
0.70	-	-	-	-	-	-	2.52E+06	1.31E+06
0.75	-	-	1.73E+06	6.20E+05	2.08E+06	9.01E+05	-	-
0.80	-	-	-	-	-	-	2.00E+06	8.31E+05
0.90	-	-	-	-	-	-	1.69E+06	5.91E+05
1.00	9.68E+05	1.95E+05	1.84E+06	7.02E+05	1.87E+06	7.26E+05	-	-
1.20	-	-	1.29E+06	3.46E+05	1.87E+06	7.23E+05	-	-
1.50	2.02E+06	8.44E+05	-	-	-	-	-	-
2.00	2.23E+06	1.04E+06	-	-	-	-	-	-
2.50	1.33E+06	3.67E+05	-	-	-	-	-	-
3.00	1.18E+06	2.88E+05	-	-	-	-	-	-
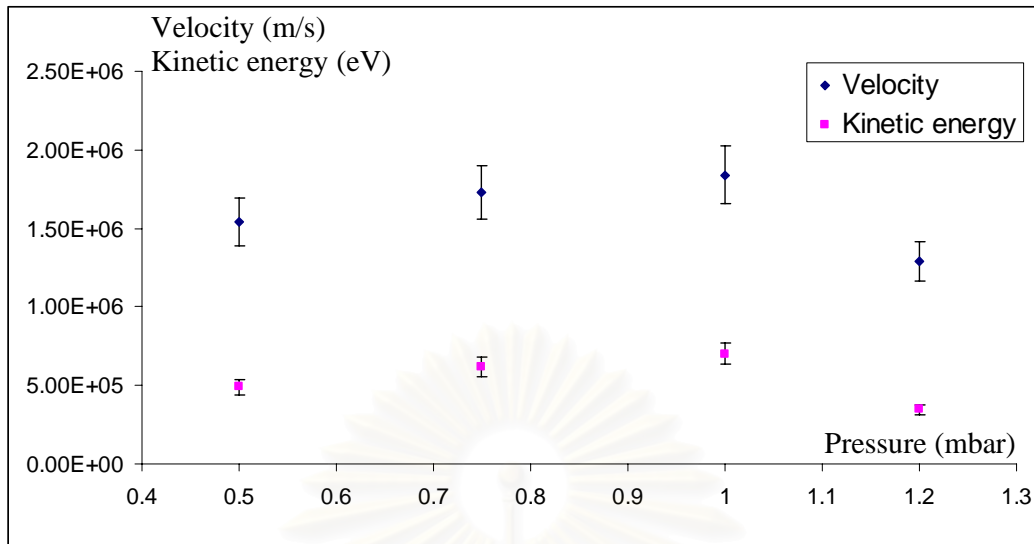
Figure 4.11: Plots showing the variation of ion velocity and energy with operating

argon gas pressure for the 16 cm anode length**.**
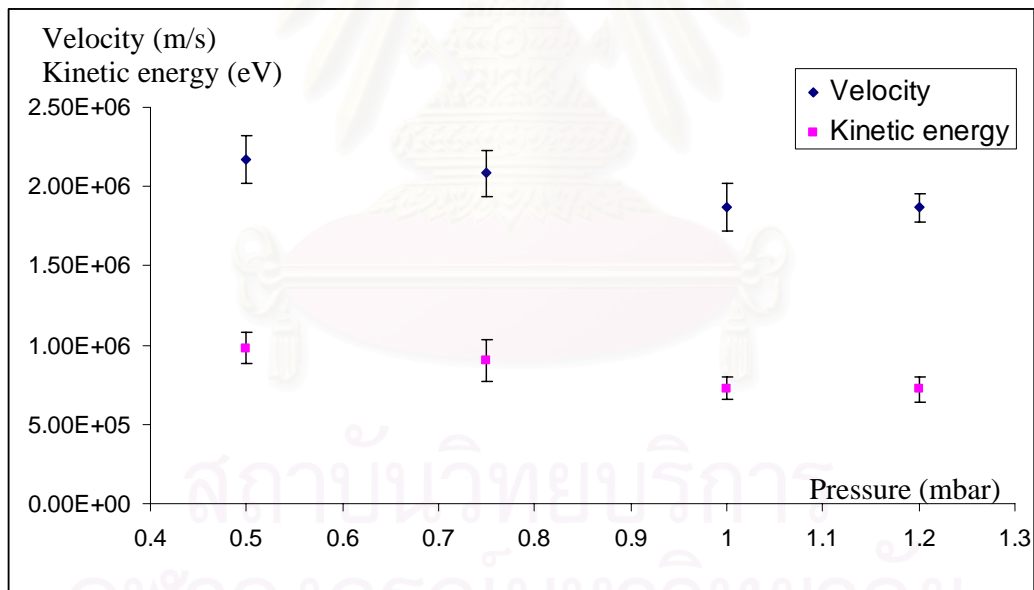
Figure 4.12: Plots showing the variation of ion velocity and energy with operating

argon gas pressure for the 19 cm anode length**.**
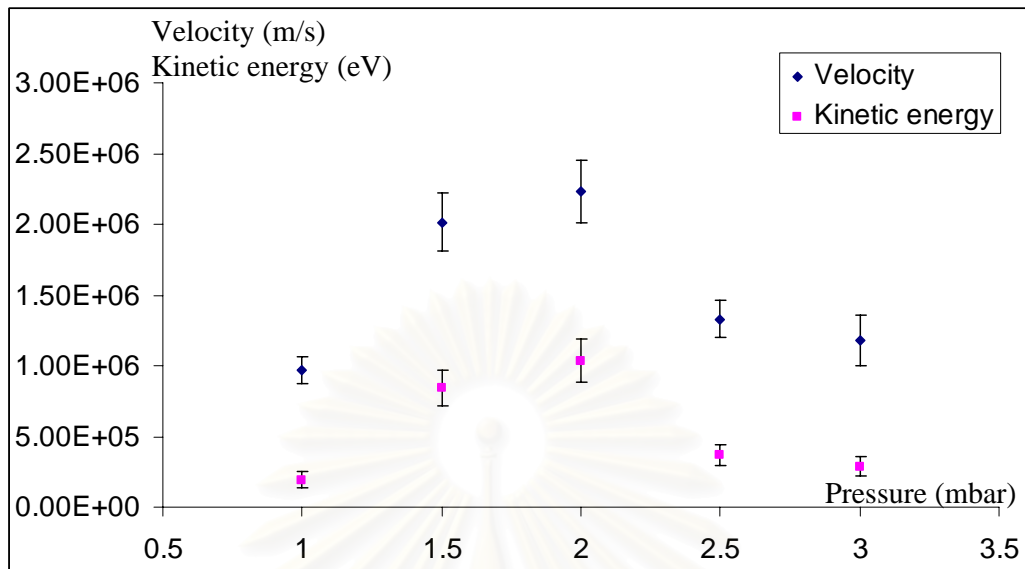
Figure 4.13: Plots showing the variation of ion velocity and energy with operating argon gas pressure for the 10.5 cm anode length.
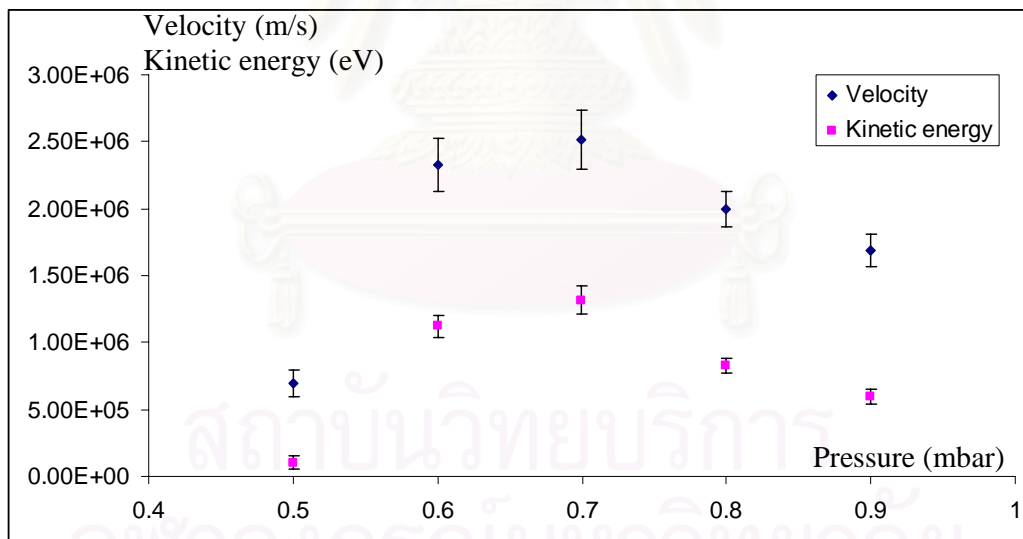
Figure 4.14: Plots showing the variation of ion velocity and energy with operating argon gas pressure for the 19cm taper anode.
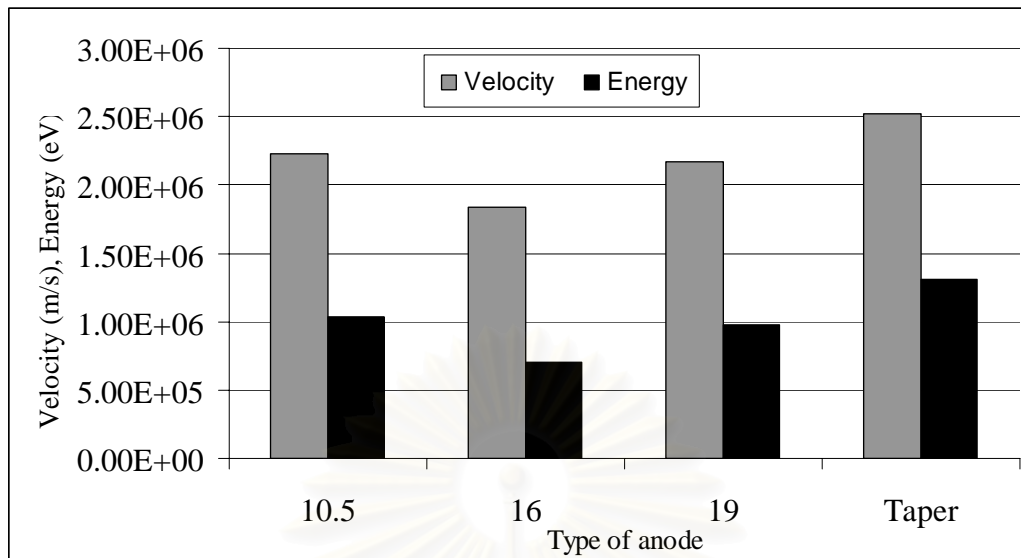
Figure 4.15: Bar chart showing a comparison of maximum ion velocity and energy for different type of anodes.

It is interesting to note that for each type of anode there are operating conditions that give maximum ion velocity and energy. From Figure 4.15, it can be seen that the taper anode produces highest ion energy around 2.52 MeV. The taper anode is able to produce high energy ion at higher pressure of 0.7 mbar where the longer taper anode produces high energy ion at much lower pressure. An analysis of this result with the simulation model will be discussed in Chapter 5.

4.4 Experiment IV: Determination of Ion beam Charge Density

The objective of this experiment is to investigate the relationship between the ion density and charge density produced at different operating conditions. Again, the experimental set up resembles that in Figure 4.2. The same energy input is applied where the charging voltage is 12.5kV. Argon gas at various pressures is used. Different anode shapes are similarly applied. The method for determination of charge density is described in Chapter 3. The area under the ion signal detected is used to determine the number of charge collected for the pulse fired.
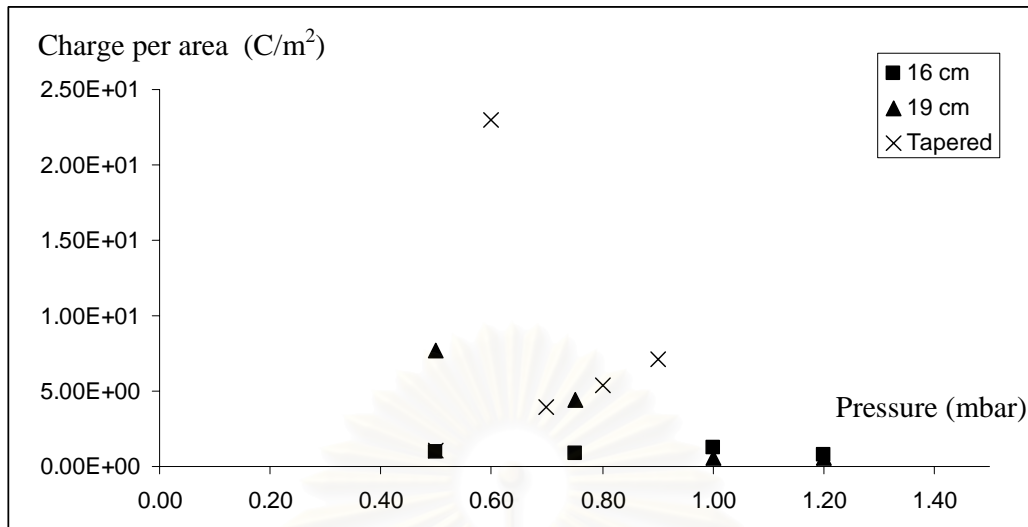
Figure 4.16: Plots showing the variation of charge density with operating argon gas pressure for three different types of anode**.**

Figure 4.16 and 4.17 show results of charge density for different operating conditions and anode types. As expected, it can be seen that the number of charge density reduces when pressure increases. This may be because of the reduction of the mean free path of ions due to more occurrence of collision when the pressure is higher. In the experiment, the energy of ion obtained is more than sufficient to travel further then the distance where the ion collector probe is placed, which means the mean free path of ion is also greater than this distance in all cases.
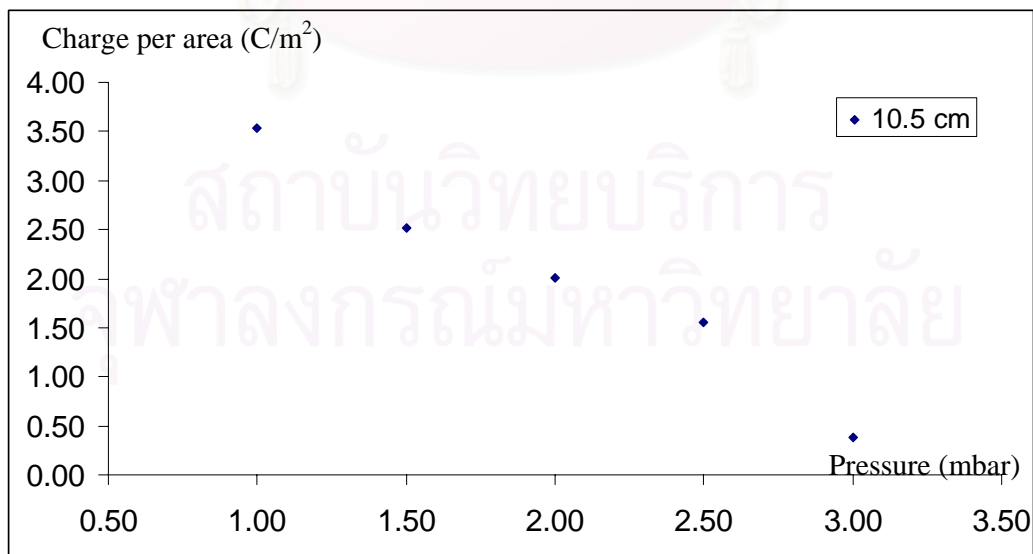
Figure 4.17: Plots showing the variation of charge density with operating argon gas pressure for anode with 10.5 cm length**.**

By assuming the ions that reach detector is mostly Ar^{+1} then the number of ion per meter of the ion density can be calculated. Figure 4.18 shows the results of ion number density for different operating conditions and anode types and the Table 4.4 shows the values. The values of ions density between 3.38×10^{19} m^{-2} to 7.17×10^{21} m-^{2} are obtained from these operating conditions. Higher ions densities are obtained from taper anode configuration.
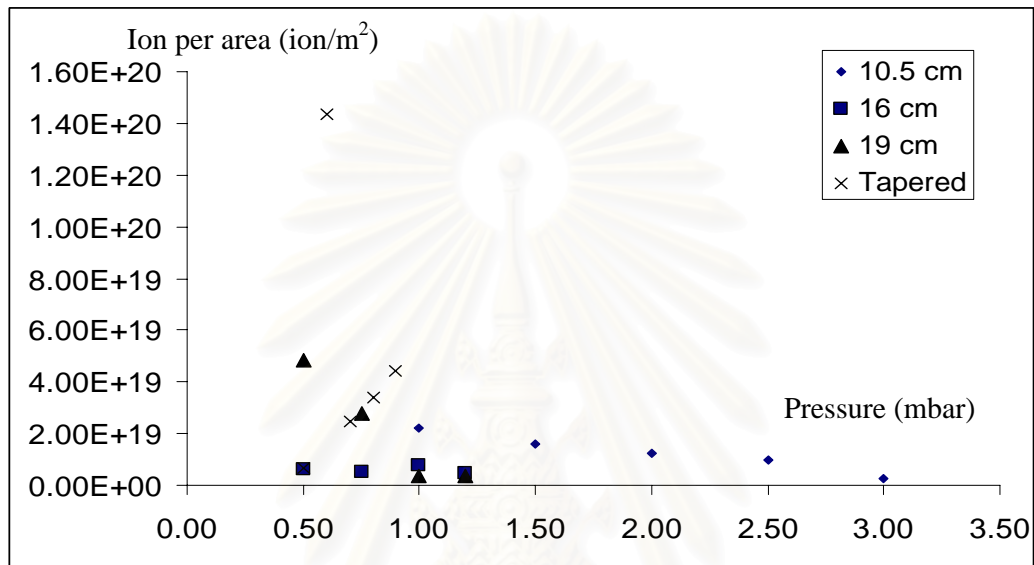
Figure 4.18: Plots showing the variation of number density with operating argon gas pressure for various anode shapes.

Table 4.4: Number of ions per area from various operating pressure and anode shapes.

Pressure	Number of ions per area (ion/m^2)			
(mbar)	10.5 cm	16cm	19 cm	taper
0.50		4.58E+20	2.41E+21	3.24E+20
0.60				7.17E+21
0.70				1.23E+21
0.75		4.18E+20	1.39E+21	
0.80				3.38E+19
0.90				2.22E+21
1.00	1.10E+21	4.97E+20	1.39E+21	
1.20		3.48E+20	1.68E+20	
1.50	7.85E+20			
2.00	6.27E+20			
2.50	4.88E+20			

4.5 Experiment V: Effect of Charging Voltage Variation to the Ion Beam Characteristics

In order to increase the energy of the ion beam and the number density of the ion, it is suspected that the initial stored energy may have significant effect. In this experiment, the initial stored energy is varied by varying the charging voltage to the 30 μF capacitor bank. The range of voltage used is from 11.5 kV to 13 kV which is equivalent to the energy range of 1.9 kJ to 2.5 kJ. The experimental set up resembles that in Figure 4.2. Argon gas at a fix 0.8 mbar pressures is used with a taper anode with 19 cm in length. For the taper anode, this condition yields the highest ion beam energy. The voltage signals for various initial stored energy are shown in Figure 4.19. Shorter axial phase period can be seen when the charging voltage increases as expected. The period varies from just more than 4 μs for 11.5 kV charging voltage to just less than 4 μs for 13 kV charging voltage. This means the speed of the plasma sheath increases as the charging voltage increases. This behavior is also expected. It can also be seen that each case produces reasonably sharp focusing peak. Figure 4.20 shows variation of the focusing voltage peaks with various charging voltage. It can be seen that peak focusing voltage increases as the charging voltage is increased. Note that the accuracy of the peak voltage is subjected to the sensitivity of the oscilloscope used. In this case a very fast oscilloscope is used to ensure the accuracy of the measurement.

Figure 4.21 shows the variation of the ion energy. It can be seen that the ion energy can be increased by increasing the initial stored energy. Figure 4.22 also shows a trend where the charge density increases with increasing initial store energy. By operating the plasma focus with taper anode at 0.8 mbar and increasing the initial stored energy to 2.5 kJ (an energy increase of 8.7%) the ion energy can be increased by 400% and 33% on the charge density.
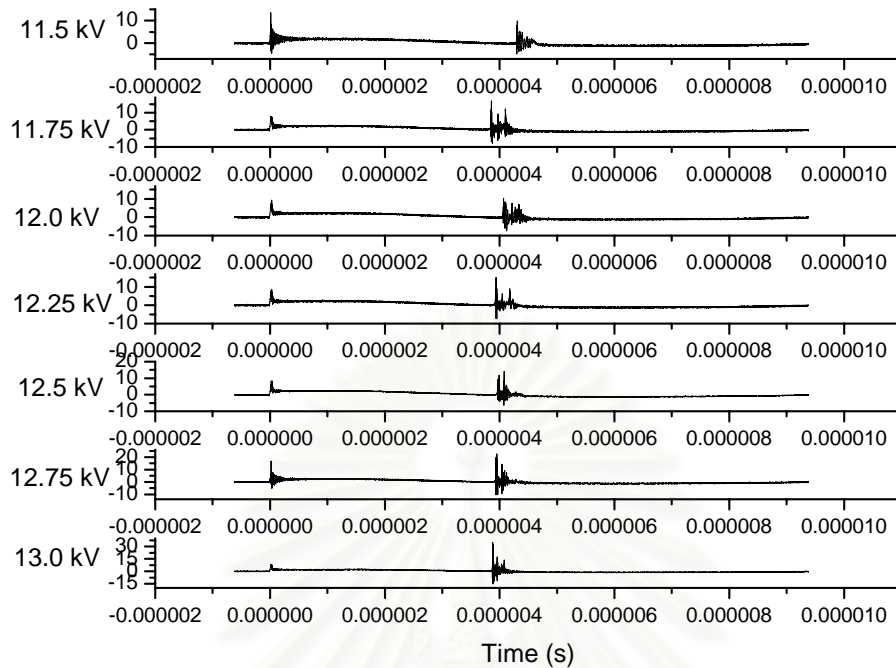
Figure 4.19: Plots showing voltage signal for various charging voltage applied to a plasma focus device operating with argon gas at 0.8 mbar and a 19 cm long taper anode.
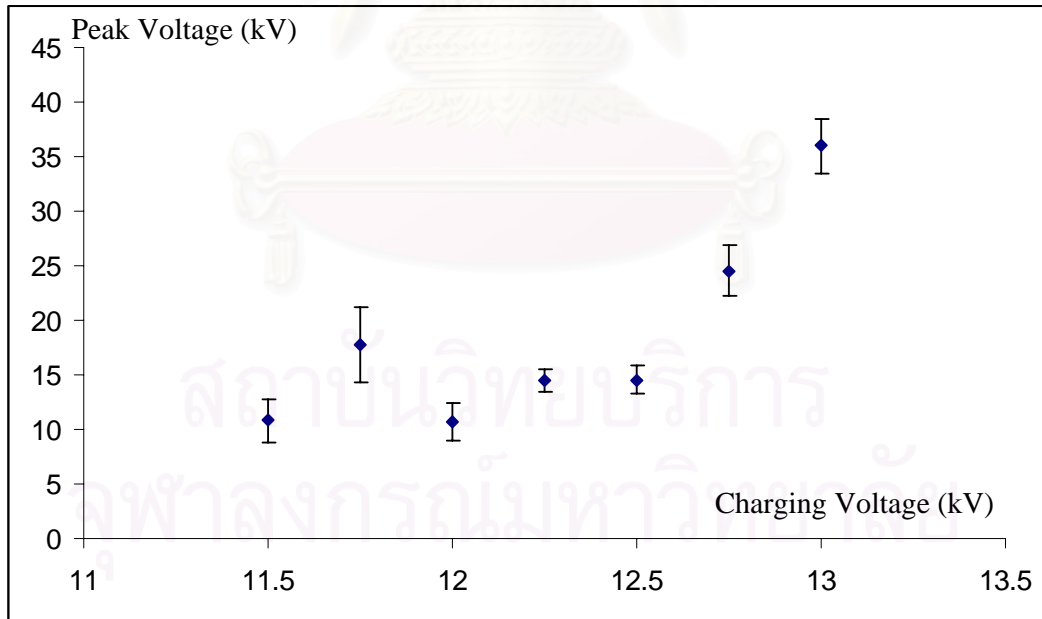
Figure 4.20: Plots showing the variation of peak focusing voltage with operating argon gas pressure for various anode shapes various charging voltage applied to a plasma focus device operating with argon gas at 0.8 mbar and a 19 cm long taper anode.
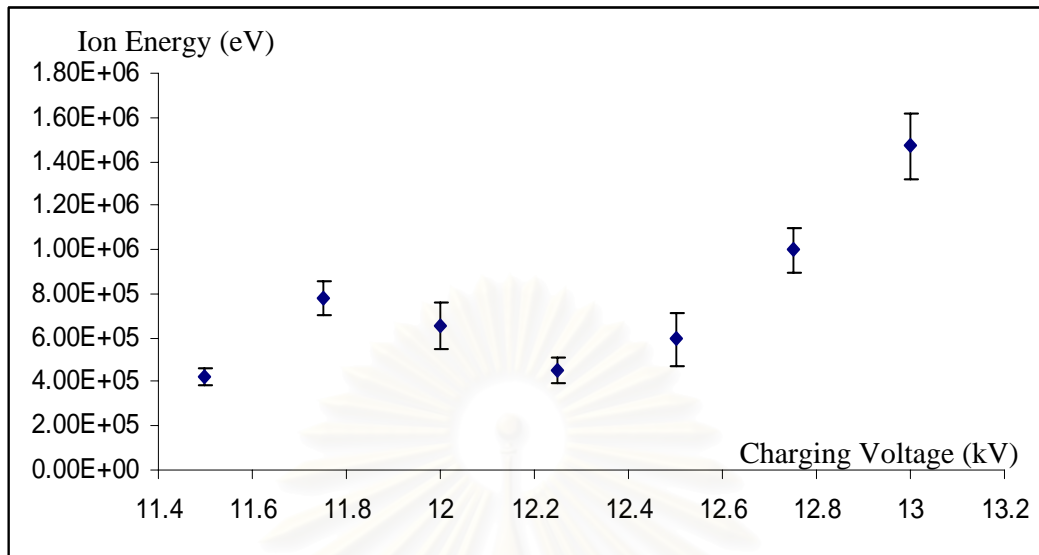
Figure 4.21: Plots showing the ion energy with various charging voltage applied to a plasma focus device operating with argon gas at 0.8 mbar and a 19 cm long taper anode.
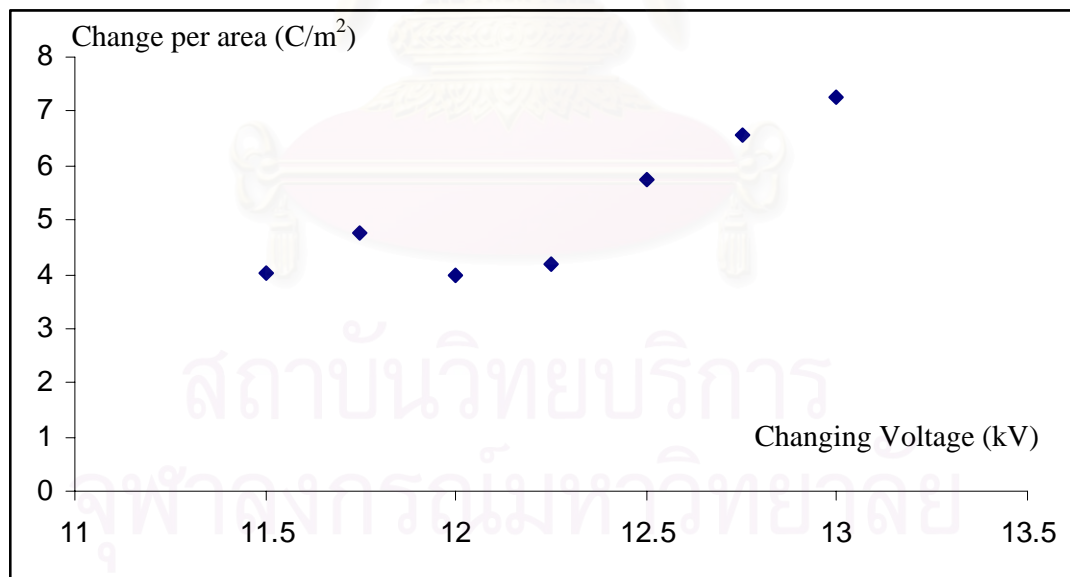
Figure 4.22: Plots showing charge per area with various charging voltage applied to a plasma focus device operating with argon gas at 0.8 mbar and a 19 cm long taper anode.

.

4.6 Experiment VI: Determination of Ion Beam Density Distribution

In this experiment, CR-39 film which is previously described in Chapter 3 is used as an ions detector. Highly energetic ions will leave tracks on the CR-39 film. By observing the track under a microscope, one can count number of ions per unit area. This should be the ion density. On the CR-39 film, a general distribution of the beam through the aperture should also be observed. The objective of this experiment is to confirm physical existence of the ions and the collimated nature of the ion beam from the focusing column of the focusing device in comparison with the electrical measurement methods.

Experimental setup for the CR-39 is shown in Figure 4.23. CR-39 is cut to about 0.5 x 0.5 cm^2 and fitted in a cylinder casing that has a pin hole with a diameter of 1.5 mm. The enclosing is placed at 12.5 cm above the end of the anode.
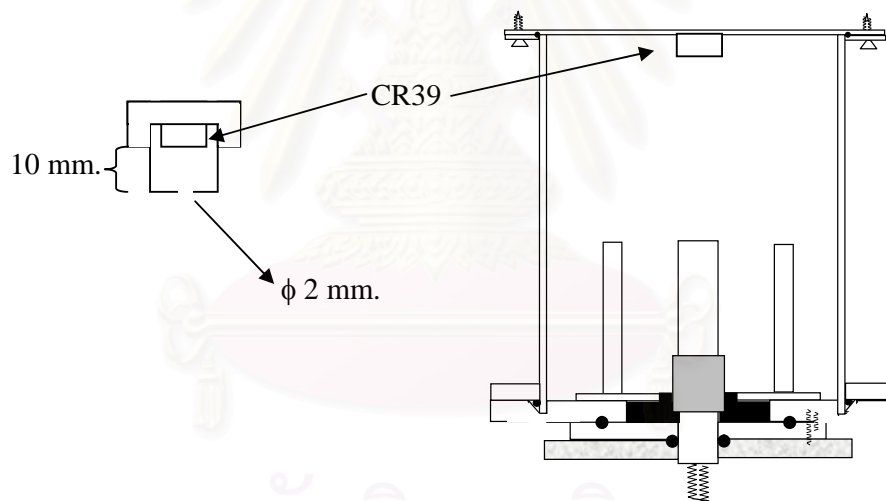
Figure 4.23: Diagram showing the setup of CR-39 film.

The experiment is carried out similar to the previous experiments by applying the same energy input where the charging voltage is 12.5kV. Argon gas at various pressures is used. Different anode shapes are similarly experimented. Again the operating conditions are chosen only that which produce focusing plasma column.

After allowing the CR-39 film to expose to the ions, the film is immersed in 6 molar NaOH solution at a temperature 70°C for 1 hour. This is to allow the solution to

etch the CR-39 film. Afterward, a light microscope Olympus Model BX-51 is used to observe the tracks or holes on the surface created by ions at x200 magnification. Figure 4.24 is a picture of unexposed CR-39 taken by the light microscope at x20 magnification. A flat smooth surface can be observed.
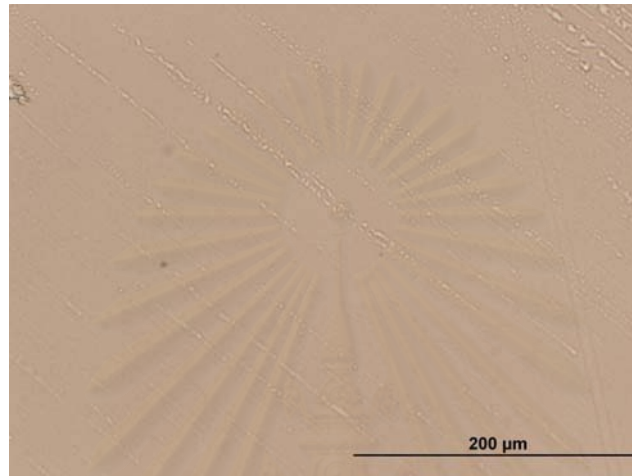
Figure 4.24: Photograph of unexposed CR-39 film taken by BX-51 light microscope at x20 magnification.
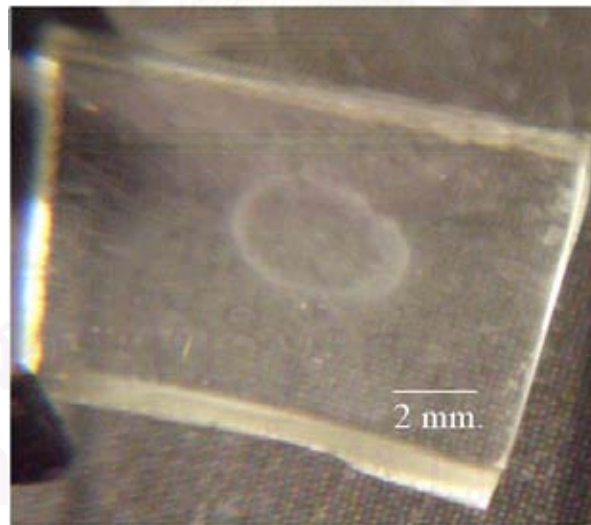
Figure 4.25: Photograph of CR-39 films that has been exposed to ions from a plasma focus operating with 16 cm long anode at 0.5 mbar operating pressure taken by a digital camera.

Figure 4.25 shows a typical ion tracks distribution on the surface of a CR-39, in this case the CR-39 has been exposed to ions from a plasma focus operating with 16

cm long anode at 0.5 mbar operating pressure. With the set up shown in Figure 4.23, the diameter of the ion distribution is measured to be about 2.5 mm.

Figure 4.27 to Figure 4.29 show the distribution of the ion tracks or holes produce on CR-39 films that are exposed to ions from a plasma focus device operating with various anode shapes and various operating pressure of argon gas. It can be seen that thee are distinct variation in roughness or the density of tracks for each operating condition. By looking closely, the most dense track population can be found in accordance to the operating condition where ions are most energetic, and not necessary where the condition that the ion density determined by the electrical measurement method is maximum. Further discussion on this issue will be made in Chapter 5.
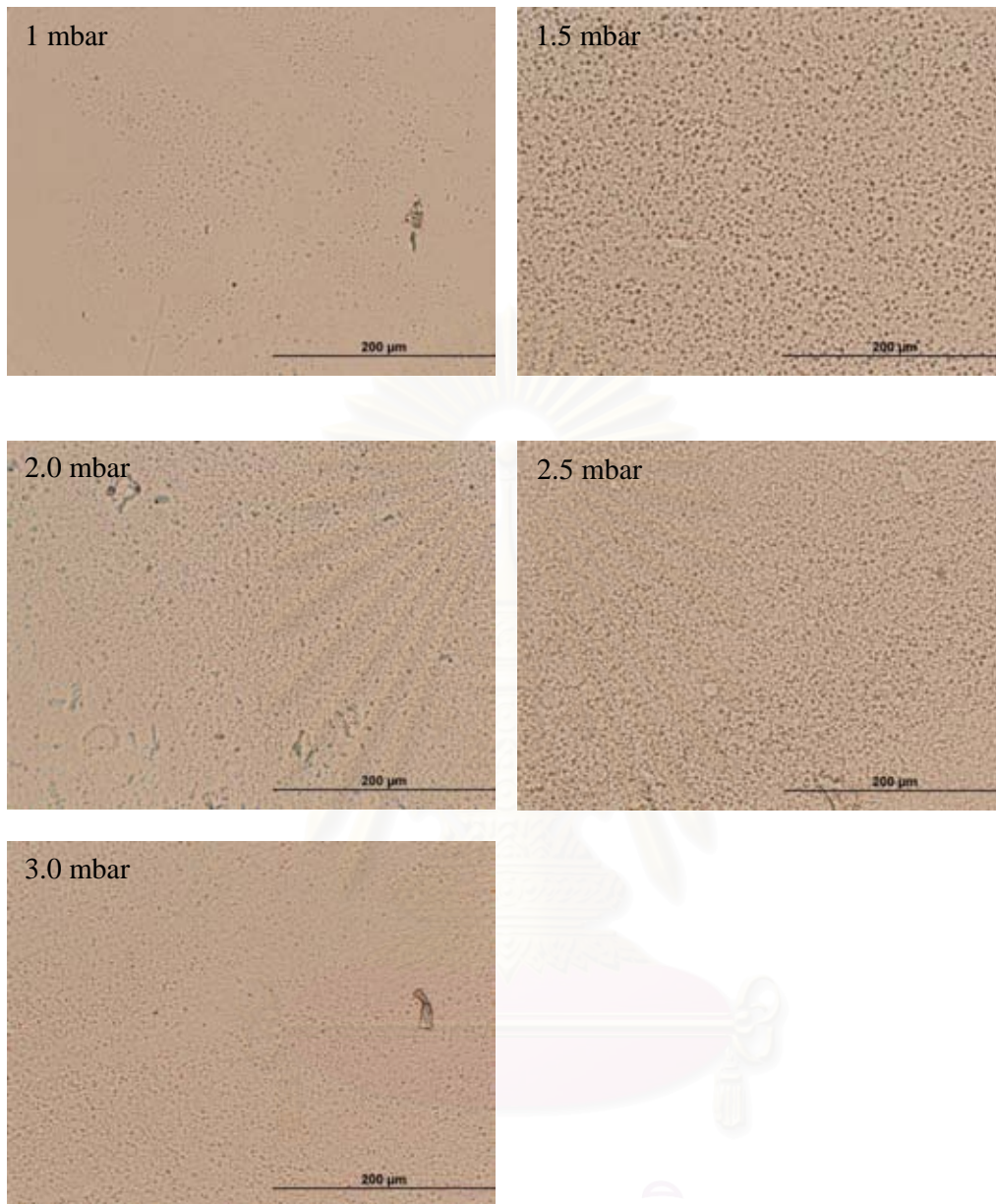
Figure 4.26: Photograph of CR-39 films that has been exposed to ion from a plasma focus operating with 10.5 cm long anode at various operating pressure taken by BX-51 light microscope at x20 magnification.
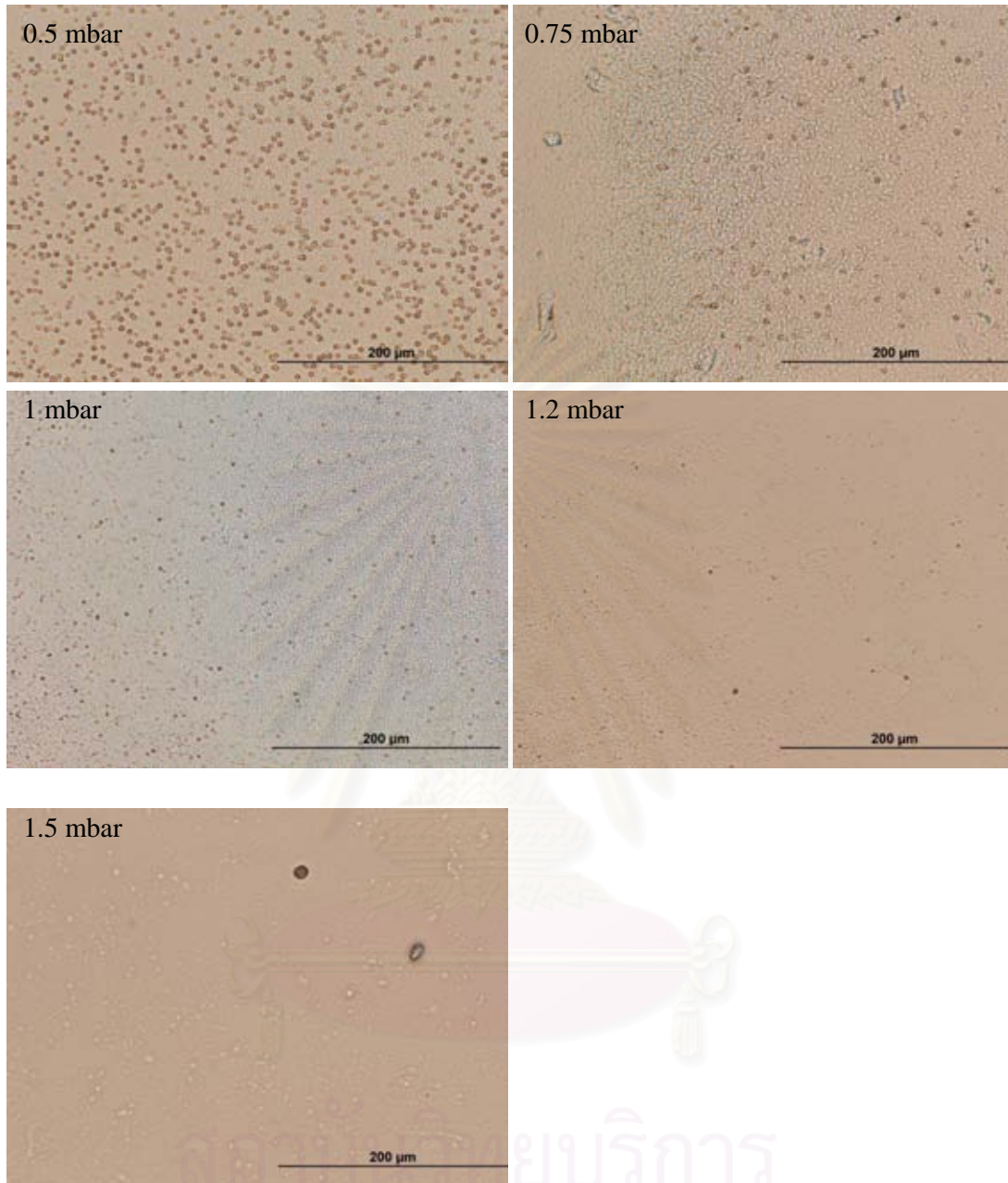
Figure 4.27: Photograph of CR-39 films that has been exposed to ion from a plasma focus operating with 19 cm long anode at various operating pressure taken by BX-51 light microscope at x20 magnification.
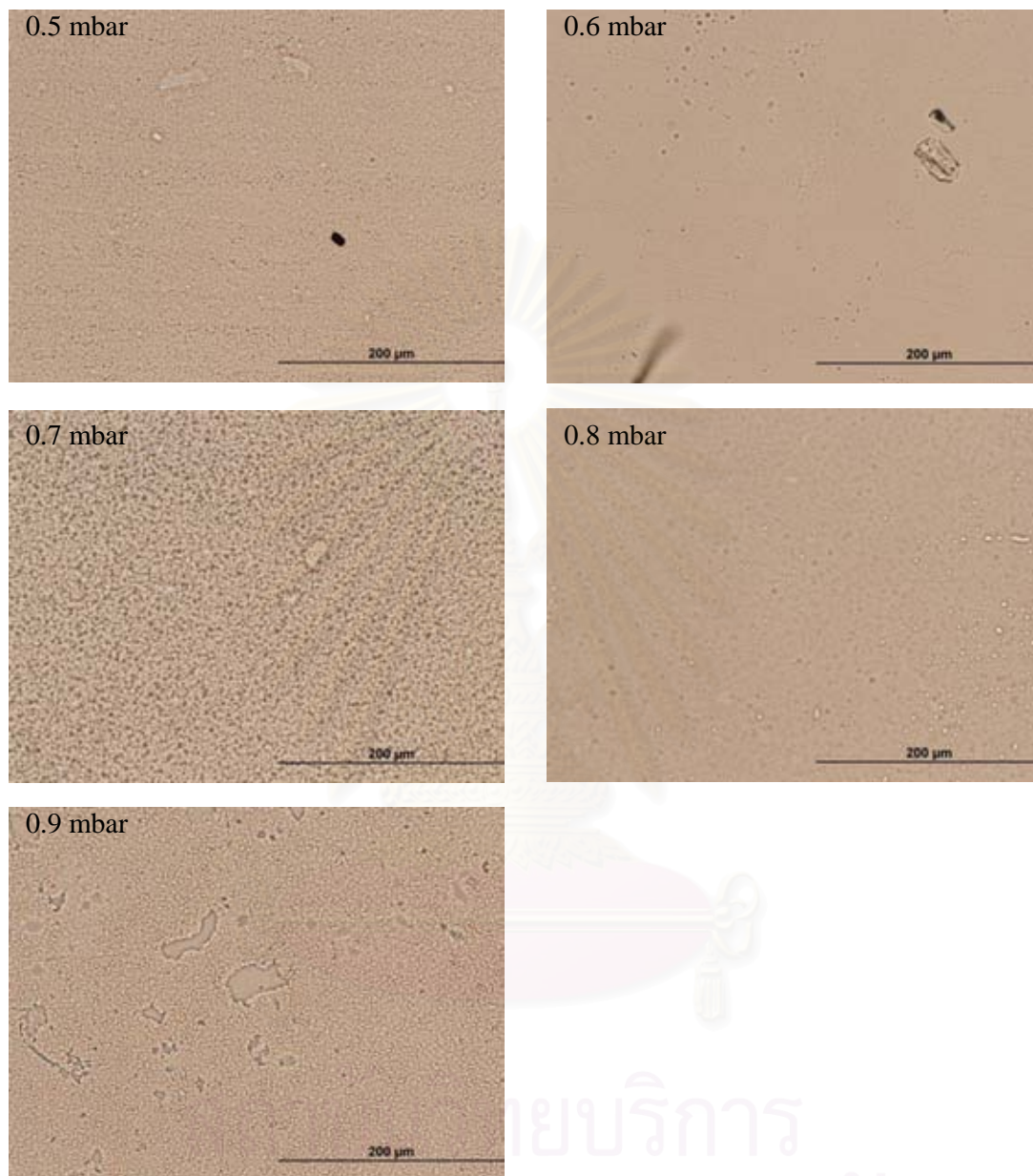
Figure 4.28: Photograph of CR-39 films that has been exposed to ion from a plasma focus operating with 19 cm long taper anode at various operating pressure taken by BX-51 light microscope at x20 magnification.
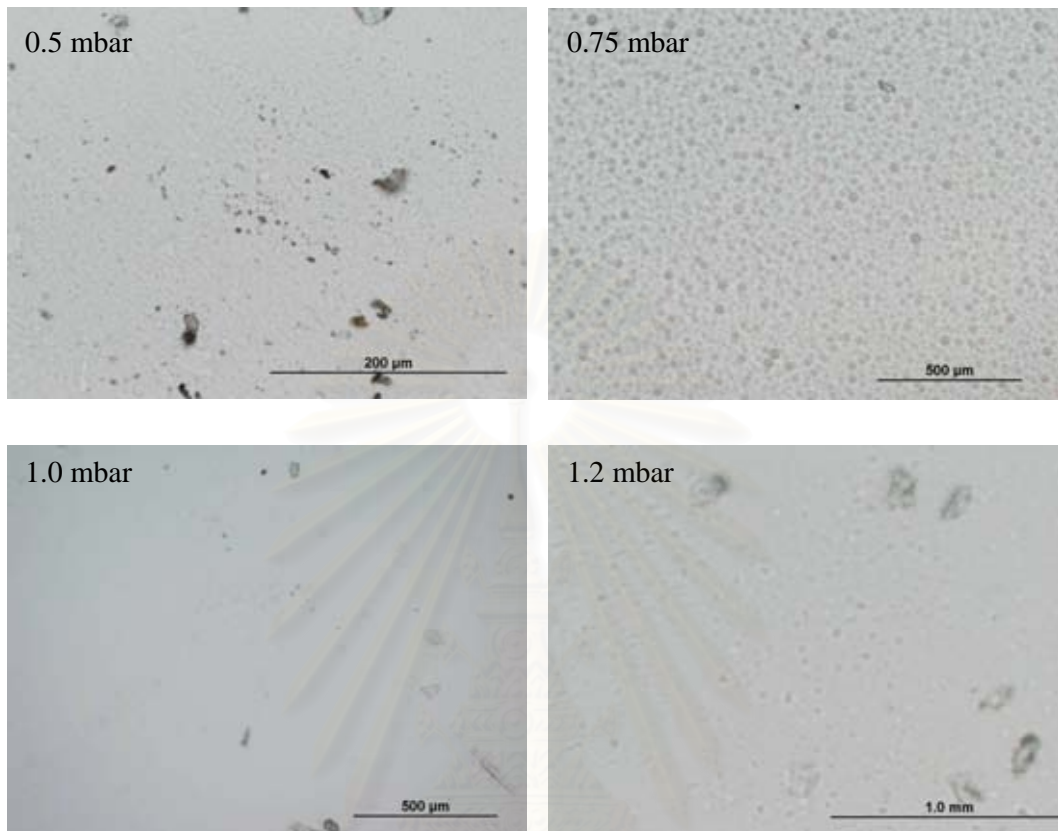
Figure 4.29: Photograph of CR-39 films that has been exposed to ion from a plasma focus operating with 16 cm long anode at various operating pressure taken by BX-51 light microscope at x 20 magnification.

CHAPTER V

DISCUSSION

In this chapter, the results obtained in Chapter 4 will be discussed and correlated to show the contributing effects of the ion beam generation by a plasma focus device. The computational model and the simulation described in Chapter 2 will be used to support the experimental results. An attempt is made to explain the mechanism of the ion beam generation process. Finally, an optimized plasma focus operating parameters for maximizing the ion beam energy and density are presented.

5.1 Focusing Limitation

In many publications, there are reports saying that the ion beam with higher energy from plasma focus device can be produced when the plasma sheath pinches [3,4,20,21,22,23,25,24,26,30,50]. The plasma column is formed during the final focusing phase. As mentioned, in Chapter 2, a plasma jet can also be produced [34] but it does not require the focusing mechanism. It is therefore believed that the mechanism for generating high energy ion beam happens or associates with the focusing phase. In the experiments, it has been shown that not all operating conditions produce focusing voltage peak which represent the final focusing phase as described in Chapter 4. A range of successful operating condition for focusing has been determined using the simulation by Lee S.[51] where a constant factor that shows the limiting condition for focusing is presented. The factor is ALT factor (used in the simulation) which is the ratio of the characteristic time t_0 to the total transit time which are component in the axial and the radial phase represented by t_a and t_r respectively. Where,

$$t_a = \left[\frac{4\pi^2 \left(b^2 - a^2 \right)}{\mu \ln(\frac{b}{a})} \right] \frac{\sqrt{f_m}}{f_c} \frac{z_0}{\left(I_o / \sqrt{\rho} \right)},$$

(5.1)

and

$$t_r = \frac{4\pi}{[\mu(\gamma+1)]^{\frac{1}{2}}} \frac{\sqrt{f_{mr}}}{f_c} \frac{a}{\left(I_o/a/\sqrt{\rho}\right)}.$$

(5.2)

These equations can be derived similarly from the model described in Chapter 2 where,

      a : radius of anode

      b : distance from centre of anode to cathode

      z_0 : length of anode

      I_0 : peak current

      ρ : density of ambient gas at operating pressure in plasma focus tube

      f_m : mass factor in axial phase

      f_c : current factor

      f_{mr} : mass factor in radial phase

      γ : specific heat for fully ionized = 1.3.

A relationship of ALT with pressure for different anode length can be determined and shown in Figure 5.1. Results from Experiment I are shown in Figure 4.5 to Figure 4.7, the equivalent ALT ratio is between 0.525 and 0.8. This is shown as a shaded region in Figure 5.1.
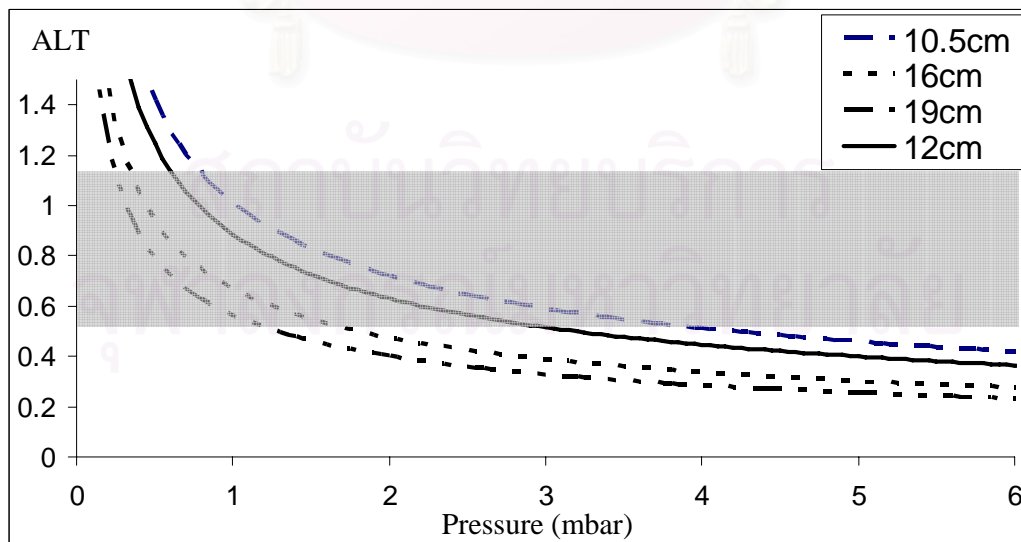
Figure 5.1: Graph showing relationship between ALT ratio and operating pressure of argon gas for different anode lengths.

Here, it can be seen that the longer anode will have a more limited operating pressure range than the shorter anode. If one needs to operate the plasma focus at a low pressure then the longer length of anode is preferable. On the other hand, for higher pressure operation, it may not be possible to reduce the length of the anode more than 5 cm as the current configuration uses a glass insulator of that length for initiating the breakdown phase. Also, it may not be preferable to operate at a higher pressure as the energy of the ion and the density of ion at a given distance will be greatly reduced due to the collision process, hence the reduction of its mean free path. This effect shall be confirmed later on in the chapter.
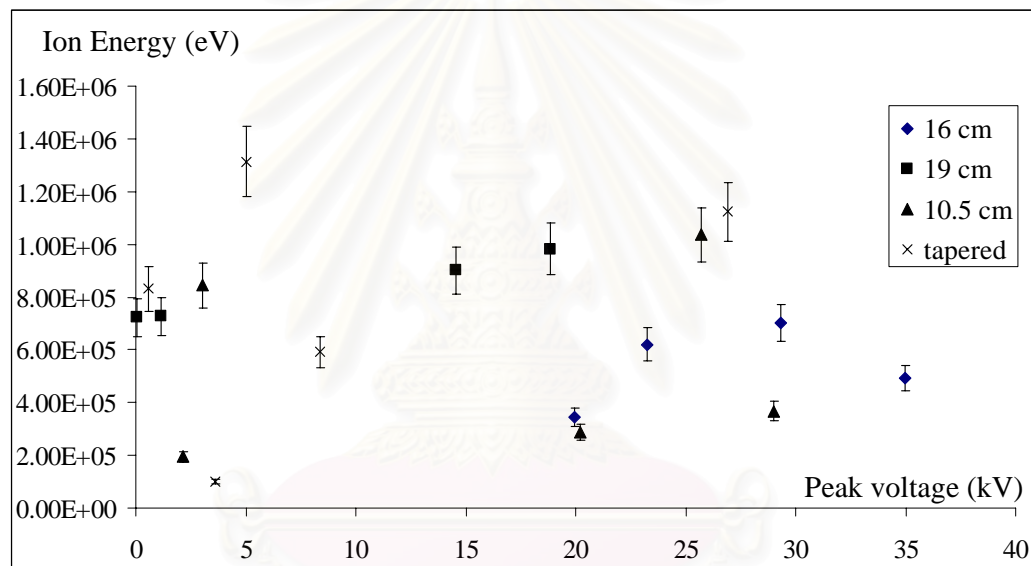
Figure 5.2: Plots showing a relationship between the focusing voltage peak and the ion energy for different anode types.

5.2 Ion Energy and Energy Transferred into Plasma

Experiment I-III in Chapter 4 are designed to give results that show contributing factor to the production of ion beam and its characteristics. In Experiment I, the average speed of plasma sheaths during the axial phase are determined. It can be seen that in different cases of the anode shape, the relationship between the average speed and the operating pressure can be established and consistent as the average speed of the plasma sheath decreases when the operating pressure increases. The simulation of the model carried out also produced similar

result with the same trend, which is expected. In the simulation, average speed is calculated by z_0/t_a. Therefore, t_a will vary with root of the density for the same discharge current. Density of gas in the plasma focus device is also proportional to the pressure by the relation $\rho = PM/RT$, where P is the operating pressure, M is molecular weight of the operating gas, R is the gas constant and T is ambient temperature.

In Experiment II, it is suspected that the strength of the voltage during the focusing phase or the peak voltage would be contributing factor for the acceleration in the ion beam. Therefore, the variation of the peak focusing voltage and pressure is examined. From Figure 4.9 and Figure 4.10, it can be seen that the voltage peaks for anode length 16 cm and 19 cm decrease when the pressure increases with exception of the taper anode where the highest peak voltage was recorded at the pressure of 0.8 mbar and 2.5 mbar for the anode length of 10.5 cm.

By examining the energy of the ions produced under these conditions from Figure 4.11, we may say that the speed of the plasma sheath may be the only factor contributing to the quality of the focusing column but not directly to the ion beam production. Although, it may has effect on the characteristic of slower plasma jet.

In Experiment III, the velocities of the ions are measured and the energies of the ion are determined when the plasma focus is operated with various pressures. It is interesting to see that whether the calculated energy transferred into the plasma during its development has any correlation with the energy of the ions produced. Figure 5.2 to 5.4 show comparative plots of the ion energy and the energy transferred into the plasma for different anode configurations. It can be seen that there is a clear correlation between these two results for those three cases. Figure 5.5 shows plots of trend between the ion energy and the energy transferred into the plasma. The trends show that the ion energy can be increased if there are more energy transferred into the plasma for each case of the anode shape. However, for each case of the anode, the maximum ion energies are also dependent on the optimum operating pressure. Chapter 2 explains the parameters involve in the energy transferred into the plasma according to the model. Equation 2.10 gives the relationship between the plasma current I_p and the plasma inductance L_p where the plasma inductance depends on the mass ratio Γ and the physical parameters of the plasma focus which are a, b and the distance that the plasma sheath has traveled z, shown in Equation 2.5. These

parameters are device specific therefore it is expected to have different values of energy transferred into the plasma for each device configuration experimented. Since the anode radius *a* and range from center of the anode to cathode *b*, were not changed in the experiments then the contribution for the variation in the results is from the plasma speed *dz/dt* and the mass ratio *Γ*. These two factors are pressure dependent as well as the initial stored energy or the charging voltage as shown in Figure 5.3 to 5.5 and Figure 5.7. It may be initially conclude that the variables that affect the ions energy are the physical parameter and the efficiency of the energy that the device is able to transfer from the stored energy into the plasma and not the peak focusing voltage that it produced as shown in Figure 5.2.
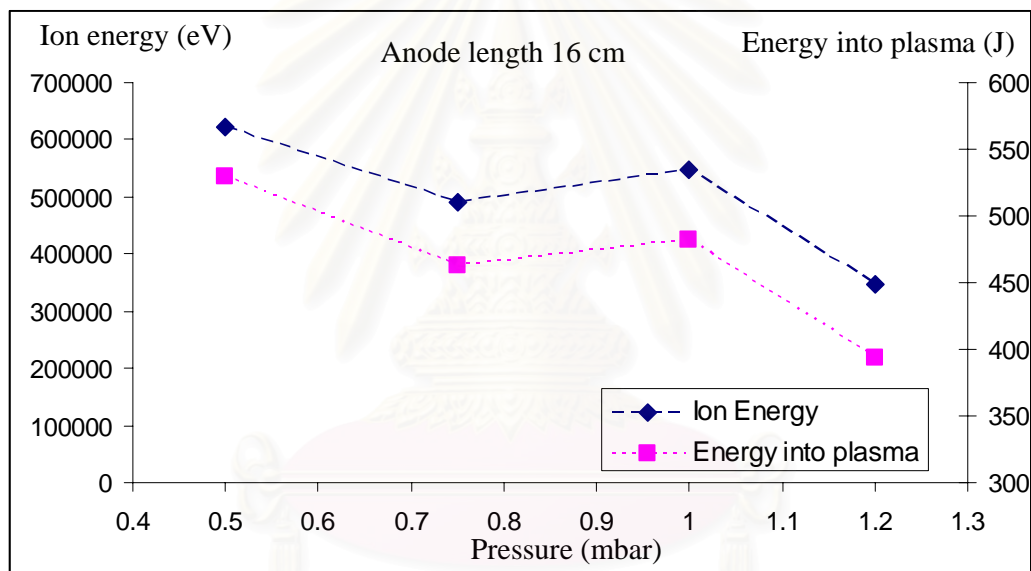
Figure 5.3: Plots showing a comparison of a relationship between ion energy with pressure and the calculated energy transferred into plasma with pressure for the anode length of 16 cm.
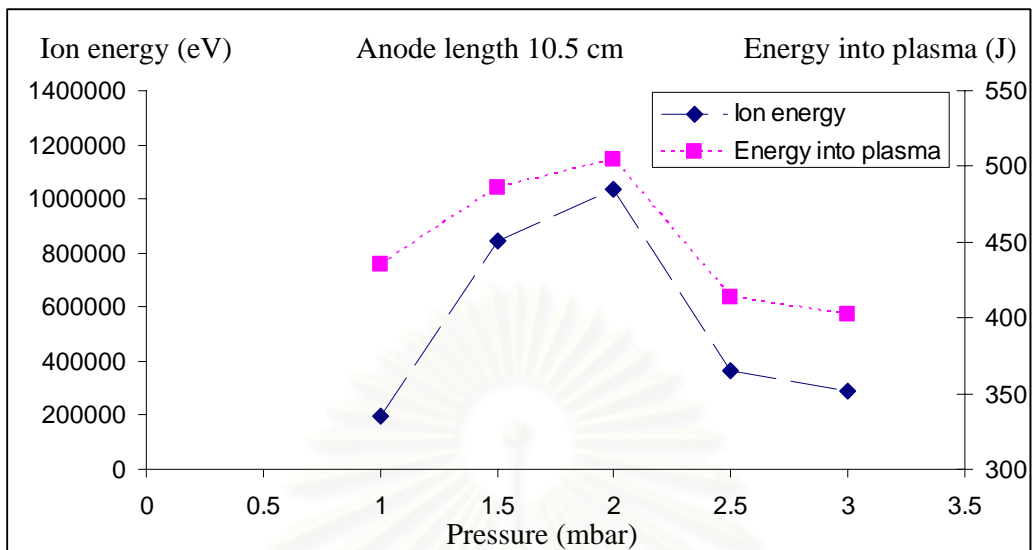
Figure 5.4: Plots showing comparison of relationships between ions energy with pressure and the calculated energy transferred into plasma with pressure for the anode length of 10.5 cm.
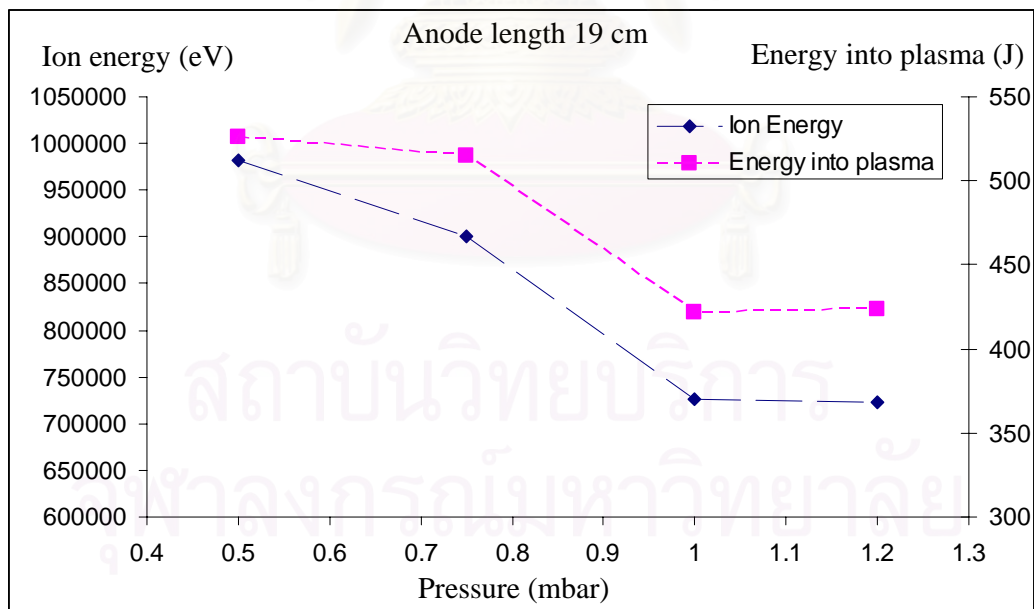
Figure 5.5: Plots showing a comparison of relationships between ions energy with pressure and the calculated energy transferred into plasma with pressure for the anode length of 19 cm.
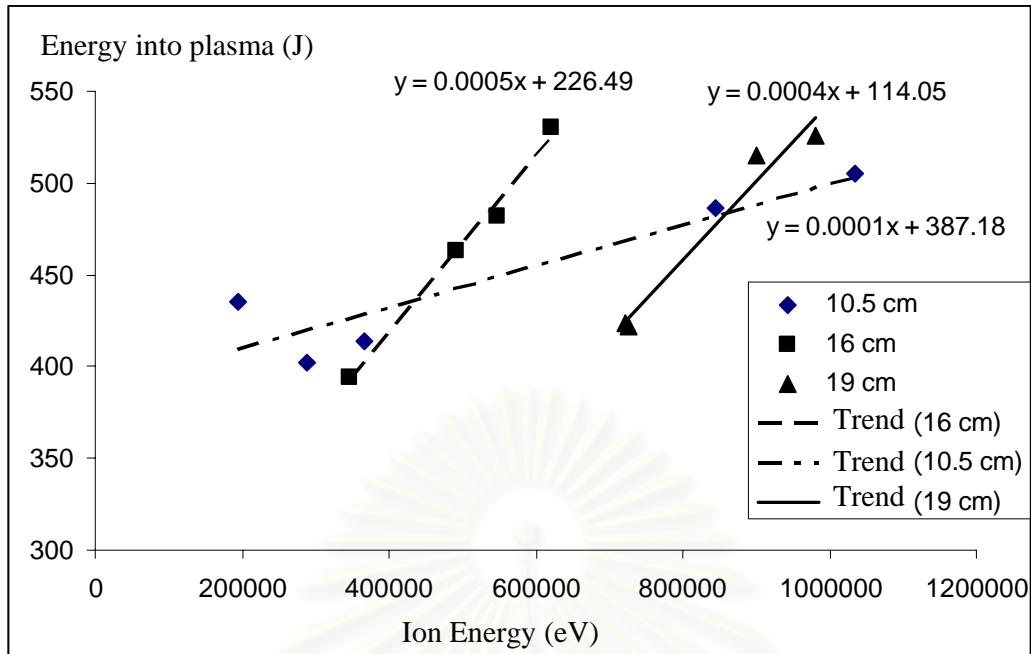
Figure 5.6: Plot showing correlations between the energy transferred into plasma and the ions energy for various anode shapes.

From Figure 5.6, the correlation between the energy transferred into plasma (E_P) and the ion energy (E_i) for the anode length of 10.5 cm, 16cm and 19 cm can be fitted with a linear graph of $E_i = 0.0001E_p + +387.18$, $E_i = 0.0005E_p + 226.49$ and $E_i = 0.0004E_p + 114.05$, respectively. The gradient of the graph represents the ratio of the energy transferred into plasma and the energy that the ions have. If the gradient is high then the configuration requires more energy transferred into the plasma to produce high energy ions. In this case, the configuration with 10.5 cm anode length produces ions with higher energy of more than 800 keV with less energy transferred into the plasma. Also from this plot, the y-axis interceptions can give us the minimum energies that should be transferred to the plasma to produce the ion beam.

From Figure 5.7, it can be seen that the ions energy varies with the initially stored energy as the initially stored energy increases the ions energy also increases. This result supports the initial conclusion that is described in earlier paragraph.
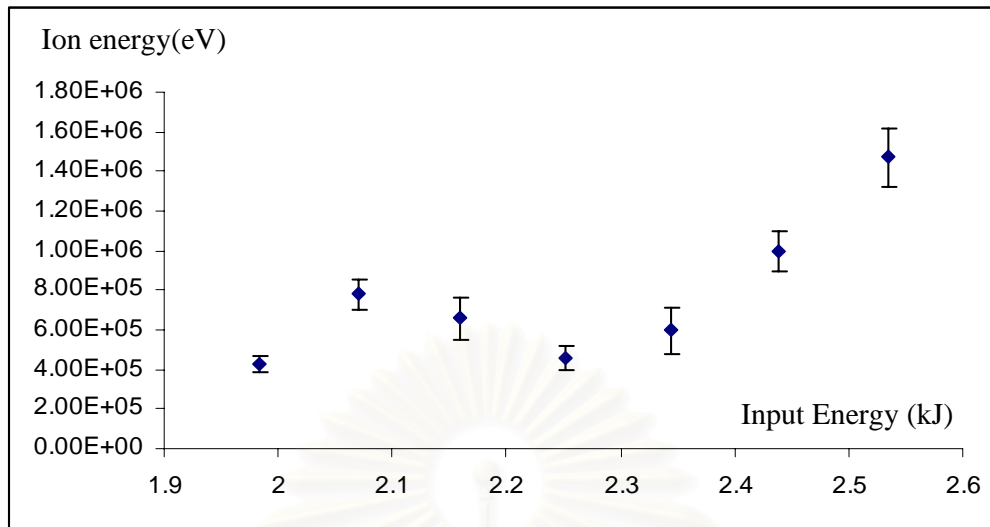
Figure 5.7: Plot showing a relationship between initially stored energy and the ion energy for taper anode of 19 cm length and operating with 0.8 mbar argon gas.

5.3 Ion Density and Energy Transferred into Plasma

Another important characteristic of the ion beam is the ion density. In this section the comparison of the relationship between the ions density and the input energies, that are obtained by changing the charging voltage, and the variation of the energy transferred into the plasma with the input energy is made. Figure 5.8 shows this comparison of the result from Experiment III and V It can be seen, as expected that, the energy transferred into the plasma can be increased when the energy input is increased. It is also interesting to see that the number of ion density also varies with the input energy similarly to the energy transferred.

By increasing the initially stored energy, the amount of the energy transferred into the plasma is also increased. As discussed earlier, this means that the ions energy increases. More ions are then expected to reach the probe which will contribute to the increase in the ion number density. Figure 5.9 shows a correlation between the ion density and the energy transferred into plasma and for the taper anode length of 19 cm operating with 0.8 mbar argon gas. The y-intercept of this linear relationship is the minimum energy transferred to produce ions that can just reach the ion collector probe at a fixed distance. In this case, the energy transferred is 328 J. The ions that have mean free path less then the distance of the probe (set at 25cm) is 350 keV.
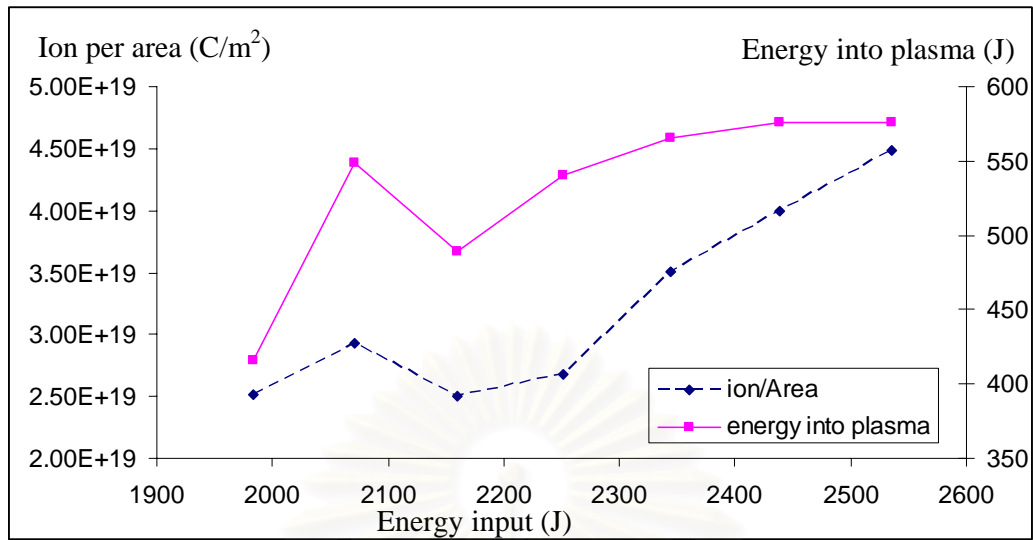
Figure 5.8: Plots showing a comparison of relationships between density of ion with the energy input and the calculated energy transferred into plasma with the energy input for the taper anode of 19 cm length operating with 0.8 mbar argon gas.
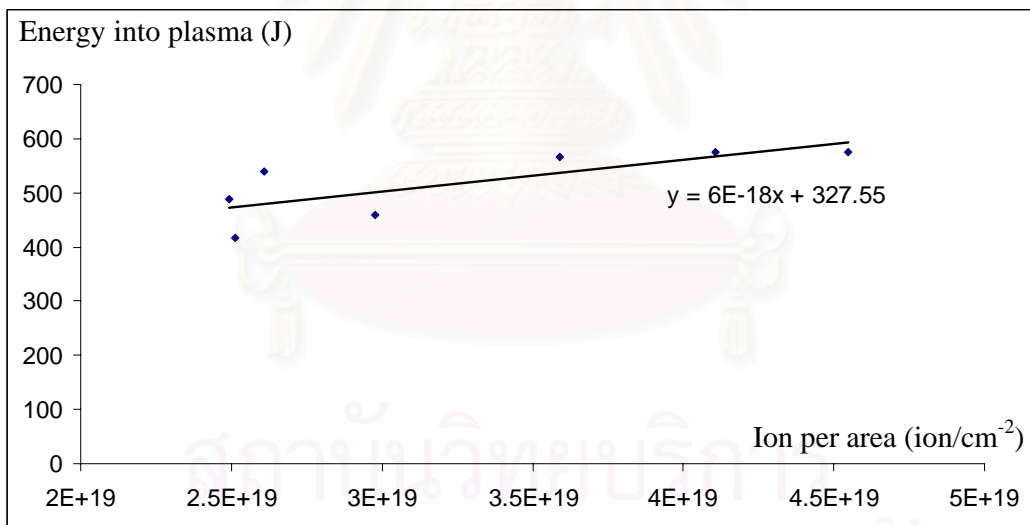
Figure 5.9: Plot showing correlations between the ion density and the energy transferred into plasma and for the taper anode length of 19 cm operating with 0.8 mbar argon gas.

5.4 Maximizing Ion energy and Ion Density

The number of experiments carried out as described in Chapter 4 has demonstrated that characteristic of ions produced can be varied according to different operating and physical parameters of the plasma focus. Table 5.1 gives an overall picture of the operating condition tested.

By taking a plasma focus device with an anode length of 16 cm as a standard (operating at 1 mbar), it can be seen that others configurations produce ions with various energies and densities. More than 50% increase in ions energy and can be achieved for the same charging voltage of 12.5 kV or the initially stored energy of 2.25 kJ. The maximum improvement of 89.4%, in these cases, is from the 10.5 anode configuration at a higher operating pressure of 2 mbar. For the 19 cm anode length, 78.7% improvement is achieved when operate at lower pressure of 0.5 mbar. It is interesting to note that the higher iosn energy is obtained when the ratio of the initially stored energy and the energy transferred into the plasma is more than 20%.

As discussed in previous section, even higher ion energy can be produced by increasing the initially stored energy or the charging voltage. An experiment with the taper anode configuration shows that 167.8% increase is obtained when having a charging voltage of 13 kV (discharging a current of 163.22 kA) or increase the initially stored by 12.4%. Again the percentage of the energy transferred into the plasma is 22.8%.

The ion density detected can be increased more than 300% for the longer anode length configuration (19 cm and taper 19cm). The effect is coming from the lower operating pressure, therefore more ions reach the ion collector probe. This means by operating with a longer anode length at a lower pressure the range of the ion can be increased. Ultimately, to maximize both ion energy and the ion density, a plasma focus device should be operated at a lower pressure and longer anode length that is within the limit of focusing criteria described in Section 5.1. As well as increase the initially stored energy by using largercharging voltage or lager capacitance value of the capacitor bank.

The shape and length of the anode may also play important part for the ions energy and ion density variation. Figure 5.10 shows diagrams of different configurations of anode with the line of force acting on the plasma sheath. It can be seen in Table 5.1 that, in general, the taper anode has a high increase in the ion

density of more than 150% to 350%. It is therefore led to believe that, by having a taper configuration, the line of force that produces the plasma sheath dynamics as described in Chapter 2 is more favorable for ion beam production than other configurations. For example, 19 cm anode length will have the force pushing the plasma more outwards; on the other hand, 10.5 cm length will have the driving force pushing inwards causing more compression and collision. This makes the taper configure behaves in manner that promote forward ion movement as well as the focusing action. Therefore more ions are directed in the z-direction giving a higher value of ion density detected by the ion collector probe. Although best ion energy gain comes from other two configurations for the same initially stored energy is applied, which may be related to the plasma sheath speed and the focusing process which are faster in the case of 19 cm and the focus is strong in the case of 10.5 cm anode length.
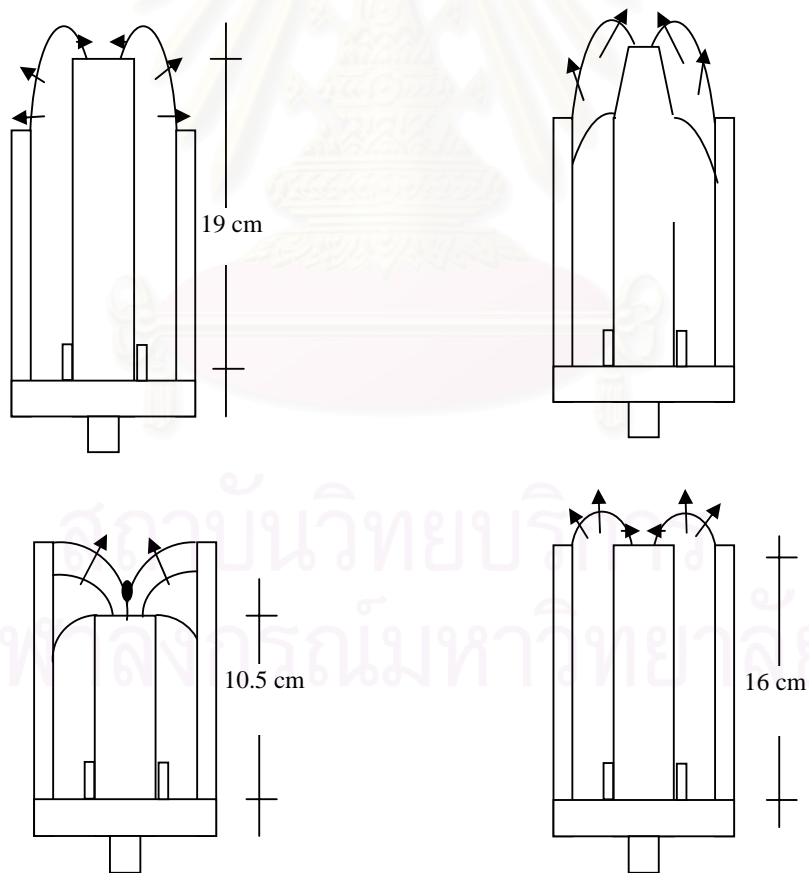
Figure 5.10: Schematic diagram showing different configurations of anode with the line of force acting on the plasma sheath.

Table 5.1: Summary of plasma focus operating parameters and ion beam characteristics

Type of anode	Pressure (mbar)	Charging voltage (kV)	Energy in put (kJ)	Current (kA)	Inductance (nH)	Ion per area (ion/m^2)	Ion energy (eV)	Energy into plasma (J)	%Ion per area	%Ion energy
10.5 cm	1.0	12.50	2.25	160.55	143	2.21E+19	1.95E+05	435 (19.3%)	122.11	-64.48
	1.5	12.50	2.25	155.41	147	1.57E+19	8.44E+05	486 (21.6%)	57.79	53.73
	2.0	12.50	2.25	163.72	140	1.25E+19	1.04E+06	505 (22.4%)	25.63	89.44
	2.5	12.50	2.25	164.03	140	9.75E+18	3.67E+05	414 (18.4%)	-2.01	-33.15
	3.0	12.50	2.25	164.72	144	2.39E+18	2.88E+05	402 (17.8%)	-75.98	-47.54
16.0 cm	0.5	12.50	2.25	150.97	154	9.15E+18	6.22E+05	530 (23.6%)	-8.04	13.30
	0.75	12.50	2.25	157.68	141	8.36E+18	4.91E+05	463 (20.6%)	-15.98	-10.56
	1.0	12.50	2.25	157.59	141	9.95E+18	5.49E+05	482 (21.4%)	0.00	0.00
	1.2	12.50	2.25	159.89	137	6.96E+18	3.46E+05	394 (17.5%)	-30.05	-36.98
19.0 cm	0.5	12.50	2.25	156.21	154	4.81E+19	9.81E+05	526 (23.4%)	383.42	78.69
	0.75	12.50	2.25	153.11	147	2.79E+19	9.01E+05	515 (22.9%)	180.40	64.12
	1.0	12.50	2.25	166.76	133	2.79E+19	7.26E+05	422 (18.8%)	180.40	32.24
	1.2	12.50	2.25	163.67	140	3.35E+18	7.23E+05	424 (18.8%)	-66.33	31.69
Tapered	0.5	12.50	2.25	154.48	148	6.49E+18	1.01E+05	-	-34.77	-
	0.6	12.50	2.25	154.48	148	1.43E+20	1.12E+06	-	1337.19	-
	0.7	12.50	2.25	154.48	148	2.47E+19	1.31E+06	-	148.24	-
	0.8	12.50	2.25	154.48	148	9.28E+18	8.31E+05	540 (24.0%)	-6.73	51.37
	0.9	12.50	2.25	154.48	148	4.44E+19	5.91E+05	-	346.23	-
	0.8	11.50	1.98	142.14	156	2.52E+19	4.24E+05	416 (21.0%)	153.27	-22.77
	0.8	11.75	2.07	150.55	141	2.93E+19	7.81E+05	549 (26.5%)	194.47	42.26
	0.8	12.00	2.16	154.39	143	2.51E+19	6.58E+05	489 (22.6%)	152.26	19.85
	0.8	12.25	2.25	154.48	148	2.68E+19	4.55E+05	540 (24.0%)	169.35	-17.12
	0.8	12.50	2.34	157.54	147	3.51E+19	5.95E+05	566 (24.2%)	252.76	8.38
	0.8	12.75	2.43	161.85	145	3.99E+19	1.00E+06	576 (23.7%)	301.01	82.15
	0.8	13.00	2.53	163.22	147	4.49E+19	1.47E+06	576 (22.8%)	351.26	167.76

CHAPTER VI

CONCLUSION

6.1 Conclusion

The objective for this research is to study further the aspect of ion production process of a UNU/ICTP Plasma Focus and to optimize the plasma focus device for better ion beam production. This includes the measurement of the ion beam characteristics by various diagnostic techniques. Furthermore, it is also important to investigate experimentally and numerically the effect of the dynamics and the energy of the plasma current sheath on the ion beam generation.

A simulation based on the snow plow model for axial phase has been used to understand the mechanism and determine the energy transfer into plasma. It is assumed that the energy transferred into the plasma focus tube has components from the inductive impedance, the work done by piston motion of the plasma and joule heating. These energies can be separated into magnetic energy and mechanical work. The energy into plasma that contributes to the magnetic energy is described by Equation 2.11. A simulation of the magnetic energy in comparison with experimental result has been done. A good fit of the results has been obtained by varying the mass factor shown in Figure 2.22. The factor is then used for the determination of possible focusing pressures for different anode configurations. The results also correspond to the experimental results which are shown by the focusing voltage peak detected by the voltage probe. It was found that ranges of pressure that standard or modified UNU/ICTP plasma focus device has a pinching of plasma or focusing are between 1 mbar to 3.5 mbar for 10.5 cm anode length and 0.5 mbar to 1.2 mbar for 16cm and 19 cm anode length. For tapered anode, it was found experimentally that the range for focusing is 0.5 to 0.9 mbar.

For experimental works, different diagnostics have been developed and tested, so that they are suitable for their respective measurements. Ion collector probe is used to detect the ion beam. Several methods have been experimented and discussed in Chapter 3. It was found that a suitable ion collector probe requires a negative bias of 18 V and the detection areas are 3.14×10^{-9} cm^2 and 3.84×10^{-5} cm^2 for the near and far

probe respectively. These probes gave suitable ion beam signals. The probe positions were chosen to be at 28 cm and 68 cm from the end of the anode. A small 1.5 cm diameter aperture was used to collimate the ion beam. It was also found that the probes are sensitive to the EM-wave produced by the plasma focus. For the ion measurement this photoelectric effect can be eliminated as one can assume that the photons are emitted at the same time when the plasma pinches. PIN diode was also used to detect X-ray radiation to confirm the existence of these photons.

Different anode modifications on the plasma focus were made and experimented. Three lengths of cylindrical anode of 10.5 cm, 16 cm and 19 were used as well as a taper shape 19 cm long anode. For each configuration, the average ion energy and the ion density were determined where suitable assumption had been made. The results obtained are compared with the standard UNU/ICTP plasma focus with 16 cm long anode. Six different experiments had been carried out.

In Experiment I, it can be concluded that the peak of voltage signal that represents the effect of plasma pinching or the focusing reduces when the operating pressure is increased for all types and shapes of the anode. The average speed of the plasma sheath was deduced for each operating conditions and found to decrease when pressure increases. The average speeds of plasma sheath are between 3 cm/μs to 7 cm/μs..

For Experiment II, it can be concluded that the focusing voltage peaks are not linearly dependent with the change in operating pressure and therefore the speed of the plasma sheath. The focusing voltage peaks should be associated with the quality of the pinch. Experiment III further investigates the variation of ion velocity which was found to vary with the operating pressure. As the velocity of the ion associates with the energy, it was found that kinetic energy when operating with 10.5 cm long anode are between 100 keV to 1 MeV when using pressure of 1 mbar to 3 mbar. The 16 cm and 19cm long anode produce focus when the pressure is between 0.5 mbar to 1.2 mbar and 0.5 mbar to 0.9 mbar, respectively. The ion energies produced are between 300 keV to 700 keV. For the taper anode, the operating pressure range is between 0.5 mbar and 0.9 mbar which produced kinetic energy between 500 keV to 1.3 MeV.

Experiment IV explores the ion beam charge density or the ion density which were found to have charge between 0.5 C/m^2 to 25 C/m^2 for all types of anode. It can be concluded that the number of charge density reduces when pressure increases, because of the reduction of the mean free path of ions due to more occurrence of collisions when the pressure is higher. For Experiment VI, the variation of the initially stored input energy in a range of 1.9 kJ to 2.5 kJ was investigated when fixing the operating pressure at 0.8 mbar. The results show that the average speed of plasma in the axial phase, peak voltage, charge density, the energy of ion and ion density increase when the initially stored energy is large.

Experiment VI was done to confirm the amount and the energy of ion beam produced by using CR39 film. It was found that the CR38 films were attacked by the ion beam. Various depths of ion tracks can be seen though an optical microscope. The results are marginal and are difficult to count and analyze. Finally the correlations of the results are shown in Chapter 5 where it is believed that peak voltage and ion energy do not relate strongly to one another but the voltage peak does relate with the initially stored energy and pressure. The average speed of plasma sheath does not relate with ion energy but it relates with pressure.

For the overall result we believe that ion beam energy relates to the energy transferred into the plasma and the ion density relates to the initially stored energy to the capacitor bank. It has been demonstrated that more than 300 % increase in ion density and 80% of the ion energy from the original UNU/ICTP Plasma Focus configuration is obtained. The standard UNU/ICTP Plasma Focus configuration has anode length of 16 cm and optimally operating with argon gas at a pressure of 1 mbar and the initially stored energy about 2.3 kJ. The ion density of 9.95×10^{18} ions per m^2 and the ion energy of 543 keV are obtained. In comparison with UNU/ICTP Plasma Focus that operate at 0.01 to 0.8 mbar [12,17] the ion density is 3.4×10^8 cm^{-2} and ion energy are between 23 keV to 8 MeV as presented in Table 1.1. It is interesting to note that, the method of ion detection may vary due to the position and the sensitivity of the detector because of the collision of ions and possible photon from the plasma causing the photoelectric effect.

In order to obtained high Ar ion density and high Ar ion energy, 19 cm long taper anode operating with 0.8 mbar Ar gas with the stored energy of 2.53 kJ has been demonstrated to produce ions with average energy of 1.47 MeV and approximately 4.49×10^{19} ions/m^2.

6.2 Further work

From the results of the ion energy and ion density presented, the modified UNU/ICTP plasma focus can still be further improved in many aspects. The objective of improvement will depend on the intended applications. For example, as proposed by E. Learner, a plasma focus can be used as a source of electrical energy through the highly energetic and dense ion beam propelled from a nuclear fusion reaction. The fusion reaction happens during the pinching of the plasma or the focusing phase. In this case, further works needed to be done is in the scaling of the plasma focus as well as making it a repetitive source of ion beam. Another application such as a repetitive neutron source using a plasma focus could also be further investigate by using either the fusion process from the deuterium ions or using deuterium ion beam to collide with tritium target to produce 2.54 MeV or 14 MeV neutrons respectively.

Other aspect of improvement could be the extension of the numerical modeling work where the radial compression phase could be considered in more detail and to use it to predict the inductive voltage induced. The result from this simulation could then be used to find the correlation between the inductive voltage induced to the measured ion beam energy. Possible improvement could also be done on the diagnostics such as the ion spectroscopy and fast framing camera in order to observe the instabilities during the focusing phase. Finally, further work should involve the application aspect of the ion beam obtained from the plasma focus for material surface processing which is currently gaining many interests from plasma focus laboratories around the world.

REFERENCES

[1] Moshe Gai, "Production of fast neutron with a plasma focus device" ,Proceeding of science International Workshop on Fast Neutron Detectors and Applications, April, 3 - 6, 2006, University of Cape Town, South Africa.

[2] A. Patran1, R. S. Rawat, J. M. Koh, S. V. Springham, T. L. Tan, P. Lee, and S. Lee, "A High Flux Pulsed Neutron Source Using a Plasma Focus Device", 31st EPS Conference on Plasma Phys. London, Vol.28G, 28 June - 2 July 2004, pp-4.213

[3] Silva, P.; Favre, M.; Choi, P.; Dumitrescu-Zoita, C.; Chuaqui, H.; Wyndham, E. "Ion beam measurements in a small plasma focus operating inhydrogen/gas mixtures", Proceedings of the 12th International Conference ,Vol 2, (1998) pp. 595 - 598

[4] H.R. YOUSEFI, Y. NAKATA, H. ITO and K. MASUGATA, "Characteristic Observation of the Ion Beams in the Plasma Focus Device", Plasma and Fusion Research: Vol 2, (2007) S1084

[5] S. R. Mohanty, T. Sakamoto, Y. Kobayashi, I. Song, M. Watanabe, T. Kawamura, A. Okino, K. Horioka, and E. Hotta, "Miniature hybrid plasma focus extreme ultraviolet source driven by 10 kA fast current pulse" Rev. Sci. Instrum. Vol. 77, (2006) 043506

[6] I.V. Fomenkov, N. Böwering, C.L. Rettig, S.T. Melnychuk, I.R. Oliver, J.R. Hoffman, O.V. Khodykin, R.M. Ness and W.N. Partlo, "EUV discharge light source based on a dense plasma focus operated with positive and negative polarity", J. Phys. D: Appl. Phys, Vol. 37 (2004) pp.3266-3276

[7] Eberle, H Krompholz, R Lebert, W Neff, R Noll, "Plasma focus as a radiation source for X-ray lithography", Microelectronic Engineering, Vol 3, 1-4 December 1985

[8] S. Lee, V. Kudryashov 1 , P. Lee, G. Zhang, A. Serban, M. Liu, X. Feng, S.V. Springham, Feng, S.V. Springham, "SXR LITHOGRAPHY USING A HIGH PERFORMANCE PLASMA FOCUS SOURCE", 1998 ICPP&25th EPS Conf. on

Contr. Fusion and Plasma Physics, Praha, 29 June - 3 July. Vol. 22C (1998) pp.2591-2594.

[9] E P Bogolyubov, V D Bochkov, V A Veretennikov, L T Vekhoreva, V A Gribkov, A V Dubrovskii, Yu P Ivanov, A I Isakov, O N Krokhin, P Lee, S Lee, V Ya Nikulin, A Serban, P V Silin, X Feng[2] and G X Zhang, "A Powerful Soft X-ray Source for X-ray Lithography Based on Plasma Focusing", Phys. Scr. Vol 57 (1998) pp.488-494

[10] T. Kulkoulprakarn, D. Ngamrungroj, P. Kamsing, C. S. Wong and R. Mongkolnavin, "X-Ray Source Structures of a Small Plasma Focus Device", J. Sci. Res. Chula. Univ.,Vol. 32(2007), pp. 55-60

[11] R. Mongkolnavin, D. Ngamrungroj, C. Leeviriyalard and C.S. Wong, "Effect of X-Ray from a Small Plasma Focus on Colorless Synthetic Corundum", Jurnal Fizik Malaysia, Vol. 25 (2004), pp. 87-92.

[12] M Nisar, F Y Khattak, G Murtaza, M Zakaullah and N Rashid, "Sequential focusing in a mather-type plasma focus", Phys. Scr. Vol 47 (1993) pp.814-816

[13] L. Rico, B.J. Go´mez , J. Feugeas , O. de Sanctis , "Crystallization of amorphous zirconium thin film using ion implantation by a plasma focus of 1 kJ", Applied Surface Science , Vol 254 (2007) pp. 193–196

[14] บุญเหลือ เงาถาวรชัย, รัฐชาติ มงคลนาวิน, ดุสิต งามรุ่งโรจน์ และไพรัช คำสิงห์, "การทำความสะอาดผิวหน้าโลหะโดยใช้เครื่องพลาสมาโฟกัส", วารสารวิจัยวิทยาศาสตร์ จุฬาลงกรณ์มหาวิทยาลัย (Section T), Vol. 3(1), (2547) pp. 11-18.

[15] H Kelly, A Lepone, A Márquez, D Lamas and C Oviedo, "Coating on metallic samples produced by a small energy plasma focus", Plasma Sources Sci. Technol. Vol 5 (1996) pp 704-709

[16] M Hassan, A Qayyum, R Ahmad, G Murtaza and M. Zakaullah, "Nitriding of titanium by using an ion beam delivered by a plasma focus", J. Phys. D: Appl. Phys. Vol 40 (2007) pp.767-777

[17]Chhaya R. Kant, M.P. Sivastava, R.S. Rawat, "Thin carbon film deposition usig energetic ions of a dense plasma focus", <u>Physics Letters A</u> , Vol 226(1997) pp 212-216.

[18] B.B. Nayak, B.S. Acharya, S.R. Mohanty, T.K. Borthakur and H. Bhuyan, "Surface nitriding of graphite substrate by plasma focus device towards synthesis of carbon nitride coating" , <u>Surface and coatings Technology</u> ,Vol 142 (2001) pp 8-15.

[19] R. Mongkolnavin, J. Srisawat, D. Ngamrungroj and V. Pimpan, "A Plasma Focus Application for Enhancing Lamination Process of Polypropylene/Polyester/Cotton Composites", <u>Jurnal Fizik Malaysia</u>, Vol. 28 (2007)

[20] H. Bhuyan, H Chuaqui, M Favre, I Mitchell and E Wyndham "Ion beam emission in a low energy plasma focus device operating with methane", <u>J. Phys. D: Appl. Phys</u>. Vol 38 (2005)

[21] H´ector Kelly, Alejandro Lepone, and Adriana M´arquez, "Nitrogen Ion Spectrum from a Low Energy Plasma Focus Device" <u>IEEE TRANSACTIONS ON PLASMA SCIENCE</u>, VOL. 25, NO. 3, JUNE 1997

[22] Kazuto Takao, Yasuhiko Doi, Satoshi Hirata, Masaki Shiotani, Iwao Kitamura, Takakazu Takahashi and Katsumi Masufata, "Characteristics of ion beam produced in a plasma focus device", <u>Jpn. J. Appl. Phys.</u> Vol. 40 (2001) pp. 1013-1015.

[23] Choiw San Wong, Peter Choi, Wee Song Leong and Jasbir," Generation of high energy ion beams from a plasma focus modified for low pressure operation", <u>Jpn. J. Appl. Phys</u>. Vol. 41 (2002) pp. 3943-3946.

[24] G. Gerdin, W. Stygar, and F. Vwnneri, "Faraday cup analysis of ion beam produced by a dense plasma focus" , <u>J. Appl. Phys</u>. Vol. 52 issue 5, May 1981 pp. 3269-3275

[25] L. Jakubowski, M. Sadowski and J. Zebrowski, "Measurements of charged particle beams from plasma focus discharges" , <u>Nucl. Fusion</u> Vol 41 (2001) pp755-759

[26] Hoon Heo, and Duck Kyu Park, "Correlations between Argon Ion Beams and X-Rays in a Plasma Focus", Jpn. J. Appl. Phys. Part 1, No. 5A,,Vol. 41 (2002) pp. 3120–3124,

[27] M Zakaullah, Imtiaz Ahmad, A. Omar, G. Murtaza and M.M. Beg "Effect of anode shape on plasma focus operation with argon" , Plasma sources Sci. Technol. Vol 5 (1996) pp 544-552. Printed in yhe UK

[28] Sharif Al-Hawat "Axial Velocity Measurement of Current Sheath in a Plasma Focus Device Using a Magnetic Probe" IEEE TRANSACTIONS ON PLASMA SCIENCE, Vol. 32, NO. 2, APRIL 2004

[29] Shaista Zeb, Mehboob Sadiq, A. Qayyum, Ghulam Murtaza, M. Zakaullah, "Deposition of diamond-like carbon film using dense plasma focus" Materials Chemistry and Physics, Vol. 103 (2007) pp 235–240

[30] H´ector Kelly, Alejandro Lepone, Adriana M´arquez, Marek J. Sadowski, Jaroslaw Baranowski, and Elzbieta Skladnik-Sadowska, "Analysis of the Nitrogen Ion Beam Generated in a Low-Energy Plasma Focus Device by a Faraday Cup Operating in the Secondary Electron Emission Mode" IEEE TRANSACTIONS ON PLASMA SCIENCE, Vol. 26, No. 1, February 1998

[31] S. Lee, B.C. Tan, C.S. Wong, and A.C. Chew. Laser and plasma Technology Proc. Second Tropical College on Applied Physics: World Scientific, 1986.

[32] H Bruzzone and R. Vieytest, "The initial phase in plasma focus devices", Plasma Phys. Control. Fusion Vol. 35 (1993) pp 1745-1754, Printed in the UK

[33] C.S. Wong "Plasma Focus", Class note, University of Malaya , 2000.

[34] Dusit ngamrungroj, "Plasma focus modification for material surface treatment", thesis of master degree , Department of Physics Faculty of Science, Chulalongkorn University, 2002

[35] C.H. Lee, D. Ngamrungroj, C.S. Wong, R. Mongkolnavin, Y.K. Low, J. Singh and S.L.Yap "Correlation Between The Current Sheath Dynamics in The Axial

Acceleration Phase of The Plasma Focus and Its Ion Beam Generation", <u>Journal of Science and Technology for the Tropics</u>, Vol. 1 (2005),pp. 49

[36] AAAPT. <u>TWELVE YEARS OF UNU/ICTP PFF-A REVIEW</u>, The United Nation University: 1963.

[37] V.I.Krauz, V.V.Myalton, E.Yu.Khautiev, V.P.Smirnov,A.N.Mokeev, M.A. Karakin et al. <u>PLASMA FOCUS RESEARCH AT THE KURCHATOV INSTITUTE</u>. Institute for High Energy Densities of Associated Institute for High Temperatures Russian Academy of Sciences, Moscow: 1999.

[38]http://video.google.com/videoplay?docid=-1518007279479871760&q=Google+ tech+talks+lerner&pr=goog-sl, Eric Lerner , Oct 06, 2007

[39] Gureev, K. G.; Filippov, N. V.; Filippova, T. I. "Numerical simulation of current sheet separation in a plasma- focus -type device", <u>Fizika Plazmy</u>, Vol. 1, Jan.-Feb. 1975, pp. 120-126

[40] M. Scholz and I. M. Ivanova-Stanik, **"**Initial phase in plasma focus device — model and computer simulation", <u>Vacuum</u> Vol 58, Issues 2-3, August 2000, pp. 287-293

[41] Shan Bing, "<u>COMPARATIVE STUDY OF DYNAMICS AND X-RAY EMISSION OF SEVERAL PLASMA FOCUS DEVICES</u>", Ph.D. Thesis, PHYSICS DIVISION, SCHOOL OF SCIENCE NANYANG TECHNOLOGICAL UNIVERSITY (2000)

[42] Bing Shan, Pual Lee and S.Lee, "Improveing Energy Efficiency of Plasma Focus", Sing. <u>J. Phys</u>. Vol. 16, No. 1(2000) pp25-35

[43] R. Mongkolnavin, D. Ngamrungroj and C.S. Wong, "<u>Efficiency of Energy Transfer in a Small Plasma Focus Device</u>", *Solid State Phenomena*,Vol. 107 (2005), pp.95-98.

[44] K. E. Nalty, R. C. Zowarka, L. D. Holland.; "Instrumentation for EM Launcher Systemst", <u>IEEE Transactions on Magnetics</u>, Vol 20, no 2, March 1984. pp 328-331

[45] R L F Boyd, "The Mechanism of Positive Ion Collection by a Spherical Probe in a Dense Gas", <u>Proc. Phys. Soc</u>. Vol 64 (1951) pp 795-804

[46]http://www.theledlight.com/UV.html&h=300&w=391&sz=17&tbnid=arjbCDY8cW EJ:&tbnh=92&tbnw=120&hl=th&start=13&prev=/images%3Fq%3DWavelength%2Buv %2B%26hl%3Dth%26lr%3D%26sa%3DN

[47] http://www.df.unibo.it/macro/intercast/charact.htm

[48] www.mercateo.com

[49] <u>Titisak Kulkoulpr</u>, "<u>Investigation of x-ray emission from a small plasma focus device</u>", thesis of master degree , Department of Physics Faculty of Science, Chulalongkorn University, 2005

[50] S.P. Moo, C.K. Chakrabarty, and S. Lee, " An Investigation of the ion beam of plasma focus Using a metal obstacle and deuterated target", <u>IEEE TRANSACTIONS ON PLASMA SCIENCE</u>, VOL. 19, NO. 3, JUNE 1991

[51] S. Lee,"<u>Radiative Dense Plasma Focus Model Computation Package RADPFV5.008</u>" NTU/NIE NSSE Plasma Radiation Source Laboratory, Singapore. (November 2005) [http://eprints.ictp.it/85/]

BIOGRAPHY

NAME   Mr.DUSIT NGAMRUNGROJ

BIRTH   16 NOVEMBER 1977

EDUCATION 2000 – 2002 M.Sc. Physics , Department of Physics, Faculty of Science, Chulalongkorn University, In 1996 - 1999 Bachelor's Degree from Chulalongkorn University, gpax 3.06, In 1990 - 1995 High School at Angthong Patthamarot Wittayakhom, gpax 3.26,In 1984 – 1989 Primary School at Anubanwat Angthong

PUBLICATIONS

- R. Mongkolnavin, **D. Ngamrungroj**, C. Leeviriyalard and C.S. Wong, "Effect of X-Ray from a Small Plasma Focus on Colorless Synthetic Corundum", *Jurnal Fizik Malaysia*, 2004, **25**(3&4), 87-92.
- R. Mongkolnavin, **D. Ngamrungroj** and C.S. Wong, "Efficiency of Energy Transfer in a Small Plasma Focus Device", *Solid State Phenomena*, 2005, **107**, 95-98.
- C.H. Lee, **D. Ngamrungroj**, C.S. Wong, R. Mongkolnavin, Y.K. Low, J. Singh and S.L.Yap "Correlation Between The Current Sheath Dynamics in The Axial Acceleration Phase of The Plasma Focus and Its Ion Beam Generation", *Journal of Science and Technology for the Tropics*, 2005, **1**, 49.
- R. Mongkolnavin, J. Srisawat, **D. Ngamrungroj** and V. Pimpan, "A Plasma Focus Application for Enhancing Lamination Process of Polypropylene/Polyester/Cotton Composites", Jurnal Fizik Malaysia, 2007, 28(1)
- T. Kulkoulprakarn, **D. Ngamrungroj**, P. Kamsing, C. S. Wong and R. Mongkolnavin, "X-Ray Source Structures of a Small Plasma Focus Device", *J. Sci. Res. Chula. Univ.*, 2007,**32**, 1, 55-60

- บุญเหลือ เงาถาวรชัย, รัฐชาติ มงคลนาวิน, **ดุสิต งามรุ่งโรจน์** และไพรัช คำสิงห์, "การทำความสะอาดผิวหน้าโลหะโดยใช้เครื่องพลาสมาโฟกัส", *วารสารวิจัยวิทยาศาสตร์ จุฬาลงกรณ์มหาวิทยาลัย (Section T)*, 2547, **3**(1), 11-18.

- **Dusit ngamrungroj**, "Plasma focus modification for material surface treatment", thesis of master degree, Department of Physics Faculty of Science, Chulalongkorn University, 2002
- Final year project report, "Development of an Electronic Circuit for Controlling High Voltage Charger", 1999

Conference

- 2nd Mathematics and Physical Science Graduate Congress December 4-6 2006, "High Frequency Electric Probe for Measuring Ion Generated from a Small Plasma Focus", Faculty of science National University of Singapore, Singrapore
- R. Mongkolnavin, D. Ngamrungroj, Wong, C.S. Yap, S.L. Low, Y.K. "Effect of pressure on the axial phase dynamics of a small plasma focus", Plasma Science, 2003. ICOPS 2003. IEEE Conference Record - Abstracts. The 30th International Conference on
- P. Kamsing, R. Mongkolnavin and **D. Ngamrungroj**, "Use of Theta Pinch for Corundum Treatment", *Abstracts to The 12th Academic Symposium of Faculty of Science, Chulalongkorn University*, 18-19 March 2004, Bangkok, Thailand.